Engineering Doctorate (Intl.)

Innovation Report

Modelling and Predictive Performance of Lithium Titanate

Michael Brunell

This work has been submitted in partial fulfilment of the requirements for the degree of Doctor of Engineering (EngD)

Warwick Manufacturing Group, University of Warwick

27th Nov 2020

Executive summary

Altairnano, a manufacturer of lithium titanate (LTO) battery cells, sponsored the work contained within this innovation report to explore the unique characteristics of its chemistry. Altairnano also sought to improve its business processes and capabilities via various projects conducted during this research.

A large portion of the work, that continued throughout the four years of the doctorate, involved exploring the capabilities of Altairnano's LTO cells. Towards this goal, a study was put together regarding the hypothesis that their commercial cells could be stored at 0 V, a voltage level that causes damage to standard lithium ion batteries. This capability could enable a unique selling point and competitive edge, while also increasing safety level of its cells during transport, storage, and system manufacturing. Through this study the cells, which were stored at 0 V, had their performance after storage periods characterized and contrasted against Altairnano's standard storage method. Following upon this doctorate and this research, the capability for low voltage storage has been evaluated by Altairnano's customers to address various application and storage needs. This includes a unique application where due to environmental conditions charging cannot be guaranteed and extreme low voltages are possible. With the customer's previous batteries, when it reached the low voltage state the battery would need to be replaced at significant cost and difficulty. Whereas due to Altairnano's cell chemistry demonstrated capabilities, per this research, to withstand low voltage conditions without damage they are now able to bring a portable charger to raise the voltage back up and continue operation, significantly reducing cost for transportation and replacement.

A separate project worked to achieve the goal of improving Altairnano's business capabilities. Towards this goal a framework tool was built around its multiple independent battery performance, aging, and thermal models. This tool would provide a platform for Altairnano's future work on

modelling. In addition, the platform simplified and streamlined the interaction between the models creating an expanded accessibility, both internal and external to the company, to its modelling knowledge and capabilities. This work and the tools developed have been implemented into Altairnano's day-to-day operation, significantly reducing the turnaround time for modelling a customer's application. This work has also been released to a customer directly to improve the quality of application needs discussed with Altairnano. This was achieved through the tool by allowing the customer to pre-qualify the estimated performance of a proposed system to meet their application requirements. This pre-qualification was not previously possible and helps to reduce the workload on Altairnano's limited resources.

Further building upon that platform and modelling work, a new model was built for Altairnano that would utilize a novel method for generating a parameterization signal. The new method would incorporate real application data collected from a grid operator for frequency regulation, a commercial industry that Altairnano's products participate in. The parameters from this signal would be incorporated into an equivalent circuit model, expanding Altairnano's modelling capabilities beyond their original model while also increasing modelling accuracy. This work has not been implemented into Altairnano's workflow due to testing resource constraints within the company, but it is planned for when resources become available to evaluate suitability in use with Altairnano's newest generation chemistry.

Contents

Executive summary i
List of Figures v
List of Tables viii
Acknowledgements ix
List of Acronyms x
1 Project Context 1
2 Background 3
2.1 Introduction to Altairnano 3
2.2 Background on Lithium Titanate Chemistry 4
2.3 Aging and Degradation 10
2.3.1 Aging of LTO 12
2.4 Project Flow 16
3 0 V storage of Lithium Titanate 18
3.1 Background 18
3.2 Alternates to Standard Lithium Ion Battery Configurations 21
3.2.1 Current Collector Material 21
3.2.2 Lithium Titanate Cells 22
3.3 Electrochemical Characterisation of 0 V cells 24
3.3.1 Half-cell Research 24
3.3.2 Full Cell Research 36
3.3.3 Incremental Capacity Analysis 42
3.3.4 Three electrode Cell Research 52
3.4 Brief Discussion of Results 56
3.5 Innovation and Impact on Industry 57
4 Continued Development and Integration of Altairnano's Model 60
4.1 Altairnano Model Background 60
4.2 A Technical Brief of Modelling 64
4.3 Model Integration 65
4.4 Innovation and Impact on Altairnano 69
5 Development of New Parametrization Signal and Implementation into an Equivalent Circuit Model 72
5.1 Common Issues with Testing for Parameterization and Model generation 73
5.1.1 Simulating Actual Conditions in Testing and Models 73
5.1.2 Hybrid Pulse Power Characterization (HPPC) 73
5.1.3 Development of a Novel Parameterization Signal and Method 77

5.1.4 Implementation into an Equivalent Circuit Model 83
5.2 Innovation and Impact on Altairnano 109
6 Conclusions 111
6.1 Limitations 113
6.2 Future Work and Opportunities 115
7 Conference Presentations..... 117
8 References 118

List of Figures

Figure 1: Comparison of LTO and Graphite anode [2] 4
Figure 2: View of an uncycled graphite particle versus Altairnano's nano lithium titanate (nLTO) agglomerate 5
Figure 3: Crystal structure of LTO from spinel ($Li_4Ti_5O_{12}$) to rock salt ($Li_7Ti_5O_{12}$) [28] 7
Figure 4: Comparison of stresses caused by Li-ion insertion 7
Figure 5: Voltage curve of LTO vs Lithium [31] 8
Figure 6: Voltage curve comparison of $LiCoO_2$ versus graphite and LTO anodes [25] 9
Figure 7: Voltage ranges for LTO full cells (right) vs other lithium ion full cells (centre to left) [33] 9
Figure 8: Cell voltages of various cells comprise of a varying cathode materials pair with a LTO anode [9] 10
Figure 9: High number of interdependent mechanisms that can affect aging in cell and create difficulties in modelling [50] (RT – room temperature, LT – low temperature, HT – high temperature) 11
Figure 10: Altairnano cell cycle life at 2C charge/discharge rates [56] 13
Figure 11: Microvast cell cycle life (www.microvast.com) 14
Figure 12: Toshiba cell cycle life (http://www.scib.jp/en/product/detail.htm) 14
Figure 13: LTO/LFP cell under 15C/10C charging and 5C discharge cycling [57] 15
Figure 14: Cell voltage window over the cycle life of an LTO/LFP cell [57] 15
Figure 15: General Project Flow 16
Figure 16: Various safeguarding options to help reduce airborne fire hazards from lithium ion batteries; the strategy of reducing the state of charge or voltage is studied in this paper. 18
Figure 17: Standard carbon-based half-cell voltage curves with a zero-volt crossing point greater than the dissolution potential of copper 20
Figure 18: Half-cell voltage curves of a lithium ion cell with titanium current collector. The zero volt cross over point is shown well below the potential of the Titanium current collector, allowing the cell to safely reach 0 Volts [63] 21
Figure 19: Lithium titanate cell construction diagram, highlighting the aluminium current collector material on both sides of the cell. 23
Figure 20: Theoretical half-cell voltage curves for a lithium titanate cell, showing the current collector dissolution potential greater thhan the zero volt cross over point. 24
Figure 21: Cell 507 initial cycles 27
Figure 22: Cell 507 cycles within extended voltage range 28
Figure 23a: 1 V to 2 V cycling of LTO half-cell id 507 29
Figure 24b: 1 V to 2 V cycling of LTO half-cell id 508 and 29
Figure 25c: 1 V to 2 V cycling of LTO half-cell id 509 30
Figure 26: 1 V to 3.5 V cycling of LTO half-cell id 507 (extended voltage window to mirror possible full cell conditions of LTO electrode for 0 V storage) 31
Figure 27: Cell 507 capacity loss during cycling for each test regime 32
Figure 28: LTO half-cell charged to 3.0 V and allowed to relax to OCV and corresponding SEM image of LTO electrode 34
Figure 29: LTO half-cell charged to 3.0 V and maintained at 3.0 V for five days and corresponding SEM image of LTO electrode. 35
Figure 30: LTO half-cell charged to 3.5 V and maintained at 3.5 V for five days and corresponding SEM image of LTO electrode. 35
Figure 31: LTO electrode SEM imaging comparing (a) pristine versus (b) electrode maintained at 3.5 V 36
Figure 32: The three voltage regimes under which the cells were stored 40
Figure 33: Pre and post storage voltage curves normalized to cell capacity 41
Figure 34: Altairnano open circuit voltage and resistance curve for the 13 Ah cell from 2.0 V to 2.755 V 41

Figure 35: Full cell ICA curves....43
Figure 36: EIS plot overlaid with where series resistance R_s and charge transfer resistance R_{ct} are determined from....44
Figure 37: EIS data of all cells pre and post storage for 90% SoC....45
Figure 38: Two sigma analysis of 90% SoC data for R_s and R_{ct} (April – pre storage, Sept/Nov post storage)....45
Figure 39: EIS data of all cells pre and post storage for 50% SoC....46
Figure 40: Two sigma analysis of 50% SoC data for R_s and R_{ct} (April – pre storage, Sept/Nov post storage)....46
Figure 41: EIS data of all cells pre and post storage for 20% SoC....47
Figure 42: Two sigma analysis of 20% SoC data for R_s and R_{ct} (April – pre storage, Sept/Nov post storage)....47
Figure 43: Altairnano 13 Ah cycle life chart showing initial increase in capacity for low count cycles [77]....48
Figure 44: Full cell 26 A charge capacity....49
Figure 45: Full cell 26 A discharge capacity....50
Figure 46: 5 cycles each of 3 A (blue) and 5 A (red) cycling after storage for a cell maintained at 0 V for storage....51
Figure 47: Three electrode voltage diagram of cell being discharged to 0 V, with the 0 V crossing point noted. 54
Figure 48: Three electrode voltage diagram of the cell following a full charge discharge cycle, discharging the cell to 0 V in a single cycle with no rest. The 0 V crossing point is noted. 55
Figure 49: Altairnano performance modelling flow chart 61
Figure 50: Schematic illustration of interdependent influential mechanisms that can affect aging in cell and create challenges in modelling [50] (RT – room temperature, LT – low temperature, HT – high temperature)....64
Figure 51: Initial interface shown when the program is first initialized 66
Figure 52: Interface shown with selections that expand to show the various options including batch processing control (single input for all files versus input for each file) and module selection 67
Figure 53: Example of initial input parameters to be entered by the user based on choices selected from the previous screen....67
Figure 54: An example of the AltiCalc workflow....68
Figure 55: Expanded view of the interactions within the AltiCalc....69
Figure 56: Complete HPPC profile – USABC Battery test manual for plug-in hybrid electric vehicles [82]....74
Figure 57: Initial sequence of the HPPC profile [82]....74
Figure 58: Comparison of a Pulse Power profile versus a drive validation test for an actual vehicle [89]....75
Figure 59: Combination of a known pulse power signal with a multisine generated signal [89]....78
Figure 60: Frequency spectrum analysis of a drive cycle versus a 2C ten second pulse power signal [89]....78
Figure 61: Magnitude and frequency comparison between the drive cycle, the pulse power test and the combined signal [89] 79
Figure 62: Frequency analysis with magnitude and phase of the PJM signal. A fitted curve (orange) would provide the basis of the multisine generation signal.....80
Figure 63: Initial step of the MATLAB tool comparing the original signal (blue) to the initial generated signal (orange). From the top normalized signal (top), inverse cumulative distribution function, and the distribution of both signals.....81
Figure 64: Output from the MATLAB code showing the original signal (blue) compared to the generated signal (orange). From the top normalized signal (top), the root mean square error of the

signals (center top), the amplitude and frequency distribution of the signal (center bottom), and the distribution of both signals (bottom).....81
Figure 65: General equivalent circuit models. (Upper left: 0th order - Upper Right: 1st order - Bottom: 2nd order).....84
Figure 66: 2% incremental step equivalent circuit parameters. The x-axis in all charts is state of charge. For Ro and Rp the Y-axis is ohms. For Tau the y-axis is the RC time constant of the parallel circuit. 87
Figure 67: 2% layered incremental step equivalent circuit parameters. The x-axis in all charts is state of charge. For Ro and Rp the Y-axis is ohms. For Tau the y-axis the RC time constant of the parallel circuit. 89
Figure 68: 5% incremental step equivalent circuit parameters. The x-axis in all charts is state of charge. For Ro and Rp the Y-axis is ohms. For Tau the y-axis the RC time constant of the parallel circuit. 90
Figure 69: Combined Ro, Rp and Tau parameters plotted 1% incremental steps.....92
Figure 70: Comparison of Altairnano's pulse power resistance values and equivalent circuit based on parameterization from the frequency regulation based multisine singal testing. 93
Figure 71: Estimated loaded voltage and SoC based on the equivalent circuit model, parameterized based on the frequency regulation based multisine signal in a charge depleting profile.....95
Figure 72: Absolute error between recorded and modelled cell voltages for Equivalent circuit model (blue) and Altair's model (red) for a charge depleting profile.....96
Figure 73: Estimated loaded voltage and SoC based on the equivalent circuit model, parameterized based on the frequency regulation based multisine signal in an charge sustaining profile.....97
Figure 74: Absolute error between recorded and modelled cell voltages for Equivalent circuit model (blue) and Altair's model (red) for an energy neutral profile 98
Figure 75: Estimated loaded voltage and SoC based on the equivalent circuit model, parameterized based on the frequency regulation based multisine signal in a charge increasing profile.....99
Figure 76: Absolute error between recorded and modelled cell voltages for Equivalent circuit model (blue) and Altair's model (red) for charge increasing profile.....100
Figure 77: Estimated loaded voltage and SoC based on the equivalent circuit model, parameterized based on the frequency regulation based multisine signal in a 0.12 constant current charge profile 101
Figure 78: Absolute error between recorded and modelled cell voltages for Equivalent circuit model (blue) and Altair's model (red) a 0.12 constant current charge profile, please note the Absolute error scale change versus prior charts.....102
Figure 79: Estimated loaded voltage and SoC based on the equivalent circuit model, parameterized based on the frequency regulation based multisine signal in a 0.12 constant current discharge profile 103
Figure 80: Absolute error between recorded and modelled cell voltages for Equivalent circuit model (blue) and Altair's model (red) a 0.12 constant current discharge profile 104
Figure 81: Estimated loaded voltage and SoC based on the equivalent circuit model, parameterized based on the frequency regulation based multisine signal, in a pulse power test with rests.....105
Figure 82: Absolute error between recorded and modelled cell voltages for Equivalent circuit model (blue) and Altair's model (red) for a pulse power profile 106
Figure 83: Error for EC model prior to adjustment showing an offset 106
Figure 84: Adjusted error for EC model, charge values are negative and discharge values are positive 107
Figure 85: Adjusted absolute error between recorded and modelled cell voltages for Equivalent circuit model (blue) and Altair's model (red) for a pulse power profile 108

List of Tables

Table 1: Working coin cell data 25
Table 2: Charge Depleting Test Profile - Summarization of errors for each model 96
Table 3: Charge Sustaining Test Profile - Summarization of errors for each model 98
Table 4: Charge Increasing Test Profile - Summarization of errors for each model 100
Table 5: Low Constant Current Charge Test Profile - Summarization of errors for each model 102
Table 6: Low Constant Current Discharge Test Profile - Summarization of errors for each model 104
Table 7: Pulse Power Test Profile - Summarization of errors for each model after adjustment 108

Acknowledgements

First, I would like to thank my parents for believing in my goals and supporting my journey half-way around the world, especially with my mother's severe dislike of flying. Both of you coming to visit and allowing me to share my experiences with you was something I will never forget.

Second, I would like to thank Dr Melanie Loveridge and Dr Alexander Roberts for the many pints and discussions. Your thoughts and inputs to my research helped myself, and my work grow beyond what it would have been. I would also like to acknowledge and send extra thanks to Dr Loveridge for taking over as my advisor to help me complete this resubmission. Without your help and support this document would not have been possible.

Third, I would like to thank Dr Nick Mallinson. It was with your support that I was able to attend WMG and for that I am ever grateful. I appreciate the many discussion that we had over the years and I look forward to many more in the future.

Fourth, I would like to thank Dr Dhammika Widanage for his support in allowing me to build upon his work and answering my many MATLAB questions.

Fifth, I would like to thank my industrial advisor Brad Hanauer and Altairnano for sponsoring me to pursue a higher degree and for the opportunity to complete some beneficial work.

Finally, I would like to thank WMG, its staff, and technicians for all the support over my four years at WMG and putting up with my many, many questions.

List of Acronyms

A – amp(s)

ACCD - aluminium current collector dissolution potential

Ah - amp hour

C -prefaced with a number indicating C-rate

CC - constant current

CCCDP - copper current collector dissolution potential

CLI - capacity loss index

C-rate - current rate, ratio of amp hour capacity of the cell to the current rate

CV - constant voltage

DoD - depth of discharge

ECM - equivalent circuit model

EIS - Electrochemical Impedance Spectroscopy

GUI - Graphical user interface

HPPC - Hybrid Pulse Power Characterization

HT - High temperature

I - current

ICA - incremental capacity analysis

IP - intellectual property

kW - kilowatt

kWh - kilowatt hour

LFP - lithium iron phosphate

LT - low temperature

LTO - lithium titanate oxide ($Li_4Ti_5O_{12}$)

mA - milliamp

mAh - milliamp hour

mV - millivolt

MW - megawatt

MWh - megawatt hour

NCA - lithium nickel cobalt aluminium oxide

nLTO - nano structured lithium titanate oxide

NMC - lithium nickel manganese cobalt oxide

OCV - open circuit voltage

PJM - Pennsylvania New Jersey Maryland Interconnection (US based Mid-Atlantic region power pool)

R - resistance

Rms - root mean square error

Ro - ohmic resistance

Rp - polarization resistance

RT - room temperature

SEI - solid electrolyte interphase

SEM - Scanning Electron Microscopy

SoC - state of charge

SoH - state-of-health

Tau - time constant for an RC pair

USABC - United States Advanced Battery Consortium

V - volt

W - watt

Wh - watt hour

WMG – Warwick Manufacturing Group

ZCP - zero volt crossing potential

Analysis and the modelling of battery aging to provide an accurate predictive model for battery life and future performance in a customer's given duty cycle

1 Project Context

The battery technology based on lithium titanate (LTO) is often viewed as technology of the future, a promising technology, that still awaits widespread commercial realisation. Despite this view, often stated in publications such as those by Ahn et. al [1] in 2011 and Dr Mumu Moorthi [2] in 2010, lithium titanate batteries are already seeing increasing traction in commercial applications such as electric grid stability, renewable integration and in heavy-duty electric vehicles (buses, trains, trams, etc.) as deployed by Altairnano as early as 2008. As with any energy storage technology, to increase usage and uptake, a deeper operational knowledge of this material is needed.

The research conducted within this Engineering Doctorate focused on expanding the current knowledge of lithium titanate (LTO) into areas that have little or no research. It also seeks to create opportunities for innovation within the field and the sponsor company.

The first section presented, which challenges standard industry operation, looked at storing a lithium titanate battery cell at 0 V. Generally, a battery cell below its stated operational lower voltage limit especially at 0 V is considered an unusable or inactive cell which has been over-discharged [3–5]. With many conventional lithium battery chemistries, discharging a cell to low voltages can cause deleterious reactions and risk a thermal event or failure happening. By using a lithium titanate anode with an aluminium current collector, many if not all of the hazards can potentially be avoided. Little research regarding lithium titanate or commercial cells at very low voltage has been done to show this capability providing an impetus for the research presented below. Beyond the expansion of existing knowledge this research could have significant impact for industry in terms of maintenance costs and increased safety. The research will be demonstrated over multiple scales of cell formats, from coin cell to full pouch. This will enable a greater understanding of the behaviour of individual components within the cells (coin cell level) to the battery as a full system (commercial

pouch). Furthermore, this research is expected to unearth additional questions and lead to avenues for future research possibilities.

The second section of the research focused on modelling and predictive performance of an LTO battery in various applications. This part was subdivided into two main aspects:

- The integration of multiple tools to increase the accessibility of a model currently in use by Altairnano. This creates innovation within the company's current operating processes.
- The development of new methods of characterization and alternative modelling techniques, which could be incorporated into the previous modelling tool.

Within Altairnano, modelling performance is used to provide critical information to the marketing and sales team, customers, as well as the Engineering team. In addition, the modelling provides direction and feedback to Research & Development to inform the development of the chemistry to meet future customer needs. As such, developing useful tools which extend to wider user communities within the company, and the development of new and innovative techniques for characterization and modelling of battery performance, are the key drivers of the research.

From the sponsor company, Altairnano, several high-level goals were set prior to the start of the program as seen below:

- Data generation
    - Validation of Altairnano's model
    - Additional cycle life data (from the research and testing phase)
- MATLAB tool for aging models
    - Initial code to be based on current model
    - MATLAB tool with friendly user interface
    - Future code to be improved based upon research and data
- Journal publications and IP generation

- Undefined but it has been anticipated by both Altairnano and WMG that there will be some IP and paper generated as part of the outcome from the program

These goals, the impact within the organization, and the research will be discussed in the following sections following a background piece on the sponsor company and its battery chemistry. Each section discussing the research will be organized in the following order: background information, methodology, a results and discussion of the research program, and finally the innovation or new knowledge developed as well as the impact on the company.

2 Background

2.1 Introduction to Altairnano

The sponsor company, Altairnano [6], is a small, US based battery system manufacturer incorporated in 2006 with a focus on secondary battery cells utilizing the lithium titanate anode chemistry. In addition to its US operations, Altairnano operates in China through a wholly foreign owned entity (W.F.O.E.) Altair Nanotechnologies (China). The company provides lithium titanate powder, cells, modules, and battery systems as its main products. These products are sold into several industries including automotive, grid scale energy, heavy-duty transportation and other industrial applications. Products are provided to a number of customers throughout the world, operating in California, Hawaii, New Jersey, Puerto Rico, Denmark, Sweden, Czech Republic, Slovakia, Poland, Finland and China [6].

Through its previous experience as a materials research & development company, Altairnano has a number of patents [6] and trade secrets in relation to the development, manufacturing and production of its proprietary chemistry and cells. This development gives Altairnano's lithium titanate material and cells its unique performance and behavioural properties. It has continued development of the chemistry and is currently in its fourth generation of cell specifications. The

research contained within this report focuses on Altairnano's second-generation cell, based on a lithium titanate anode against a 1:1:1 lithium cobalt nickel manganese oxide cathode (NMC) with a 155mAh/g specific capacity.

2.2 Background on Lithium Titanate Chemistry

Of the multiple commercially available lithium ion battery technologies, one chemistry that has started to gain traction in various markets is Lithium Titanium Oxide $Li_4Ti_5O_{12}$ (more commonly known as Lithium titanate - LTO, or as nano material - nLTO). There are several material manufacturers, which are able to manufacture lithium titanate powder for use in battery cell. Of these manufacturers there is a smaller subset which sells commercially available cells including Leclanché, Altairnano, Microvast and Toshiba, each of which have their own variant of the chemistry.

A lithium titanate cell replaces the traditional graphite or carbon anode of a standard lithium ion cell with one that is manufactured with lithium titanate. The cell stills maintain the use of standard cathode materials such as lithium nickel cobalt aluminium oxide (NCA), NMC or other mixed metal oxides. A comparison of an LTO cell versus a standard graphite cell can be seen below in Figure 1.

	Li_4Ti_5O12 (LTO)	Graphite
Volume Change	0.2% (zero strain)	12%
Lithium Diffusion Coefficient	10^{-8} cm^2s^{-1}	10^{-10}-10^{-11} cm^2s^{-1}
Working Voltage vs Li^+/Li (V)	1.55	~0.1
Solid Electrolyte Interface (SEI)	none to inconsiderable	forming in 1st charge
Theoretical Capacity (mAh g^{-1})	175	372

Figure 1: Comparison of LTO and Graphite anode [2]

A comparison of a graphite particle and the LTO material manufactured by Altairnano can be seen below in Figure 2.

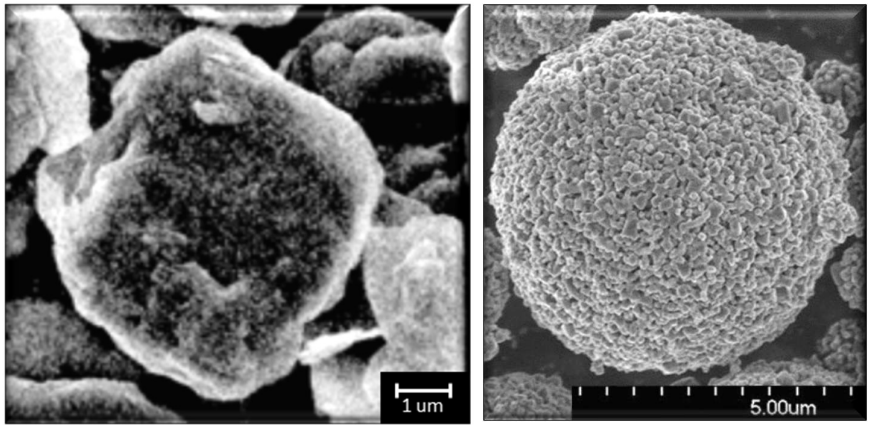

Figure 2: View of an uncycled graphite particle versus Altairnano's nano lithium titanate (nLTO) agglomerate

The replacement of the standard anode with one made of lithium titanate has a number of effects on the performance of the battery [2,7–20]. These effects include:

- A lower cell operating voltage range
- minimal to negligible solid electrolyte interface (SEI) layer formation
- wider functional operating temperature range
- generally lower energy density
- higher power density
- longer calendar life
- lower self-discharge rates
- considerable increase in cycle life
- higher operational current ratings especially on charge
- wider usable state of charge range with minimal impact on life
- increased safety.

Each of these effects will be discussed greater detail in the following paragraphs.

In the mid-1980s J.B. Goodenough and his group published a paper [12] exploring the superconducting-semiconducting transition in LTO spinels which built upon previous work completed in the 1970s. In 1989 Colbow et al. [21] continued the work and looked at the chemistry's cycle reversibility and voltage profile, but discusses the chemistry as a cathode rather than an anode of modern day LTO cells. In the 1990s and on into the 2000s research on lithium titanate occasionally emerged, with the chemistry often discussed as "an excellent *potential* electrode for battery applications" due to its characteristics in safety and cycle life [22–25]. As noted in the introduction, the status of LTO is often referenced in the literature "as a *promising* anode material" [15]. By this wording it implies that LTO requires considerable time in development prior to being introduced into commercial usage. However, LTO batteries are already being deployed commercially by several manufactures such as Altairnano and Toshiba, in addition to Microvast, Leclanché and Enerdel among others. Despite referencing commercial entities in their paper Sandhya et al. [15], and many other authors referenced in this and previous paragraphs, still refer to LTO as a technology of the future, rather than a technology of the present.

2.2.1.1 Structure

One feature of a LTO electrode is that the chemistry is considered a zero strain material [15,17,25–28]. During lithium ion and electron insertion and extraction there is no noticeable change in lattice dimension, or volumetric expansion with changes from the $Li_4Ti_5O_{12}$ state to $Li_7Ti_5O_{12}$, as seen in Figure 3. This results in electrodes, and further full cells, which do not exhibit volume changes during cycling operation due to electrode swelling.

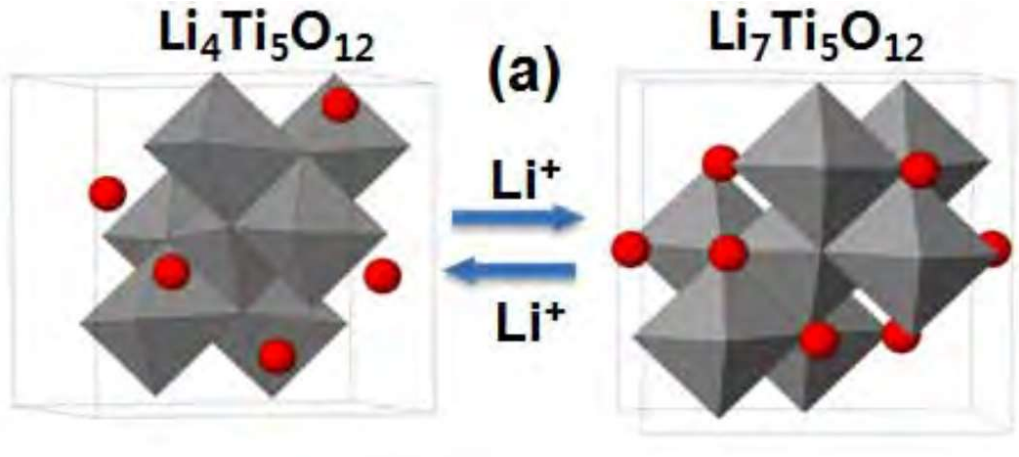

Figure 3: Crystal structure of LTO from spinel ($Li_4Ti_5O_{12}$) to rock salt ($Li_7Ti_5O_{12}$) [28]

With no expansion fractures due to dimensional changes at the SEI layer or at grain boundaries (please see Figure 4), failures due to damage to the material are not seen in LTO electrodes [29]. This stability of the crystalline structure through its various phases helps to support the long cycle life exhibited by LTO cells and avoid one of the main aging mechanisms of other Li-ion batteries based on carbon, graphite or silicon, mechanical stress and exfoliation of the material.

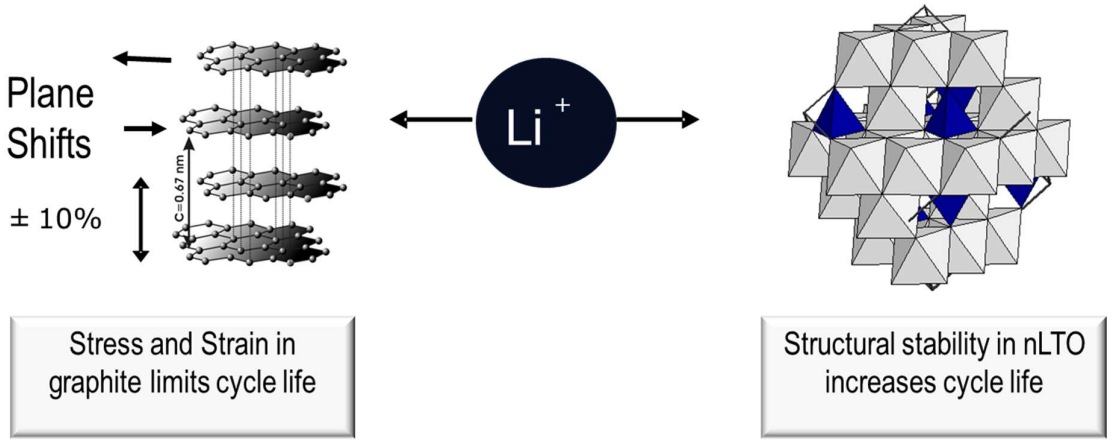

Figure 4: Comparison of stresses caused by Li-ion insertion

2.2.1.2 Voltage

Despite the benefits that LTO battery cells bring, there are a number of perceived negatives which have impacted the widespread adoption in commercial applications. The first of which is the lower

operating voltage of full LTO cells when compared to tradition Li-ion batteries. A lower cell voltage has implications in module and system design as it will take additional cells to reach a specific voltage as compared to higher voltage cells, which can increase weight and cost of a system. LTO electrodes have a stable operating voltage vs lithium of 1.5-1.6 V [9,11,29–32] as seen in Figure 5.

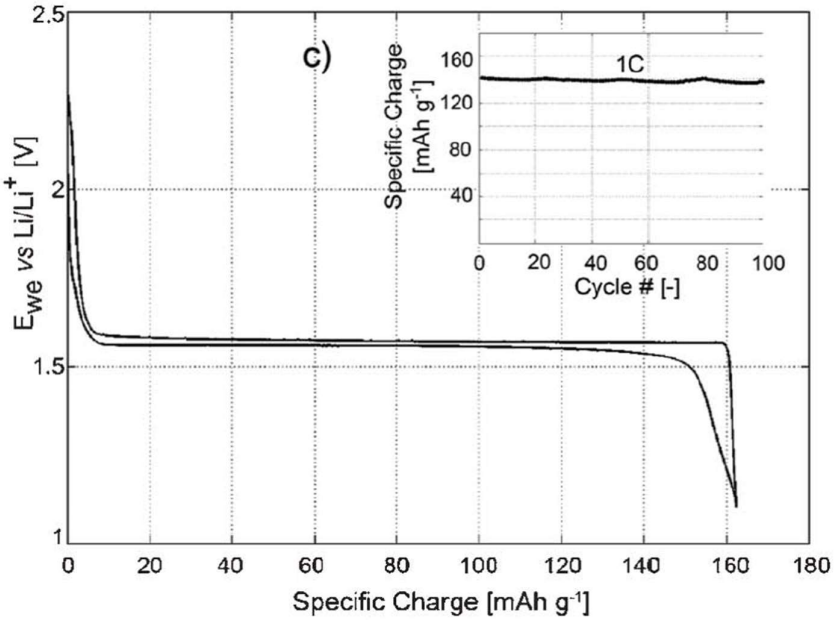

Figure 5: Voltage curve of LTO vs Lithium [31]

When a LTO electrode is combined in a cell with either a lithium nickel manganese cobalt oxide (NMC) or a lithium nickel cobalt aluminium oxide (NCA) electrode, the full cell will have an operating voltage range of 1.5-1.9 V to 2.8-2.9 V with a nominal voltage between 2.2 – 2.3 V as seen in Figure 6.

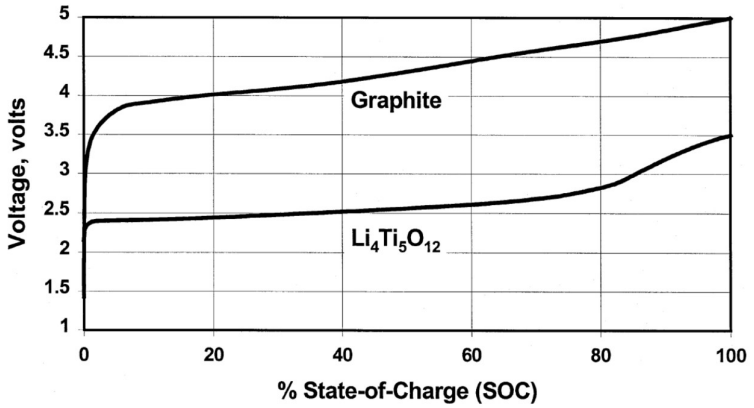

Figure 6: Voltage curve comparison of $LiCoO_2$ versus graphite and LTO anodes [25]

This nominal voltage is lower than standard lithium ion cells, such as lithium iron phosphate (LFP) which has a nominal voltage range of 3.3-3.4 V, or for various other lithium ion chemistries such as NMC, NCA, or Mn which have nominal values of 3.6-3.8 V as seen in Figure 7. Cells that pair an LFP cathode with an LTO anode have proven to be a safe and thermally stable cell, but with an even lower nominal voltage of 1.9 V seen in the right hand side of Figure 8 [15,30].

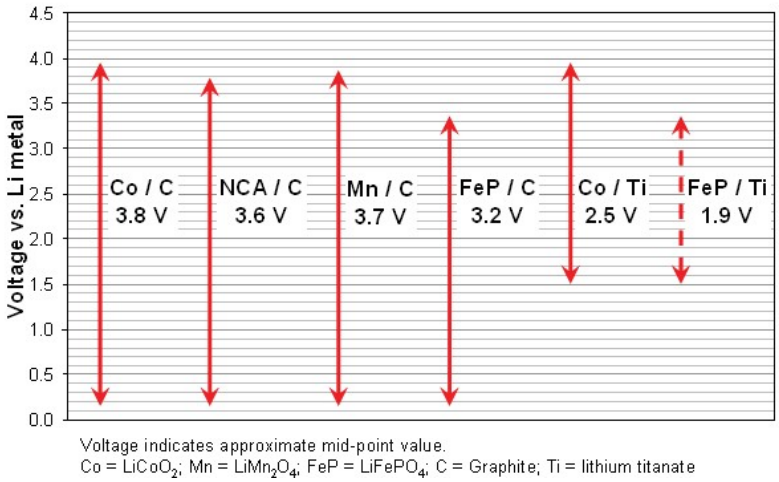

Figure 7: Voltage ranges for LTO full cells (right) vs other lithium ion full cells (centre to left) [33]

A lower full cell voltage of an LTO cell has a large influence on the engineering and system design:

- By increasing complexity (as more cells are needed to reach specified operational voltages of pack which increases the number of connections that must be made).

- When the lower operating cell voltage is compounded by a lower energy content (watthour, Wh) the choice of an LTO cell can drive an overall heavier system when the system is sized to reach a desired Wh, kWh, or MWh goal often requested by end users.

There has been work on higher voltage LTO cells such as the study by Yi et al. who paired LTO with various other cathodes as seen in Figure 8 with a goal of building a higher voltage LTO cell. [20] This goal comes with its own unique challenges including the need for stable high voltage electrodes and high voltage electrolytes that do not degrade at the higher voltage potentials vs lithium.

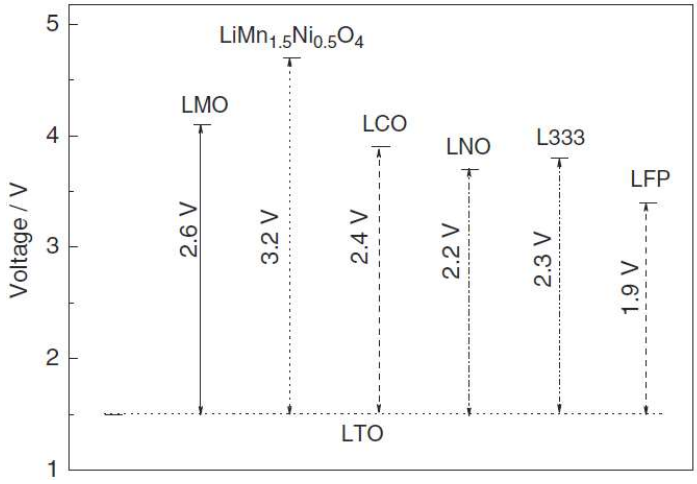

Figure 8: Cell voltages of various cells comprise of a varying cathode materials pair with a LTO anode [9]

2.3 Aging and Degradation

As mentioned throughout literature understanding battery aging is a highly challenging and complex issue [34–48]. As such, one of the hardest things to achieve when modelling lithium ion battery performance is predicting how the battery will degrade or age and determining the effect that this predicted degradation will have on the cell's performance over time. This degradation can be from either age effects or usage effects, and often with a lithium ion battery how the cell is used throughout its life (duty profile or usage profile) varies significantly and can be hard to quantify [49]. There are several variables which can impact how a cell ages when the battery is not used in a stable consistent manner over its lifetime:

- The actual age of the cells (calendar aging).
- The current rate at which the cell is charged or discharged (C-rate).
- How many times the cells have been either charged or discharged (cycle life).
- The depth of charge or discharge during each cycle (DoD).
- How the temperature of the cell changed throughout usage and storage.
    - High temperature (HT) cycling and excursions
    - Low temperature (LT) cycling

Each of these factors vary continuously and often simultaneously in an application and rarely remain constant similar to the web seen in Figure 9 [50], these compounding factors increase the complexity of understanding and isolating specific aging behaviours within a cell.

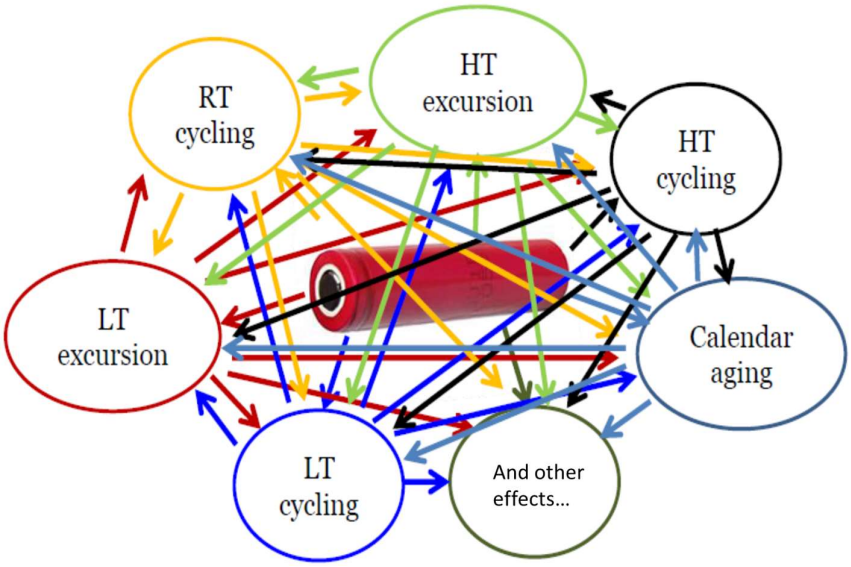

Figure 9: High number of interdependent mechanisms that can affect aging in cell and create difficulties in modelling [50] **(RT – room temperature, LT – low temperature, HT – high temperature)**

Larger applications with longer lives and more complex operating environments are driving an increased interest and need to understand how a lithium ion battery cell will degrade under a wider range of conditions [35]. In small-scale applications such as portable electronic devices, with non-replaceable batteries, the upgrade/replacement cycle of the devices is generally shorter than the life span of the battery. In these small-scale applications, the understanding of aged cells was of less

concern as the device was disposed of, discarded or replaced prior to failure of the battery. In contrast, larger format applications such as automotive, electric grid, and aerospace, all require multi-year life from the battery in a wide range of environmental operating conditions [51].

Automotive applications need batteries that can handle wide temperature ranges from diverse driving conditions across the world. Handling the variability of driving in a stop and go urban setting or driving long distances on highways or in rural environments also present variable drive cycles in addition to temperature effects. The battery is required to remain operational above 80% of the initial capacity for the length of their vehicle's warranties or longer. In many cases warranties are targeted for 5, 7 and even 10 years of life. Grid applications are looking for batteries that last like the equipment they know and are familiar with such as power plants, generators, turbines, transformers, and other industrial equipment, all which have life spans greater than 10 years. To the utility industry, equipment that is put into service on the electric grid needs to last. [52–54]

Quantifying how much a cell degrades in a single cycle that may have a variable current rate combined with a variable ambient/cooling/heating environment can be quite difficult and creates a need for modelling tools to be developed to support this. Research conducted on this topic is further discussed in following sections.

2.3.1 Aging of LTO

As noted by Svens et al. [10] currently there are large gaps in literature detailing the aging mechanisms of LTO electrodes, especially commercial LTO electrodes. Because of this gap, understanding how LTO degrades in a complete battery cell can be difficult. Where there is literature on a LTO based cell degradation, the aging of the cell is generally attributed to the cathode [10,23,25,28,55]. Due to the fact that the cathodes are standard commercial cathodes the research and literature is more readily available and accessible.

When discussing LTO cells the cycle life is often the main focus, with calendar life and capacity loss as secondary interests. Regarding its cycle life multiple commercial manufacturer have claimed and

demonstrated greater than 10,000 full 100% DoD cycles at 25 °C. Some of the manufacturers are: (i) Microvast, demonstrating greater than 20,000 full cycles (www.microvast.com); (ii) Altairnano, demonstrating greater than 16,000 cycles [56] and Toshiba which has demonstrated greater than 10,000 cycles (http://www.scib.jp/en/product/detail.htm). The long cycle life of LTO causes further complication in the collection of aging data as the time required, even with accelerated testing, is many times longer than traditional lithium ion cells. At a 1 C-rate (current rate, ratio of current to of amp hour capacity of the cell) charge/discharge cycle 10,000 cycles would take 20,000 hours or approximately two and a quarter year of non-stop testing. Because of this time commitment, empirical data to fully characterize a cell in an aging model can be difficult to come by as the time required to collect the data can be a significant detriment.

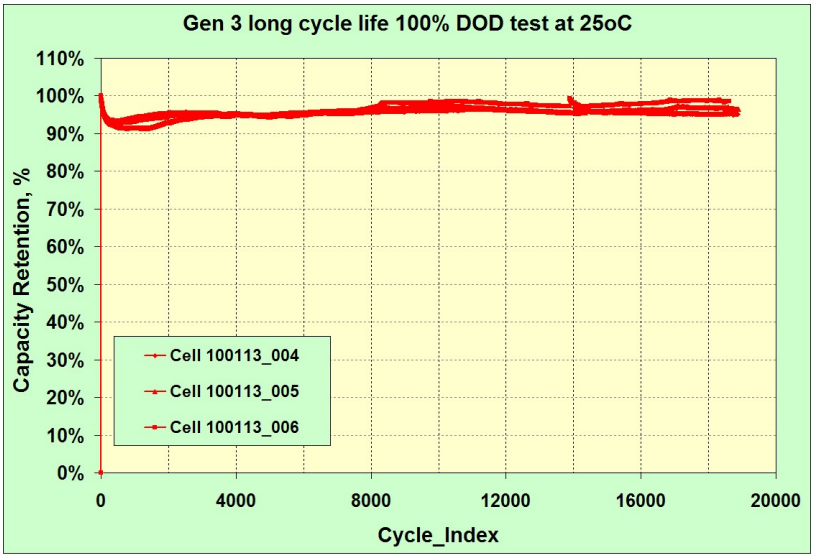

Figure 10: Altairnano cell cycle life at 2C charge/discharge rates [56]

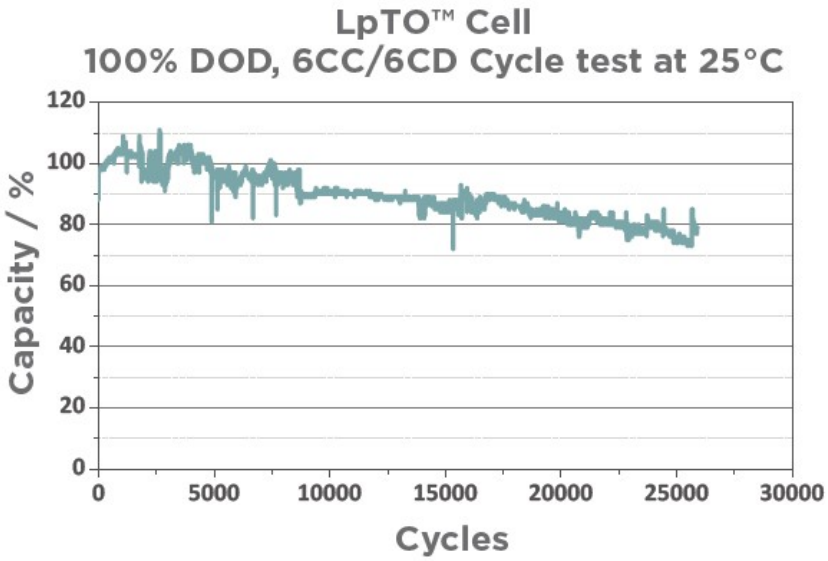

Figure 11: Microvast cell cycle life (www.microvast.com)

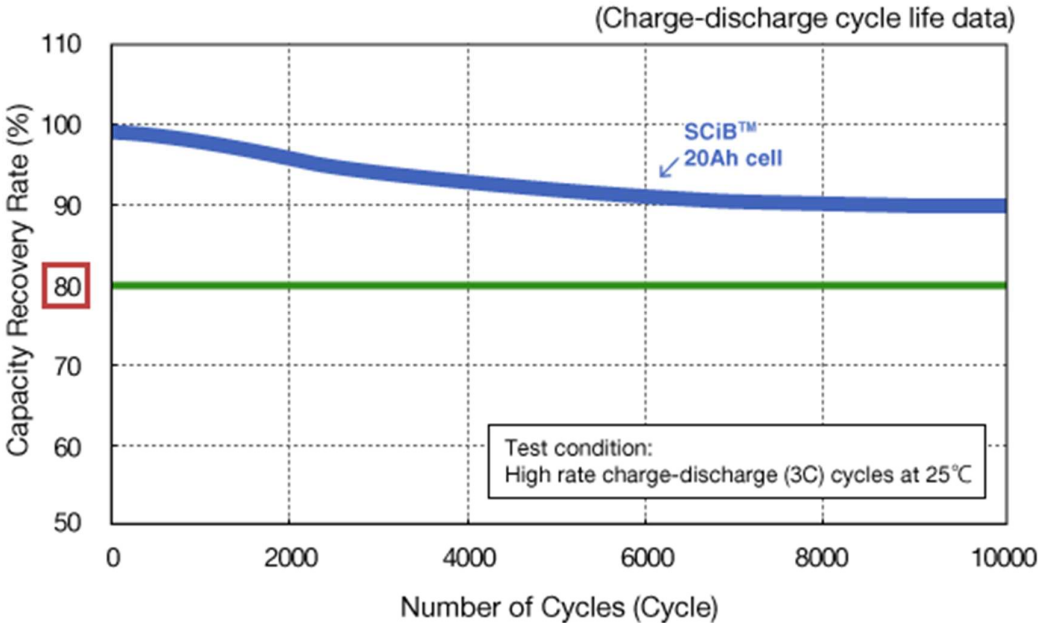

Figure 12: Toshiba cell cycle life (http://www.scib.jp/en/product/detail.htm)

Furthering the claim of extremely long cycle life Zaghib et al. have demonstrated in their lab LTO cells which exhibit greater than 20,000 to 30,000 cycles at very high current rates of 10 to 15 C charging with a 5 C discharge, significantly higher than traditional lithium ion batteries as seen in Figure 13 below [57].

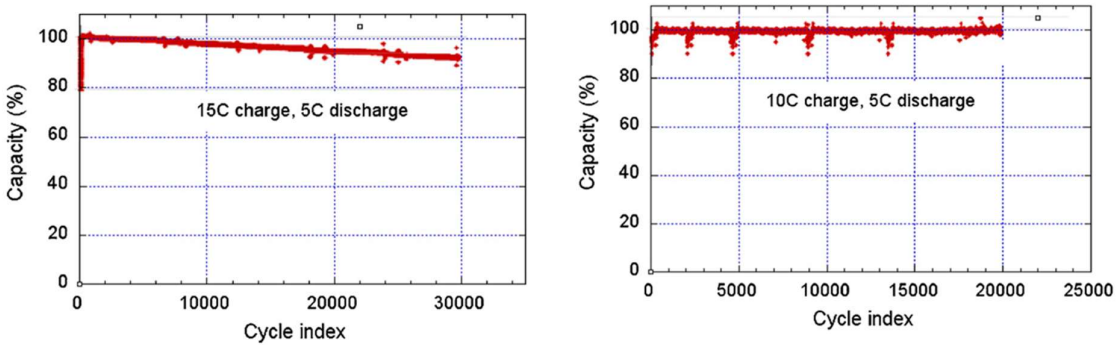

Figure 13: LTO/LFP cell under 15C/10C charging and 5C discharge cycling [57]

In addition to the long cycle life, Zaghib et al. have also demonstrated the stability of the cell voltage while cycling [57]. The voltage window for an LTO cell remains stable and consistent throughout the life of the cell during cycling as seen in Figure 14, which is ideal for supporting accurate life estimating and future performance predicting models.

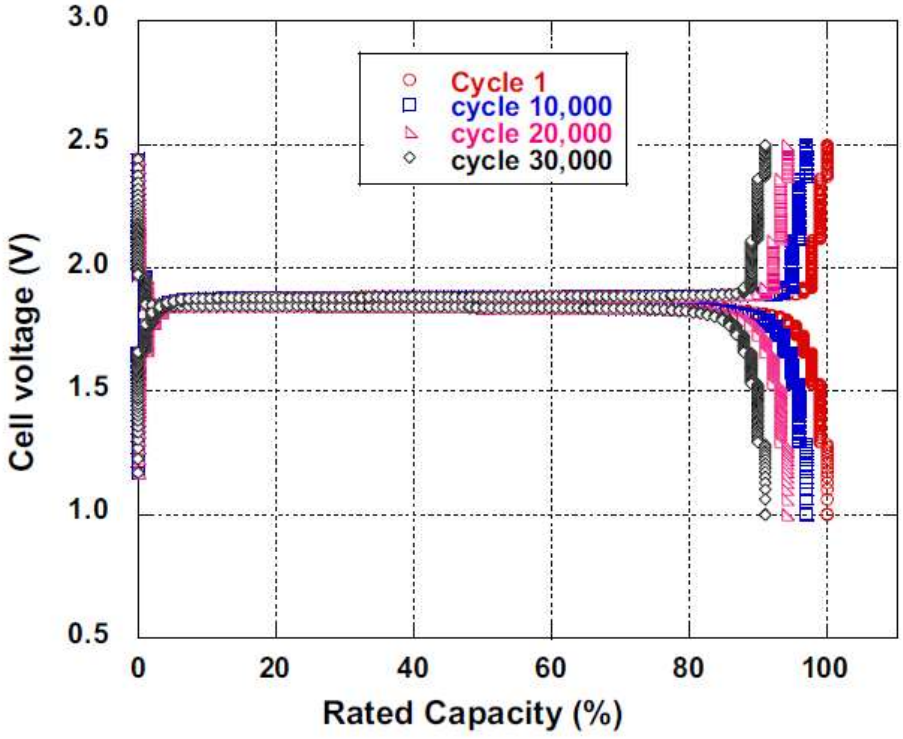

Figure 14: Cell voltage window over the cycle life of an LTO/LFP cell [57]

2.4 Project Flow

All of the projects within this research focused on Altairnano's 2nd generation chemistry of their lithium titanate cells, with much of the research conducted on the 13 Ah pouch cell format. All research conducted was in an effort to establish new knowledge and innovation within Altairnano or industry.

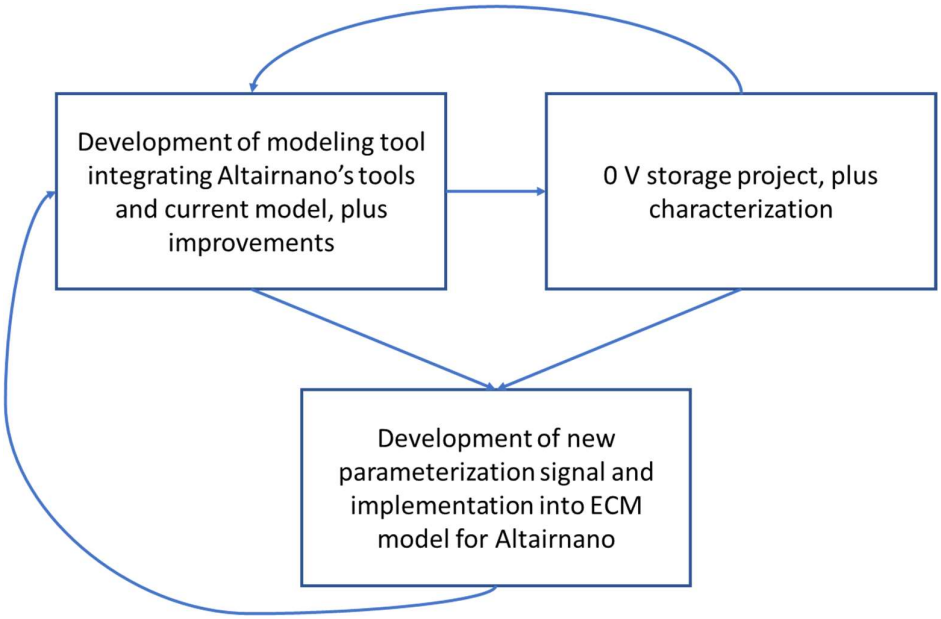

Figure 15: General Project Flow

While presented second for reading purposes, the initial project was the integration of Altairnano's model and various tools into a single tool or platform. This work provided the base from which the 0 V and new parameterization signal and ECM model developed from. This first project developing a not tool for Altairnano allowed the researcher to develop an understanding and competency with the MATLAB environment, which would support subsequent work through data analysis techniques.

The 0 V project, grew from the initial project as a way to establish a more complete understanding of Altairnano's lithium titanate chemistry and behaviour through characterization, but also to establish new knowledge. This characterization data was fed back into the initial project allowing for a more complete open circuit voltage curve to be implemented into the model, while providing evidence into the effect of storage periods at 0 V would have on the performance of the cells after aging and

storage. This knowledge is a critical piece to the understanding the aging of cells as often models do not incorporate or account for storage periods by customers.

The final project built upon the two previous projects, bringing together data developed during characterization of the 0 V cells with the modelling knowledge developed during the work with Altairnano's original model. This allowed for a model to use accurate data within the framework of the tool originally developed to process the model's inputs and outputs.

All three projects together help to build a more complete picture of the behaviour and performance capabilities of Altairnano's chemistry and cells.

3 0 V storage of Lithium Titanate

3.1 Background

As a result of the increased use of rechargeable lithium ion batteries in today's life there has been a matched increase in the volume of lithium ion batteries shipped and stored in warehouses around the world. As such, due to lithium ion's potential for explosive reactions, as has been seen in recent news, there has been an increase focus on safety during shipping and warehousing.

Figure 16 shows proposed solutions to increasing safety during shipping with the goal of reducing the significance of damage done if an event does occur. One of the ideas noted in Figure 16 is the concept of reducing the state of charge at which a cell is shipped. As energy is stored in a battery due to chemical reactions and electrical potential differences, reducing the state of charge reduces the electrochemical energy contained within the cell. Various abuse testing has substantiated that a cell at lower state of charge tends to have a reduced chance of gassing and fire [58–60], thus increased safety and increasing the ability of safety personnel to manage events that do happen.

Figure 16: Various safeguarding options to help reduce airborne fire hazards from lithium ion batteries; the strategy of reducing the state of charge or voltage is studied in this paper.

The increased need for safety and lowering the state of charge of a cell as method of achieving this goal was a catalyst for researching a lithium titanate cell's potentially unique behaviours at low voltage, down to and including a potential of zero volts which is not possible with standard lithium ion cells without causing irreversible damage or risking additional modes of failure.

Of the above methods, lowering the state of charge looks at reducing the total electrical energy contained within the cell to a minimum state and increasing safety as noted above. Uncontrolled electrical energy release can lead to chemical reactions within the cell, which lead to increased heat within the cell, which can then lead to explosion or fire. The initiation of the event is caused by an uncontrolled release of electrical energy, one such example is a short, either internal or external, to the cell. Shorts can be caused by connection of the external terminals, by external mechanical failures such as crush or puncture creating a connection between the electrodes internally, or electrochemical factors within the cell such as conductive dendrites.

By reducing the potential between the two electrodes to zero volts, the opportunity for uncontrolled electrical release causing an unwanted side reaction due to an internal or external short circuit can be eliminated.

One challenge to the approach of lowering the state of charge, or electrical energy, is that there is generally a limitation on how low the voltage of a lithium ion battery can be reduced until damage is caused within the cell. This damage can be in the form unwanted chemical reactions such as the dissolution of the copper current collector, which is often used for the anode. This dissolution can introduce impurities to the electrolyte and creates focal points for the formation of lithium plating and dendrite growth. [3,4,59,61,62] As demonstrated in Figure 17 [63] when a standard lithium ion cell is discharged to zero volts there is a cross over point where the potential between the two electrodes is zero volts. This cross over point is at a greater potential versus lithium, than the potential where copper begins to dissolve, as noted as the substrate dissolution potential in Figure 17. In standard practice a full cell voltage below the manufacturers recommended lower voltage limit is considered an over discharge event. The voltage curves for the anode and cathode shown below in Figure 17 are representative of the voltage response under a constant current load.

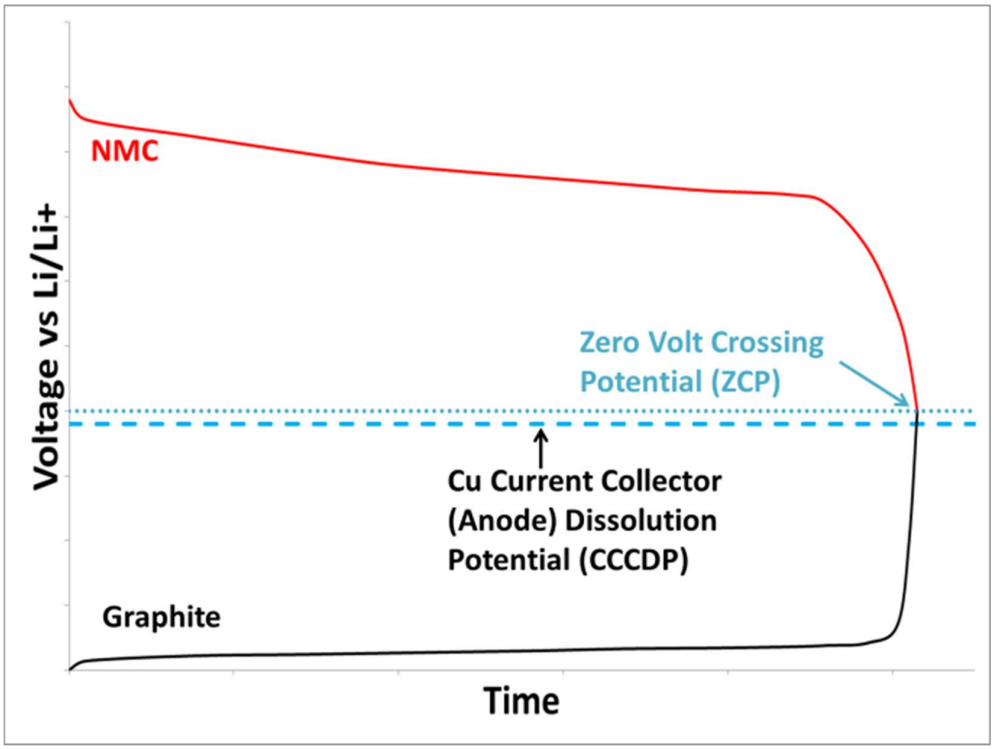

Figure 17: Standard carbon-based half-cell voltage curves with a zero-volt crossing point greater than the dissolution potential of copper

In addition to the improved safety for shipping and warehousing provided by a zero-volt cell, a potentially a more important aspect of the zero-volt cell may be for commercial pack manufacturers. During the construction of high voltage systems such as vehicle packs, bus packs or electrical grid systems these battery systems typically have a high voltage, ranging from a few hundred volts to upwards of 1100 V on grid systems. Due to the number of cells that are present in a system, the working voltage of the system quickly increases during manufacturing as cells are added in series until the voltage quickly reaches hazardous dc voltages, which includes any voltage greater than 50 V. This increases the danger to personnel building the system and requires increased safety standards, an increase in required operator training, and the need for certification of workers to handle the hazardous voltage systems. In this situation, cells which have been reduced to a zero-volt potential allows for a system to be manufactured at, or near a working voltage of zero volts. This change in operating procedure has the chance to improve the safety of the operator working on the system, creating an opportunity for less restrictive manufacturing environments, increased

worker comfort and potentially increasing assembly throughput. Novel research such as the work presented here on zero-volt storage has the potential to have significant impacts on various industries, including but not limited to shipping and manufacturing.

3.2 Alternates to Standard Lithium Ion Battery Configurations

3.2.1 Current Collector Material

One method to avoid the dissolution of the copper current collector at low voltages, and allow a cell to reach a zero volt potential without damage, is to replace the copper with another material such as titanium which has been used in over-discharge studies [64,65], or aluminium which is often used as a cathode current collector material. As shown in Figure 18, by replacing the copper current collector with another material, the dissolution potential of the current collector material can be adjusted to a potential voltage that is greater than the threshold where the full cell reaches a potential of zero volts. By moving the current collector dissolution potential to one that is greater than where the electrode voltages crossover, the risk of the current collector dissolving when the full cell voltage is low can be eliminated.

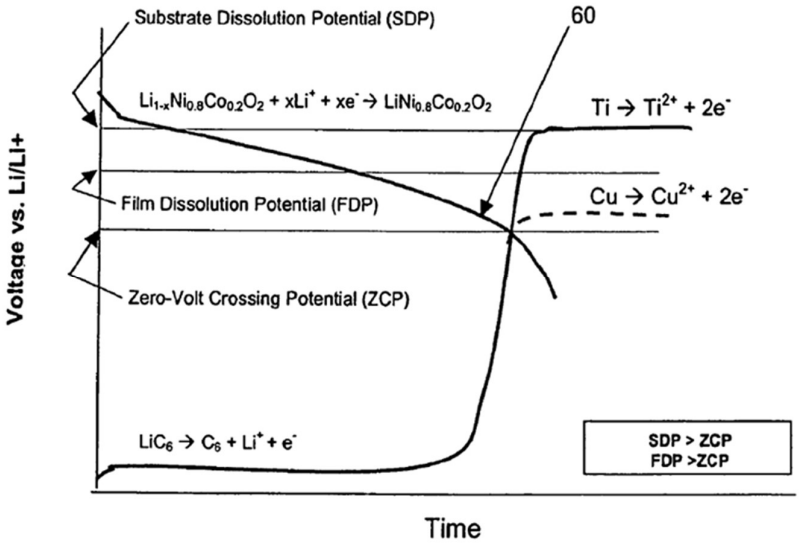

Figure 18: Half-cell voltage curves of a lithium ion cell with titanium current collector. The zero volt cross over point is shown well below the potential of the Titanium current collector, allowing the cell to safely reach 0 Volts [63]

One limitation to replacing the copper current collector in a standard lithium ion cell with alternative materials, such as aluminium, is the alloying potential for the aluminium to alloy with Li+ at the standard operating voltage of a graphite/carbon anode which has a low potential voltage versus lithium [66]. When the potential of the carbon/aluminium electrode is near that of lithium, the opportunity for the alloying process is a risk, thus an aluminium current collector is generally not an option when paired with the standard anode materials. This points to that while replacing the current collector for a graphite/carbon based cell with aluminium would solve the issue of the dissolution of copper at a zero volt full cell state, it creates new difficulties by creating a situation where alloying could occur during standard operation due to the anode's operating voltage versus lithium.

Alternatively, replacing the copper current collector with titanium while addresses both the dissolution and alloying risks, it is generally not a financially feasible solution for mass produced cell. One of the main driving goal of mass production cell manufacturers is to reduce the cost of a cell. With the cost of titanium being much higher than copper it is not a cost-effective solution, as such 0 V operation of full cells remains unfeasible with standard graphite-based cells.

3.2.2 Lithium Titanate Cells

An alternative solution to replacing the current collector material to is to replace the anode material which would allow for a change to current collector material without alloying potential. One such solution is the lithium titanate cell, which replaces the standard anode material with of lithium titanate (LTO) which allows the manufacture to also replace the standard current collector with aluminium (Figure 19). This creates a cell in which both current collectors are aluminium and, as the potential of the anode material is much greater than graphite's this cell configuration, does not have the possible reactions seen in a standard graphite-based cell.

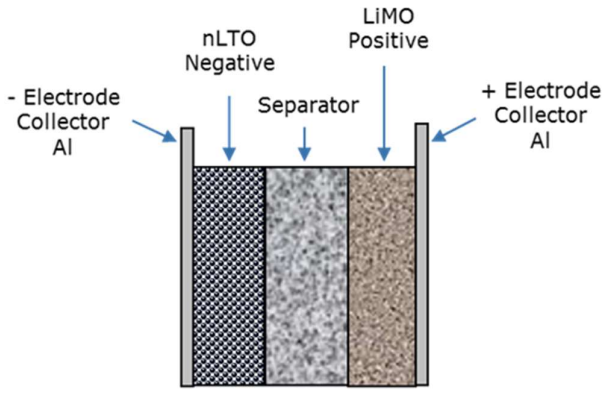

Figure 19: Lithium titanate cell construction diagram, highlighting the aluminium current collector material on both sides of the cell.

A cell manufactured in this method should theoretically allow for the potential of the full cell to be reduced to zero volts without damage internally to the cell. The concept can be seen in Figure 20, which shows half-cell voltages with the zero-volt potential crossing point and the aluminium current collector voltage potential for dissolution. As laid out by the chart, the potential versus lithium for the zero-volt crossing point is less than the dissolution potential of aluminium, this indicates that a full cell zero-volt potential should theoretically be feasible, and more importantly be feasible without damage to the cell's performance or behaviour. The voltage curves for the anode and cathode shown below in Figure 20 are representative of the voltage response under a constant current load.

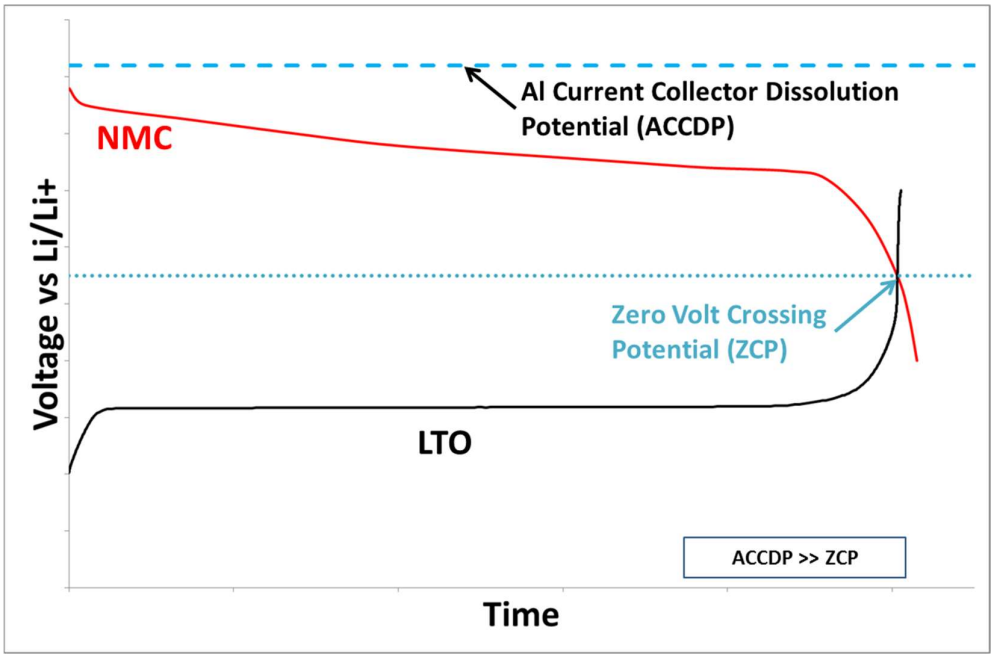

Figure 20: Theoretical half-cell voltage curves for a lithium titanate cell, showing the current collector dissolution potential greater thhan the zero volt cross over point.

The work in the following sections explores the feasibility of zero volts and further studies the effects that storing an LTO cell at zero volts may have on the performance and life of the cells.

3.3 Electrochemical Characterisation of 0 V cells

3.3.1 Half-cell Research

3.3.1.1 Half-cell Manufacture

To support understanding of the behaviour of the nano lithium titanate (nLTO) electrodes under storage conditions, i.e. at the voltages that the anode would experience during full cell zero-volt storage, four LTO half-cell coins were manufactured [10]. Upon the initial voltage check one of the four coin cells was determined to have an internal short and was discarded, with the remaining three cells to be used for testing. The LTO electrodes were harvested from a commercially available 13 Ah nano lithium titanate cell manufactured by the US manufacturer Altairnano. As seen in Table 1 below, based on the active material weight of and theoretical capacity of LTO, a capacity was estimated for each cell.

Table 1: Working coin cell data

coin cell id	initial voltage (V)	total electrode wt (mg)	avg measured al disc wt (mg)	coating wt (mg)	target proportion (nLTO)	active mat wt (mg)	LTO theoretical capacity (mAh/mg)	Coin cell theoretical capacity (mAh)
507	2.98	30.5597	9.3344	21.2253	0.9	19.10277	0.175	3.34298475
508	2.83	30.7452	9.3344	21.4108	0.9	19.26972	0.175	3.372201
509	2.45	30.7082	9.3344	21.3738	0.9	19.23642	0.175	3.3663735

As the cells were manufactured from existing commercially available 13 Ah cells, a standard electrolyte formulation (RD281) was used in place of Altairnano's electrolyte, as Altairnano's electrolyte is a proprietary formulation and was unable to be supplied. While the electrolyte differs from the one used by Altairnano, as the standard formula is missing the additives used by Altairnano to increase cycle life stability, the goal of the test was not cycle life examination but voltage behaviour of the electrode. This change was deemed an acceptable risk by the researcher in consultation with Altairnano. During initial cycling the average cell capacity was 2.6, 2.46, and 2.54 mAh respectively. Additionally, many portions of Altairnano's cells are protected by IP and/or trade secrets which precluded the exact duplication and manufacture of fresh cells in the lab for research purposes.

Due to the nature of coin cells there are several limitations and risks. Firstly, the coin cells created for the research contain a different composition than what is seen in the commercial cell. For the half cell research this includes the use of lithium disc as the counter electrode and a differing electrolyte as noted previously. Secondly, these changes create a limitation to the work as it was possible to introduce unknown side reactions between the electrode and electrolyte or between the electrode and the lithium disc. These changes also miss out on possible interactions between the commercially used cathode, electrolyte and the LTO anode.

As noted in the first paragraph of this section (3.3.1.1 Half-cell Manufacture) the goal is to isolate the LTO electrode's behaviour, not to explore the behaviour of the NMC, as such no additional work was done with the NMC electrodes but the harvested LTO anodes were tested versus a lithium counter electrode.

An addition risk with the manufacture of coin cells is the possible introduction of impurities and contaminants during manufacturing. To mitigate the introduction of moisture and other contaminants, the electrode samples were harvested and manufactured in a controlled argon environment. As half-cell work is commonly used within research and coin cells are often used for preliminary testing, the risks and unknowns were determined, acknowledged and mitigated where possible. As such, while indicative, half-cell work is not definitive and was used as a preliminary exploration of the feasibility of the concept, prior to testing of the full cell using the commercially available 13 Ah cells directly from the manufacturer. Full cell testing, and the results, are discussed in section 3.3.2 Full Cell Research, subsequent to the determination to move forward based on the results of the half-cell testing.

3.3.1.2 Half-cell Cycling Parameters

Following fabrication, the three half-cells were cycled 20 times within a voltage window of 1.0 V to 2.0 V at a 0.65 mA rate, an approximate current to capacity ratio (C-rate) of C/5 [16]. A climate-controlled chamber was set to 25 °C to maintain cell temperature. It is assumed the erratic behaviour seen during initial cycling is due to side processes happening within the coin cells between the electrolyte and the LTO, as well as any reactions due to possible contaminants and impurities such as moisture introduced during electrode harvesting and coin cell fabrication. The voltage behaviour is observed to become stable within 2 to 5 cycles, dependent upon the cell. The initial 20 cycles for cell 507, including the initial voltage response due to side reactions, can be seen in Figure 21 for illustration purposes. Full discussion of results will be handled in following section (3.3.1.3 Half-cell Electrochemical Characterization Results and Discussion).

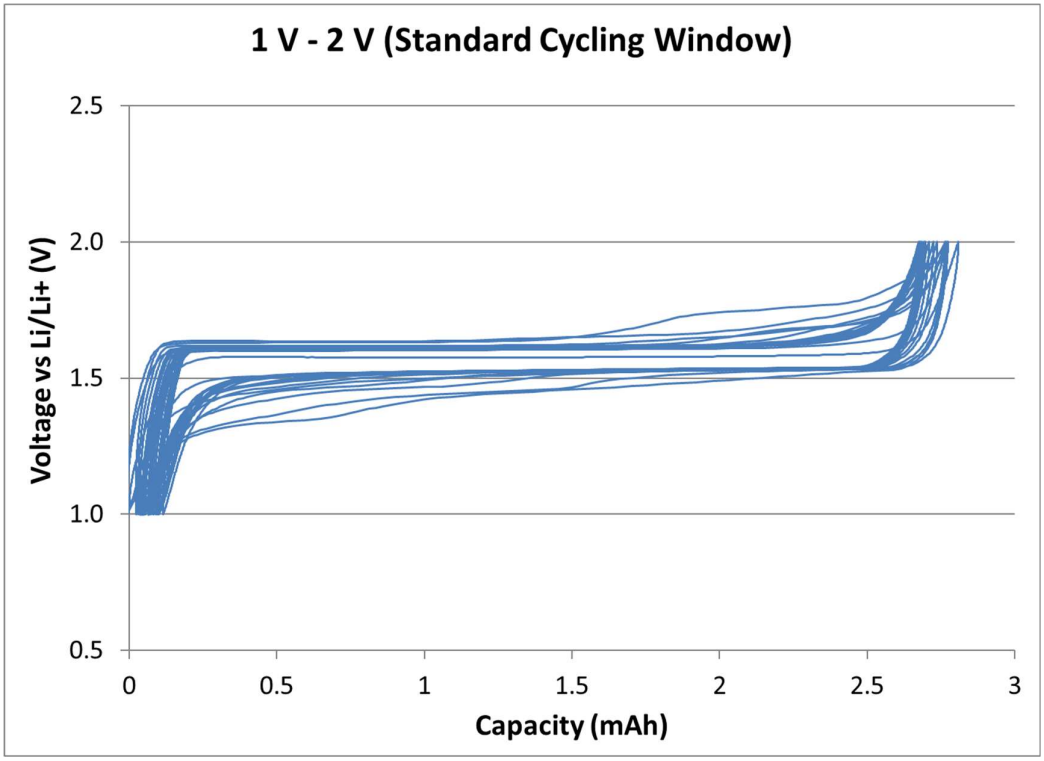

Figure 21: Cell 507 initial cycles

Following completion of the initial 20 cycles, a single cell (cell id 507) was then cycled in an extended voltage window from 1.0 V to 3.5 V for an additional 20 cycles, as seen in Figure 22, at the same 0.65 mA rate.

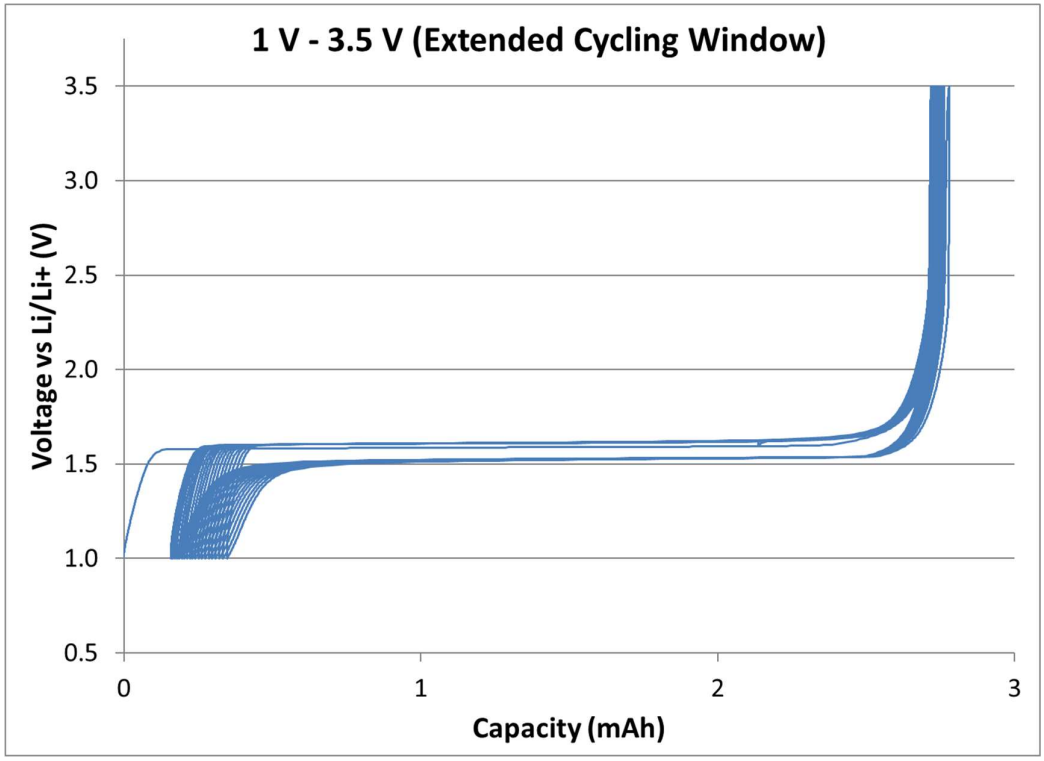

Figure 22: Cell 507 cycles within extended voltage range

As this work was preliminary and performed prior to full cell or 3 electrode testing, the extended voltage of the cycled coin cell was chosen based on the theoretical LTO half-cell voltage curve shown previously in Figure 20. This voltage range was chosen to mimic the possible voltage range that an LTO electrode would experience in a full cell configuration during discharging to zero volts. As will be seen in three electrode testing, section 3.3.4, future testing would need to extend voltage range in which the half-cell is cycle to greater than 3.6 V.

3.3.1.3 Half-cell Electrochemical Characterization Results and Discussion

In Figure 25 (a, b, & c) below, the voltage behaviour for each half-cell cycled between 1.0 V to 2.0 V can be seen. These figures exclude initial formation cycles (seen previously) for clarity purposes.

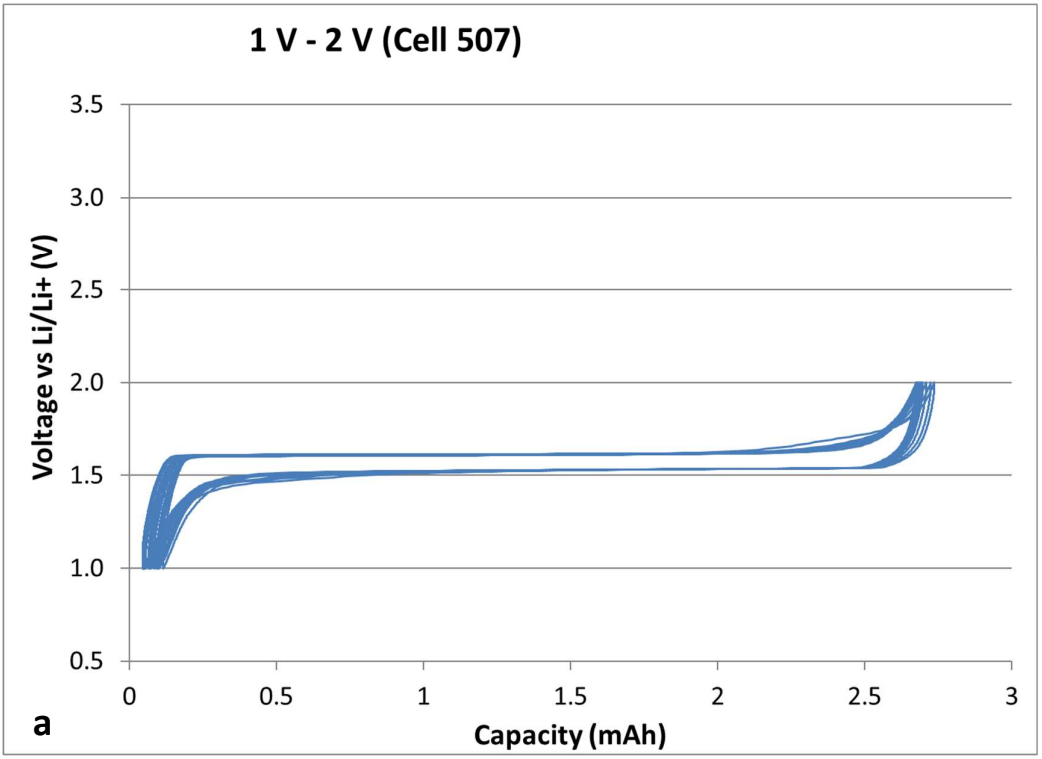

Figure 23a: 1 V to 2 V cycling of LTO half-cell id 507

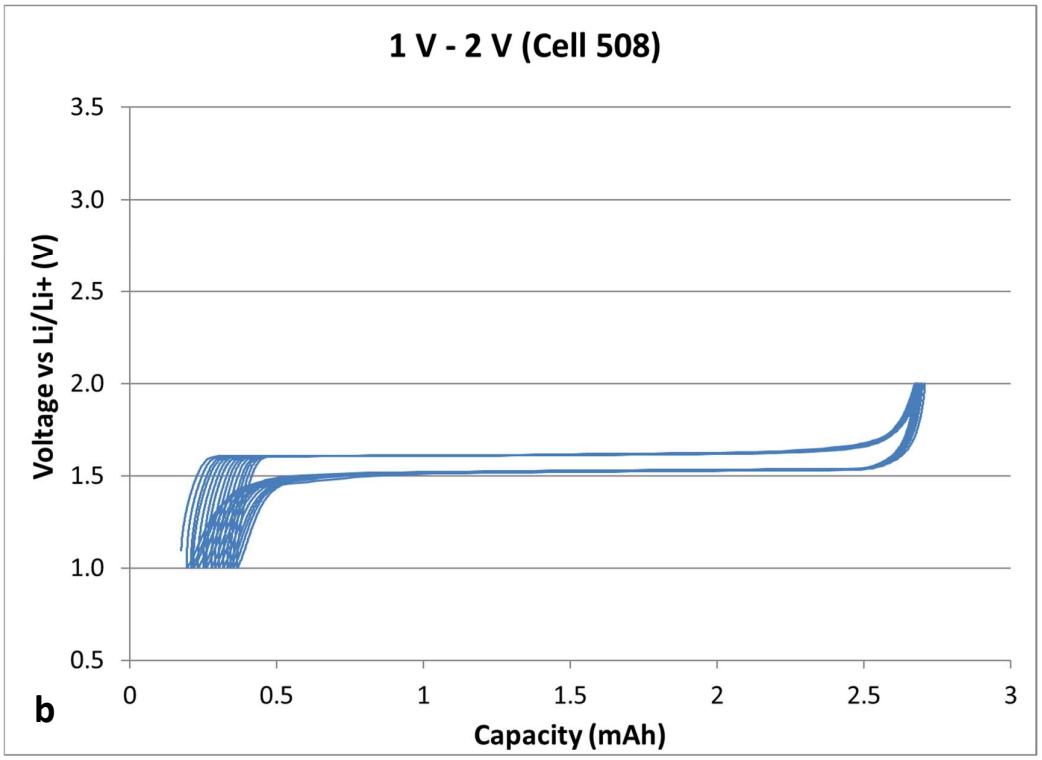

Figure 24b: 1 V to 2 V cycling of LTO half-cell id 508 and

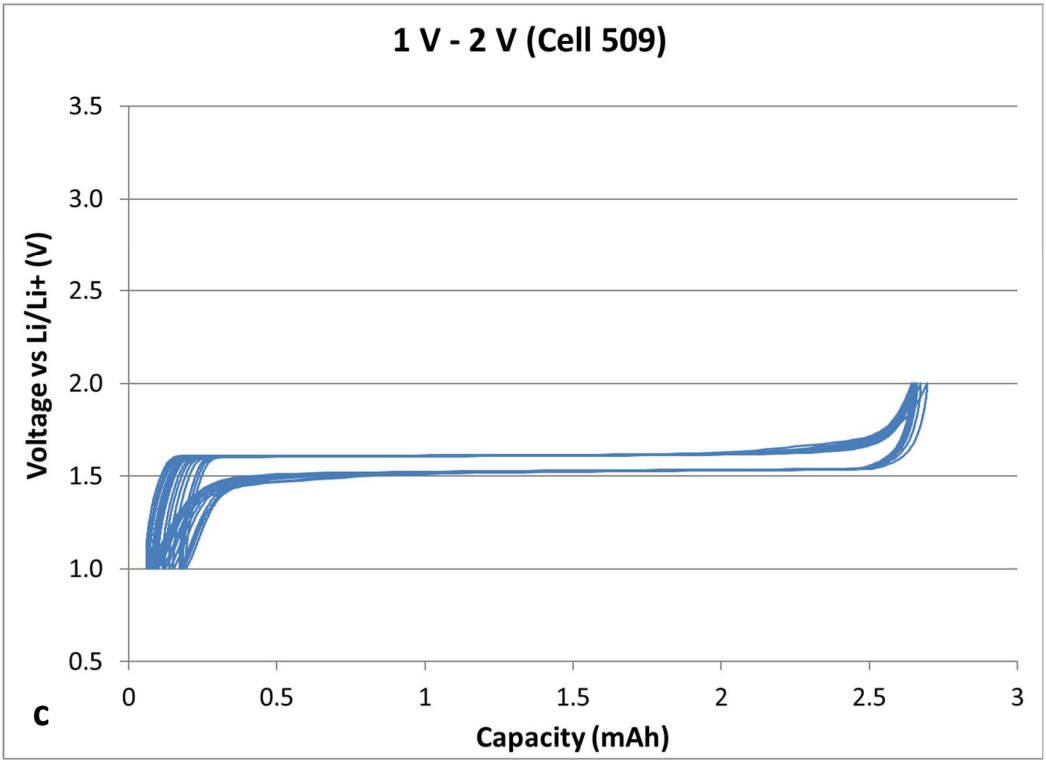

Figure 25c: 1 V to 2 V cycling of LTO half-cell id 509

These plots show a voltage plateau near 1.55 V that is characteristic of LTO electrodes [67]. With a stable plateau and no significant deviations, the cells are stable and operating within normal behaviour [31].

Following the completion of the initial 20 cycles from 1.0 to 2.0 V, cell 507 was then cycled for an additional 20 cycles between the voltages of 1 to 3.5 V the results of which are shown below in Figure 26. As noted previously the 1.0 V to 3.5 V range was chosen to demonstrate LTO electrode behaviour that may be seen within a full cell when discharged to 0 V.

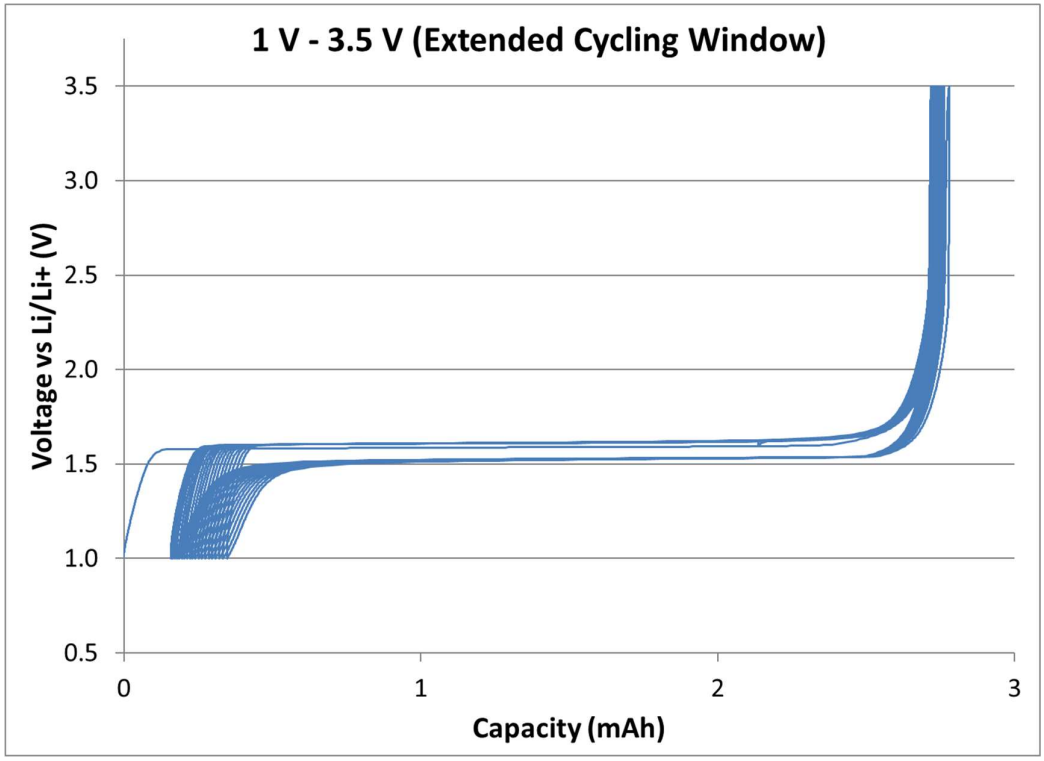

Figure 26: 1 V to 3.5 V cycling of LTO half-cell id 507 (extended voltage window to mirror possible full cell conditions of LTO electrode for 0 V storage)

In this test, as seen previously, a stable voltage plateau around 1.55 V was observed. Because the cells are half cells, cycling versus lithium and operating with a different electrolyte, the rate of capacity loss was not a focus of the testing. In the interest of cell performance disclosure, the capacity loss curve for cell 507 during both cycling regimes is presented below (Figure 27). Linearly fitting within the limited data sets for each degradation curve provides a loss of capacity rate of approximately 0.0116 mAh per cycle for 1.0 V to 2.0 V cycling, and a rate of 0.0123 mAh per cycle for 1.0 V to 3.5 V. The causes and the rate of capacity loss for these coin cells was outside the scope and goals of this research and will not be discussed further. The impact of 0 V storage on cell capacity loss for full cells is studied during the full cell testing (section 3.3.2 Full Cell Research), as all relevant factors which the half-cell tests could not account for are controlled for by using the commercial cell.

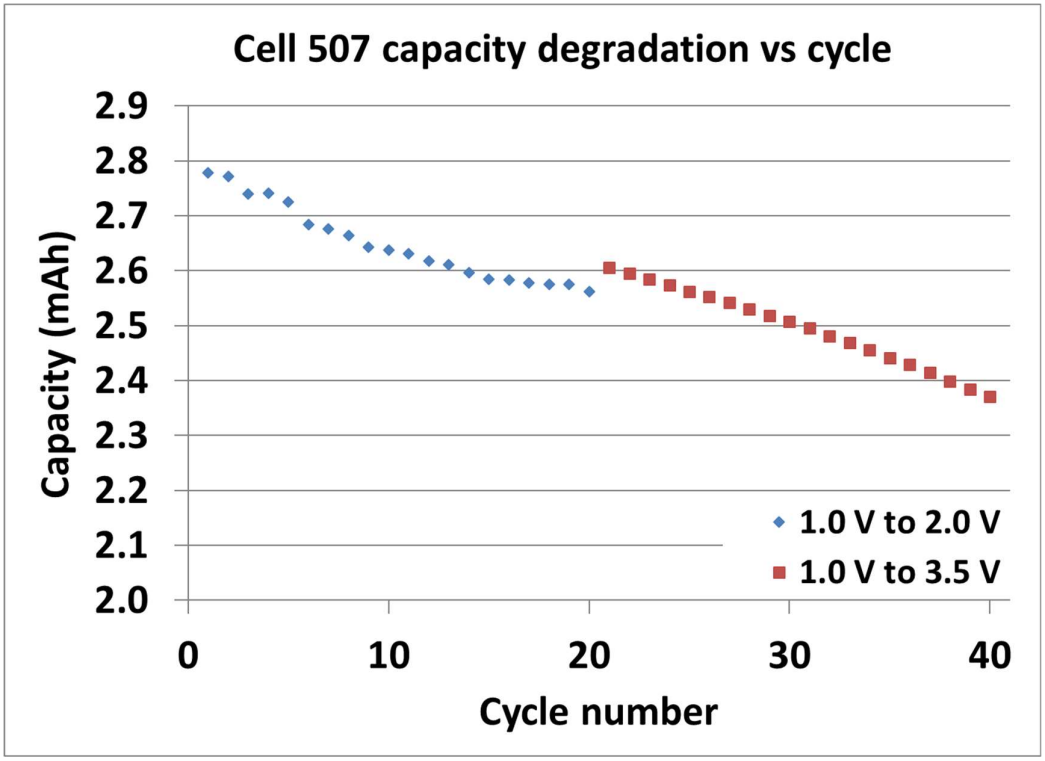

Figure 27: Cell 507 capacity loss during cycling for each test regime

Comparing the voltage data between the two cycling windows we can see that there is no significant shift or changes to the voltage plateau or voltage curve, as any shift to the plateau or change in shape of the overall voltage curve would indicate unwanted behaviour differing from standard operation. The stability of the voltage behaviour, outside of capacity loss, provided the evidence that there was no significant impact to the LTO electrode's health when cycled to 3.5 V under this limited testing. If there was deviation in the voltage behaviour during the extended voltage window cycling of the LTO electrode within a half cell, then that behaviour change would be reflected as an abnormal voltage response of a full cell. This data was important to build confidence in how the LTO electrode voltage may behave when the full cell is discharged to 0 V. In the case where a full cell is discharged to 0 V and returned standard operating voltage range, to establish the case that 0 V storage is successful the cell should continue to operate normally with no changes in the voltage response or behaviour of the full cell.

While this testing explored the behaviour of the electrode when cycled, further study would be needed to explore the behaviour of the electrode when held at a higher than standard voltage for a longer period of time (mimicking storage or shipping versus cycling).

3.3.1.4 Half-cell Storage Conditions

After completing the cycling regimes, the three coin cells were then placed into three different voltage states for a short term 5-day storage study to explore the behaviour of the electrode when held at high voltages for an extended period of time versus lithium. The voltages were chosen to mimic possible voltage states that the LTO electrode may experience during storage or shipping, when in a full cell voltage state of 0 V.

The first cell was charged to 3.0 V at a 0.14 mA rate, and allowed to naturally relax to open circuit voltage (Figure 28). This voltage behaviour was chosen to see the response of a full cell that was over discharged and allowed to relax to a natural voltage without external influence (current or resistance), as cells are often stored and shipped in an open circuit state [60].

The second cell was charged to 3.0 V at 0.10 mA constant current rate then maintained at 3.0 V for 5 days through a constant voltage (CV) regime (Figure 29). The third cell, which was previously cycled in the 1.0 V to 3.5 V window (Figure 26), was charged to 3.5 V at a 0.10 mA constant current rate then maintained at 3.5 V for 5 days through a constant voltage (CV) regime (Figure 30). These two steady state voltages were chosen as it was unknown what voltage an LTO electrode would be at during 0 V storage in a full cell. The two steady state voltages would allow for a comparison, if there was determined to be a difference (performance or structurally), between the two storage conditions.

Following storage, the coin cells were disassembled to be imaged by Scanning Electron Microscopy (SEM) characterisation. The SEM images were taken in a Carl Zeiss Gemini FEG-SEM at 5.0 kV with a 30 µm aperture.

There was no performance testing following the storage periods. Imaging was used immediately following storage to determine if there was structural damage to the electrodes. It was believed that cycling post storage may obscure any films, structural changes or other possible effects due to the storage conditions, by allowing chemical reactions to occur while cycling. Future work would include additional cells stored under identical conditions which undergo performance testing conducted prior to any imaging. These additional tests would help to provide additional support and to verify conclusions drawn on the impact of storage on the state of health of the electrodes.

3.3.1.5 Half-cell Storage Results and Discussion

Figure 28, Figure 29, and Figure 30 shown below show the three voltage states the cells experienced during storage and their corresponding SEM images, after disassembly. Qualitatively the images show no significant difference in electrode structure and no noticeable presence of film growth. The lack of structure changes when compared to a pristine sample provides support to the thought that there were no unwanted reactions forming new structural abnormalities or unwanted films on LTO after storage at the various voltage levels.

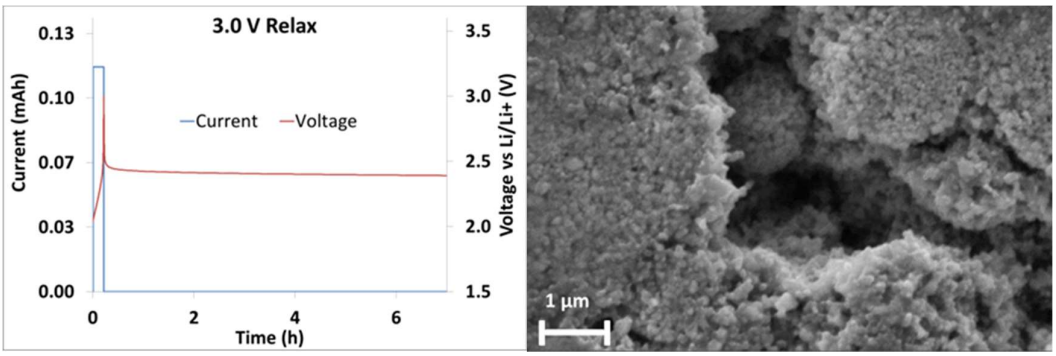

Figure 28: LTO half-cell charged to 3.0 V and allowed to relax to OCV and corresponding SEM image of LTO electrode.

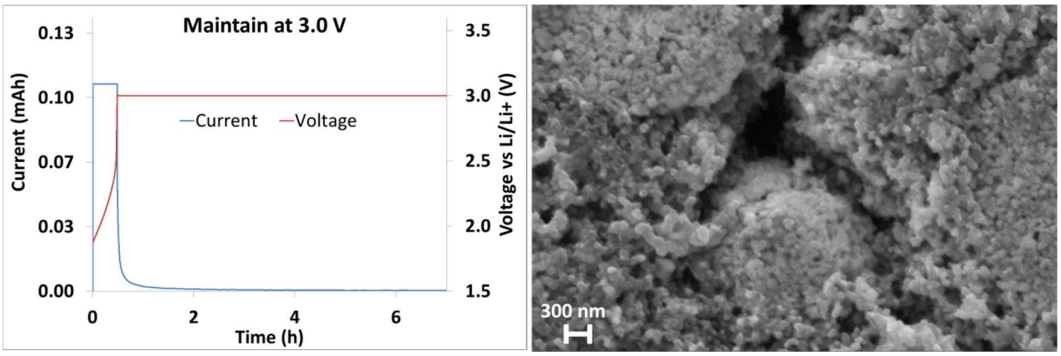

Figure 29: LTO half-cell charged to 3.0 V and maintained at 3.0 V for five days and corresponding SEM image of LTO electrode.

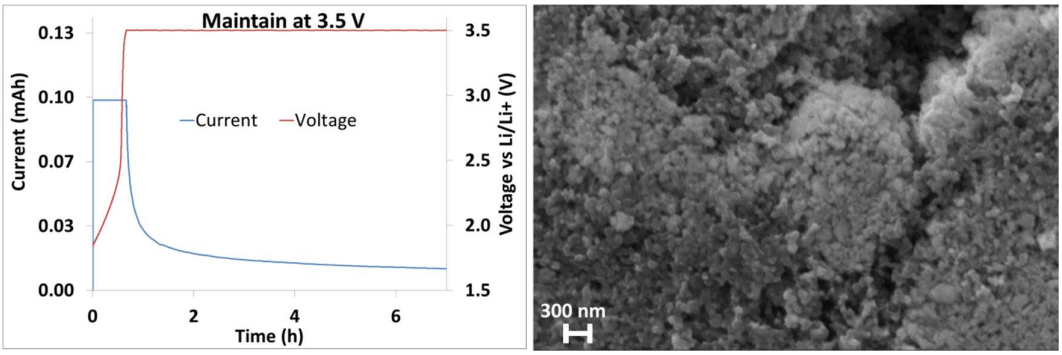

Figure 30: LTO half-cell charged to 3.5 V and maintained at 3.5 V for five days and corresponding SEM image of LTO electrode.

This data was used to build confidence in the performance of an LTO electrode in a full cell, indicating that storing a full cell at zero volts should cause no structural changes or film growth thus the cell's performance should not be impacted after storage. Again, as noted previously, future testing include performance testing would help to support this assumption.

Furthermore as seen in Figure 31, a and b, the SEM imaging provides a comparison of a pristine sample from the original electrode compared to the electrode which experienced the highest cycling voltage and was stored at the voltage of 3.5 V. Again, no visible films or other structural changes are identified, indicating no damage is experienced when comparing the electrode from pristine to an electrode after a high half-cell voltage storage state vs. Li/Li^+.

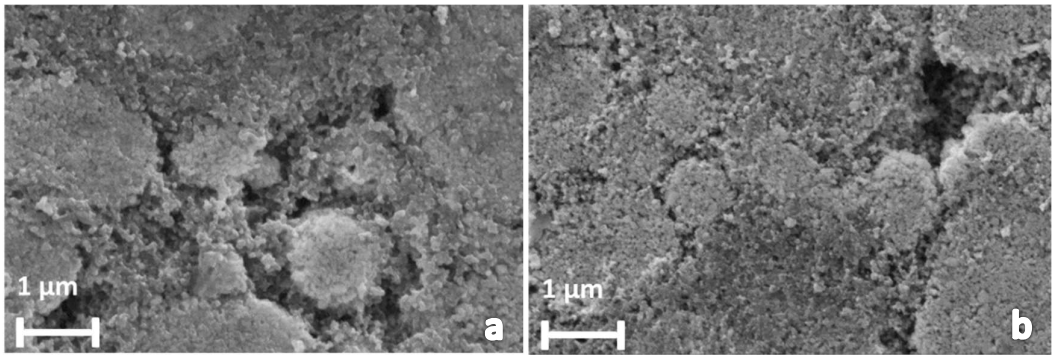

Figure 31: LTO electrode SEM imaging comparing (a) pristine versus (b) electrode maintained at 3.5 V

For this study SEM was used to visually compare samples. In future studies a more in-depth use of the technique would be recommended to include a higher number of sites imaged, broader use of the various tools and techniques available with SEM imaging including particle size estimate etc. to enhance and improve upon the results shown here. One limitation with inherent with SEM imaging is imaging enough sites such that the sample size is representative of the full electrode. Small variations in other locations could mask issues that were not identified in the images presented here.

3.3.2 Full Cell Research

Based on the results of the half-cell data, sufficient knowledge and confidence was built regarding the possible behaviour of a full cell discharged to a state of zero volts, which allowed full cell testing to proceed. Six 13 Ah nLTO cells from Altairnano were randomly selected for testing from a lot of 30 cells. The cells were removed from long term warehousing where they had been stored in a 10 °C climate-controlled container at a 10% state of charge. Each cell was thermally soaked for 8 hours at 25 °C in a thermal chamber prior to characterization.

3.3.2.1 Storage Conditions for the Study

The six cells selected were randomly sorted into three groups of two cells each. Two cells were retained as control cells (group A), to be kept in storage at near 0% SoC or approximately an open circuit voltage (OCV) of 2 V. This value is a manufacturer provided value based on their previous generation chemistries. The voltage was chosen by the company as prior generation chemistries

when rested, tended towards 2 V, so the value was chosen as their defined 0% SoC. It is part of this work's goal to challenge those previously held assumptions and expand the company's knowledge on the behaviour of their chemistry at low, full cell voltages.

A further two cells were selected to be discharged to 0 V then allowed to relax naturally to open circuit voltage (OCV) (group B). As noted previously most cells are stored in an OCV state while in storage or during transportation [60]. As such the second test group was designed to examine the behaviour of the cells if discharged to a low voltage and then allowed to relax to an OCV state, similar to the cells in standard storage group A.

The final two cells were selected to be discharged to 0 V and subsequently maintained at 0 V during the storage period through a physical short between the terminals (group C). This would keep the potential of the cell at 0 V throughout the storage period and create a path for the dissipation of any energy resulting from side reactions that may occur. Though as noted in previous sections (2.3.1 Aging of LTO, 3.3.1.1 Half-cell Manufacture), based on review of both the cathode through literature review and of the LTO anode through experimentation, it was assumed that there should be no reactions present and all systems would be stable.

The cells groups were stored were all stored together in the same thermal chamber for identical periods of time in a 25 °C climate controlled thermal chamber. During storage each cell's voltage was monitored and data collected.

At the end of each storage period all cells were then conditioned prior to characterization. Cell groups B and C were charged at 0.25 A to 1.0 V. Then all cell groups were charged at a rate of 0.5 A to 2.0 V (in the case of cell group A this was to account for any self discharge losses), followed by a 1.0 A charge to 2.8 V. All cell groups were then cycled five times at a rate of 3 A, between the voltage limits of 1.5 V and 2.8 V. This was followed by five additional cycles at 5 A, within the same voltage limits. Because behaviour of the full cell was unknown and current limitation of the cycling

equipment, the cells were cycled at two steps of relatively low current rate compared to standard capability of the cells [68]. The currents where chosen within the limits of the equipment and two differing currents were chosen to provide an easily comparable early indication of cell performance or deterioration. The cells would be fully exercised at higher currents during the characterization testing.

3.3.2.2 Full Cell Electrochemical Characterization

The characterization procedure was used prior to testing, and following each period of storage, to allow for a standard comparison of the behaviour exhibited by the various cell groups. The procedure included a capacity check, at a discharge and charge rate of 26 A, twice the capacity of the cells; followed by a low-rate 0.12 A discharge and charge cycle to observe near or pseudo OCV behaviour [69]. Voltage limits for all cycles was 2.8 V on charge and 1.5 V on discharge.

Following the low rate cycling the state of charge (SoC) was adjusted to 90 % SoC, 50% SoC and 20% SoC sequentially. At each SoC a pulse power test was conducted comprising of a 10 second discharge pulse, 30-minute rest, 10 second charge pulse followed by a 30 minute rest. Pulse current tests were conducted at increasing rates of 20 A, 40 A, 60 A, 80 A, and 100 Amps. Additionally, after completing the set of current pulses, a galvanostatic electrochemical impedance spectroscopy (EIS) [70–72] sweep to determine the AC impedance of the cells. This test was performed using a potentiostat (Solartron Modulab, Model 2100A, with a 2 A booster card). The impedance measurements were conducted in the frequency range of 10 mHz to 10 kHz with the current amplitude set to 800 mA. After the pulse power testing and EIS sweeps were completed at each SoC, the cells were cycled with a final 26 A charge/discharge cycle.

3.3.2.3 Full Cell Result and Discussion

Full cell testing was completed to compare the behaviour of the control cells (group A) with the behaviour of the cells stored under the 0 V relax regime (group B) and the cells maintained at 0 V (group C). This comparison method was chosen to establish if cells stored under these various

conditions caused changes to the performance and behaviour of the cells. As such, the analysis focuses on comparing the behaviour between the three groups for significant deviations. For example:

- If the control group's parameter increased, did the other group's parameter increase or did the different groups exhibit differing behaviour?
- Did a capacity change trend exist in all groups?

The broader focus of the research was the behaviour of the cells in context of all three cell groups, not an individual cell's changes insolation. If all groups cell capacity degraded, then that was considered similar behaviour. As such the general trends and behaviour of the various test groups were the focus of the research in an effort to determine the impact 0 V storage would have on the cells when used Altairnano's customers after such storage conditions.

In Figure 32 shown below, the logged voltage behaviour is presented for each of the three groups during a one month storage period. Altairnano's 13 Ah nLTO cells demonstrate a very low self-discharge rate of less than 1% per month as seen by the control cell's voltages flat profile.

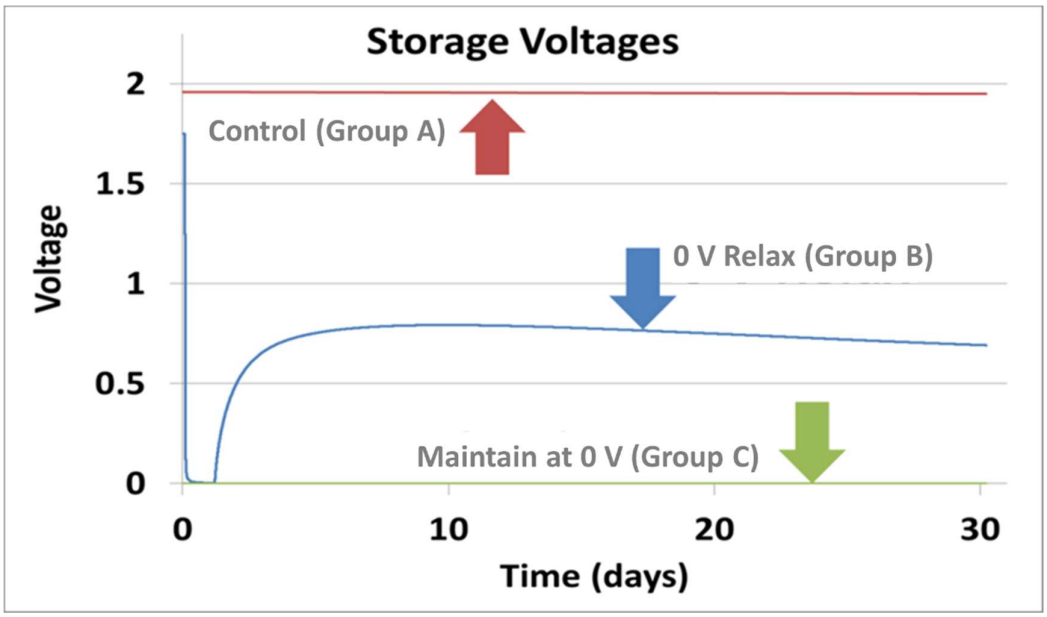

Figure 32: The three voltage regimes under which the cells were stored

The behaviour of the 0 V relax cell voltages after 5-10 days (Figure 32) is currently being explored and will be subject to future work, as such, the discussion on the rate of the voltage decay is beyond the scope of this paper.

The final set of cells which were maintained at 0 V, through a resistor short across the terminals, maintained a flat 0 V profile for the entire duration of the month.

3.3.2.4 Voltage Curve Behaviour

Figure 33 compares the 0.12 A discharge voltage profile, normalized to the capacity of each to determine if there is any significant change in the behaviour or shape of the various cell, which would indicate damage to either electrode or cell as a whole.

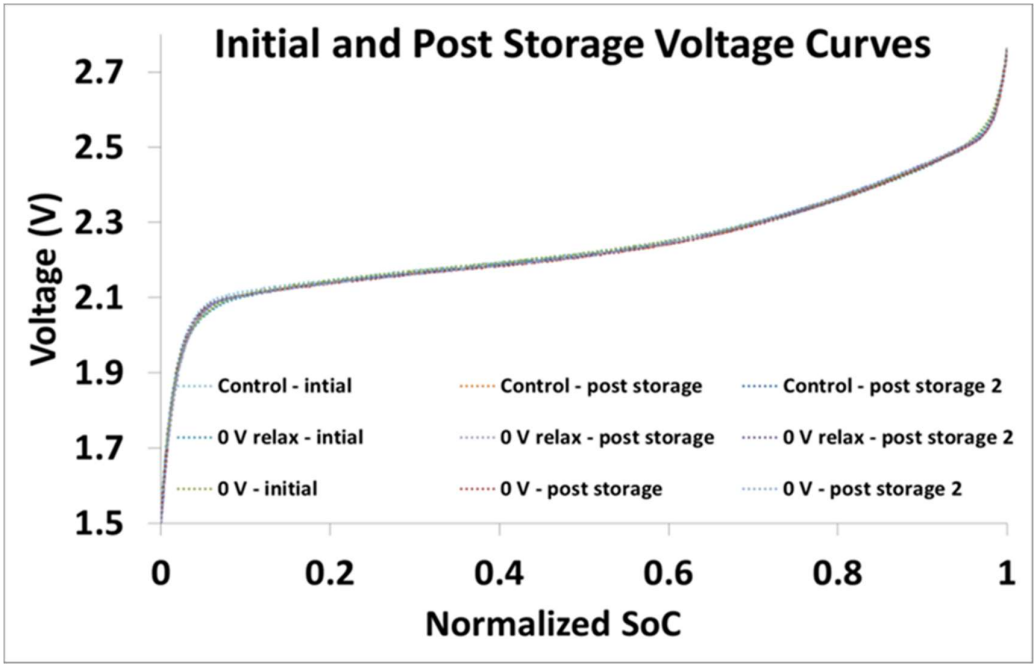

Figure 33: Pre and post storage voltage curves normalized to cell capacity

The voltage profile for all cell groups initially, and more significantly, post each storage period are overlaid in Figure 33. This chart is used to demonstrate a stable and consistent voltage profile before and after storage. The absolute maximum difference between any two cells pre- or post-storage, control or abused, was approximately 14 mV observed at approximately 96 % SoC, (a region where nLTO cells see an increased rate of change in its resistance versus very small changes in state of charge as seen in the data provided by Altairnano in Figure 34), a similar deviation is seen around 5% SoC range.

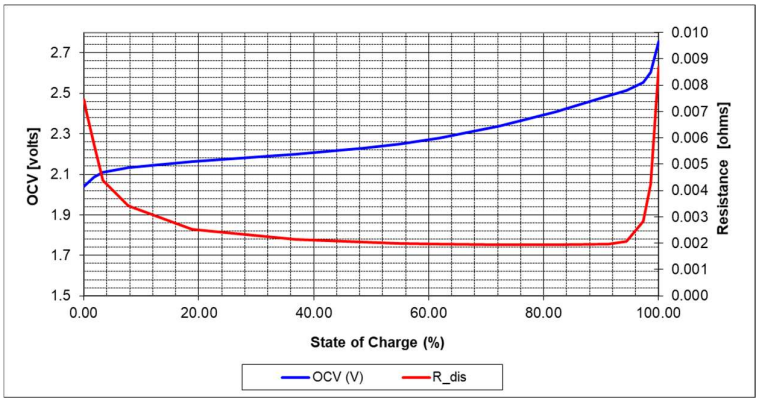

Figure 34: Altairnano open circuit voltage and resistance curve for the 13 Ah cell from 2.0 V to 2.755 V

Additionally, at 50% SoC the maximum difference between the highest and lowest voltage cells is 10 mV for initial characterization between a control cell (group A) and a '0 V relax' (group B) cell. This same voltage difference is seen between the same '0 V relax' (group B) cell and but the second control cell (group A), post storage. The difference between the same identical cells from the intimal characterization reduced to 7 mV. All other voltage differences for all other cells at 50% were less than 10 mV, indicating that there has been no significant damage to cells and their resulting voltage profiles. Furthermore, this data provides support to the theory that there is no damage to the cell for either storing at 0 V or discharging a cell to 0 V, of which both cases are normally considered an over discharge abuse event.

3.3.3 Incremental Capacity Analysis

To better understand and identify any possible damage an additional analysis on voltage behaviour, incremental capacity analysis (ICA) [10,23,72,73], was carried out for all cells based on the data obtained during the 0.12 A discharge cycle in the characterization cycle. This analysis was chosen to understand if any storage condition provided a discernible difference in voltage behaviour as any changes in the active material of the positive or negative electrodes, or lithium content would be immediately identifiable based on shifting of the curves [34,74]. Figure 35 shows all 6 cells pre- and post- storage with their respective ICA curves overlaid to compare the general shapes of the curves, and to demonstrate that the voltage curves have not significantly deviated. Based on the analysis the ICA curves' behaviour the ICA curves of the control cell are not identifiable from the ICA curve of the two other cell groups.

Through ICA any significant damage to the electrodes during the storage period would be readily identifiable based on a shifting or a change in the magnitude of various portions of the curves [74]. As seen in Figure 35 the overall general shape of the control cell's curve does not differ significantly from the cells, which underwent discharge to 0 V or maintained at 0 V. As noted by Dubarry et. al. if there was significant damage to the electrodes a shifting of the curves would occur, a change in the

overall shape of the curve, or an increase or decrease in the magnitudes if peaks seen in the ICA curves for the over discharged cells (0 V relax and maintain at 0 V) would significantly differ and be easily identifiable. An example of a shifting that can be identified is the behaviour differences clearly seen at 2.05 V and 2.5 V.

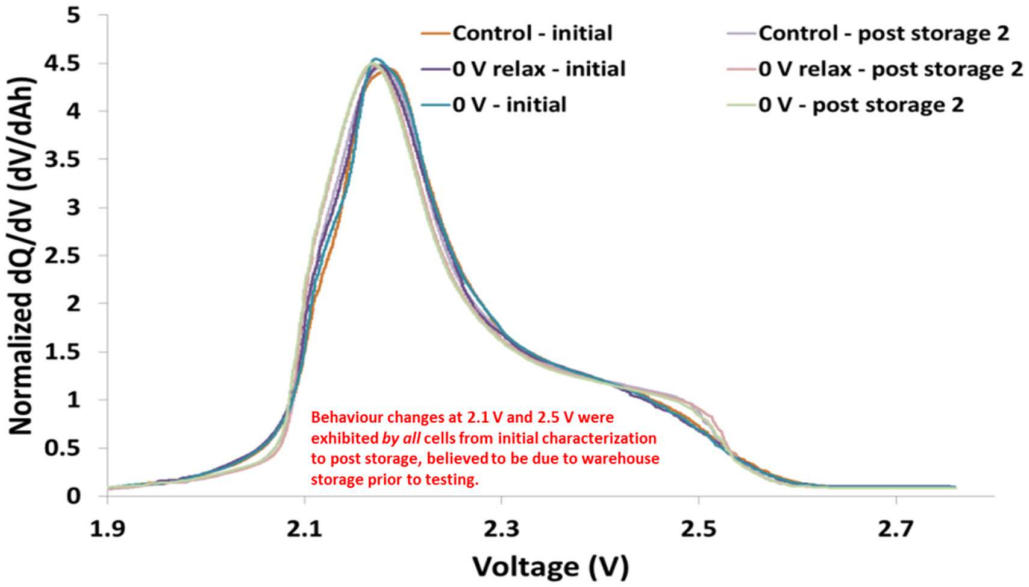

Figure 35: Full cell ICA curves

Though, it is of note that the appearance of the small peak behaviour at 2.5 V is seen in the control cells as well as over discharged cells. This behaviour, because it is seen in all cells, indicates that this change is not a symptom of discharging the cell to 0 V but rather a behaviour exhibited by all of the test samples regardless of storage condition. The same can be said of the droop in the curves at approximately 2.05 V, with all cells exhibiting the same behaviour. The exact reasoning for the change in the curve is unknown at this time, because it was exhibited by all cells it was not explored during this research. One cause of this behaviour may be result of the long-term cold storage of the cells (10 °C for longer than one year) prior to this research. Future work would be needed to explore this behaviour, but also to design an initial cycling regime for all cells to prevent such changes in behaviour from impacting future studies.

3.3.3.1 *Electrochemical Impedance Spectroscopy*

Electrochemical impedance spectroscopy (EIS) was used to identify any changes to the ohmic resistance and other processes within the cell including diffusion and kinetics [10,72,75]. Analysis of the EIS measurement focused on the series ohmic resistances (R_s) and charge transfer resistances (R_{ct}) at three states of charges for each of the three storage conditions [49,72,75,76]. As seen in Figure 36, these values can be derived from the values reported by an EIS scan.

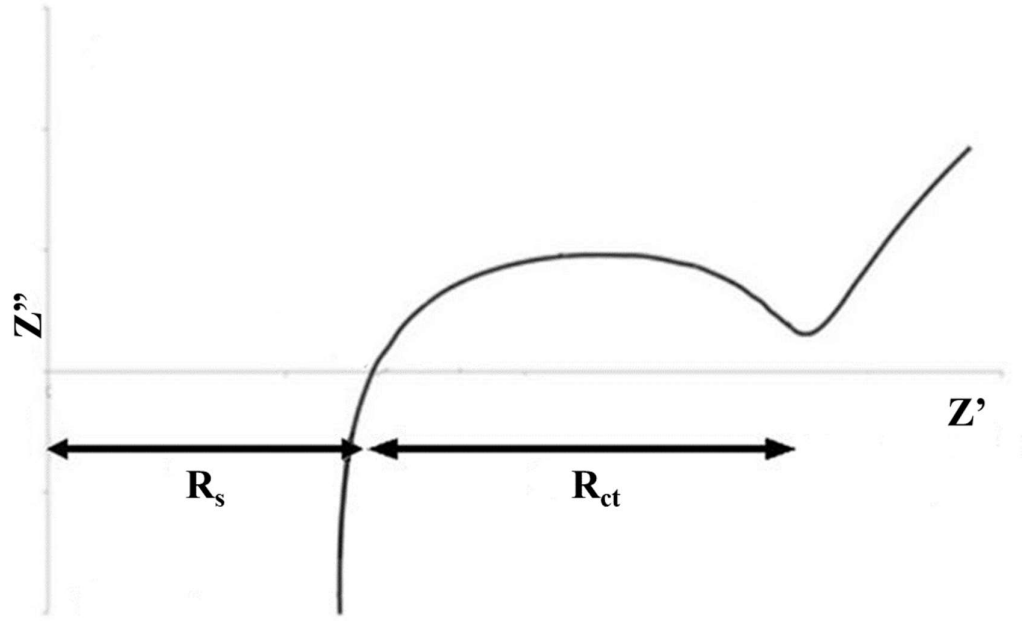

Figure 36: EIS plot overlaid with where series resistance R_s and charge transfer resistance R_{ct} are determined from

Figure 37 through Figure 42 shows, for each state of charge, all pre- and post- storage cells' EIS results as well as their resulting R_s and R_{ct} values. For the respective SoCs, data shown for April is pre-storage while data shown for September and November are post storage for each chart discussing R_s and R_{ct}.

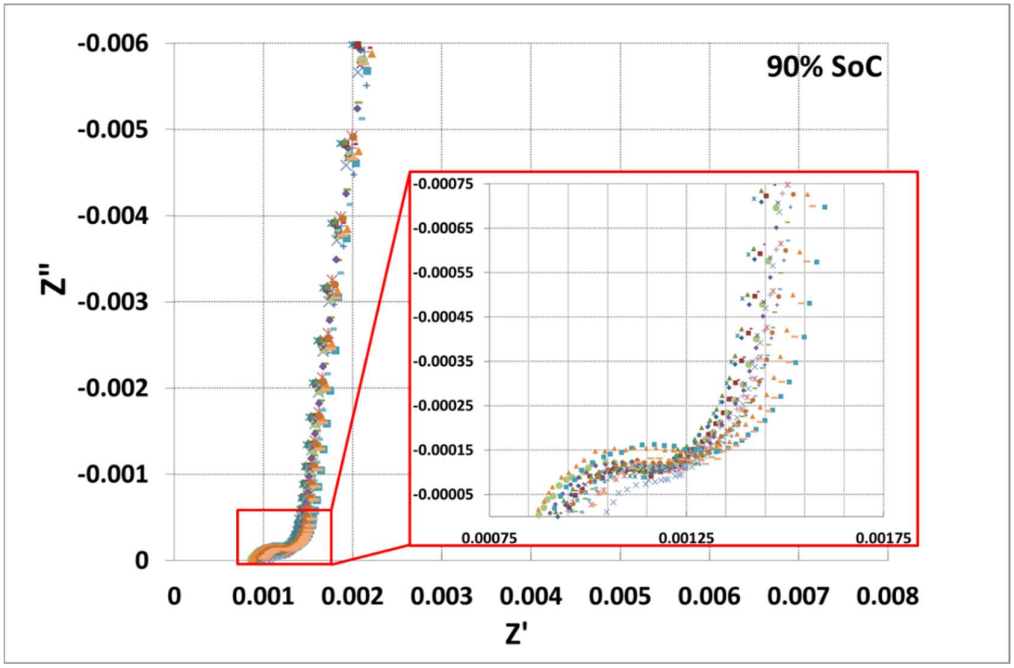

Figure 37: EIS data of all cells pre and post storage for 90% SoC

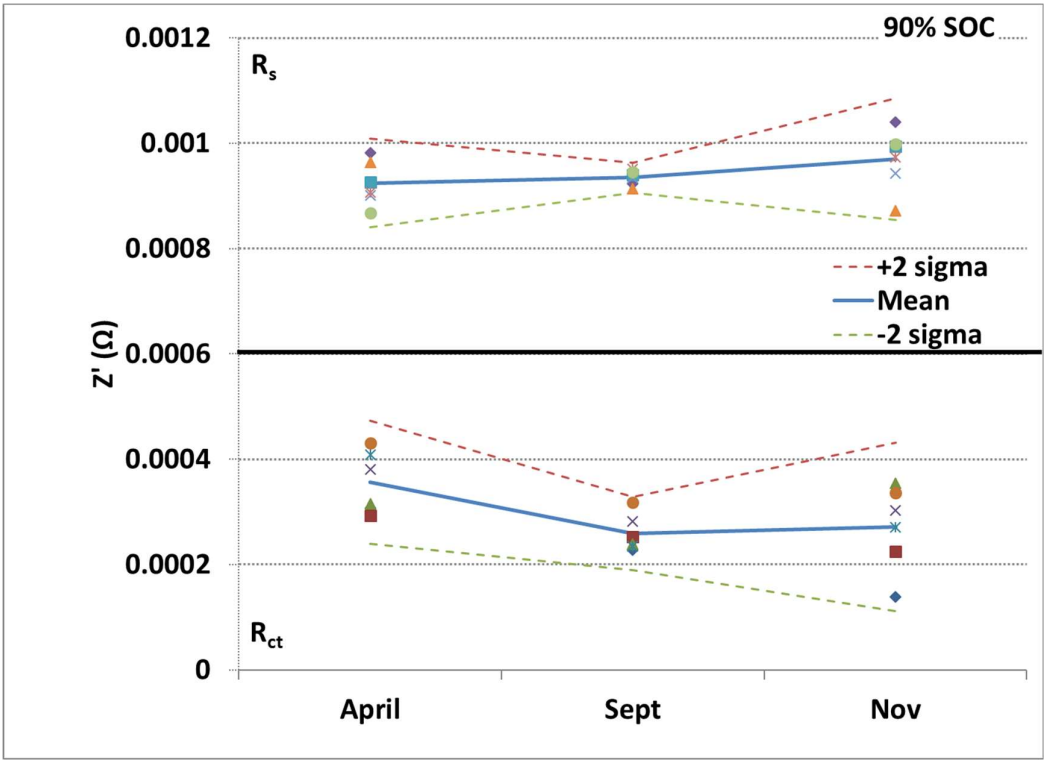

Figure 38: Two sigma analysis of 90% SoC data for R_s and R_{ct} (April – pre storage, Sept/Nov post storage)

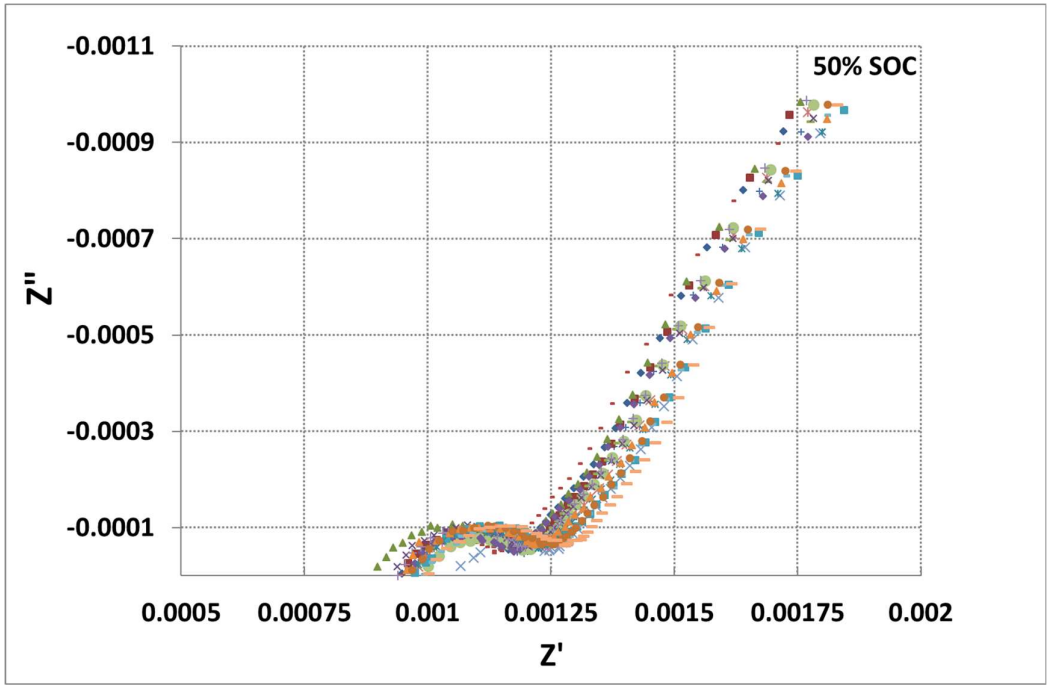

Figure 39: EIS data of all cells pre and post storage for 50% SoC

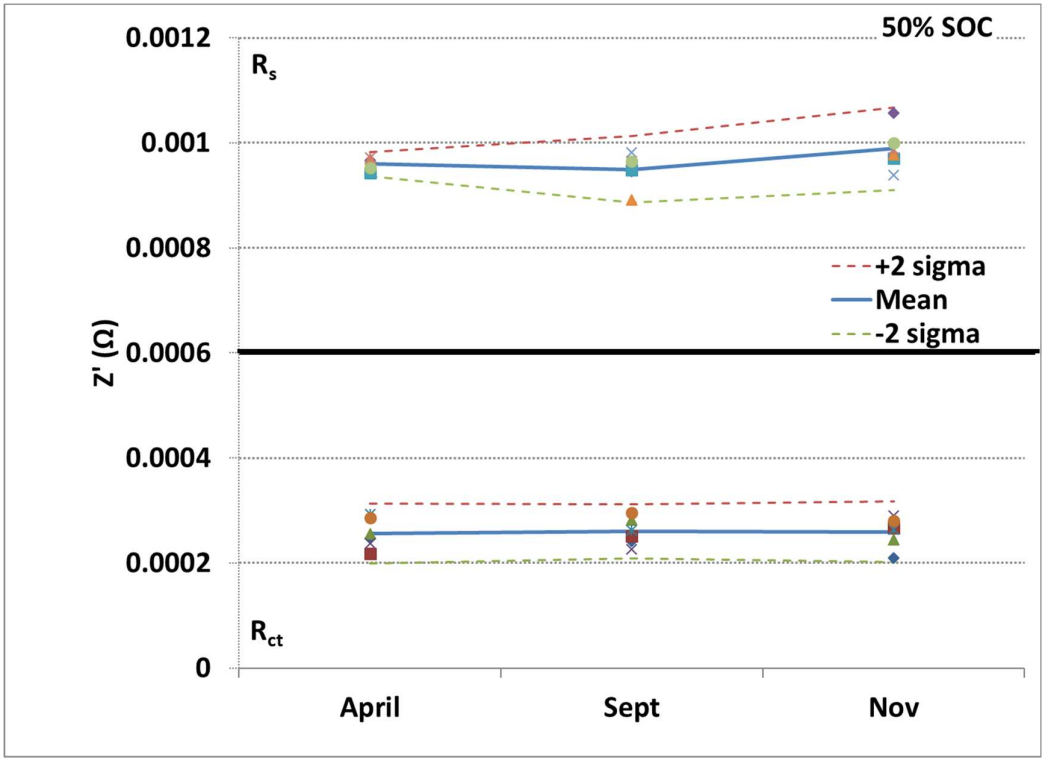

Figure 40: Two sigma analysis of 50% SoC data for R_s and R_{ct} (April – pre storage, Sept/Nov post storage)

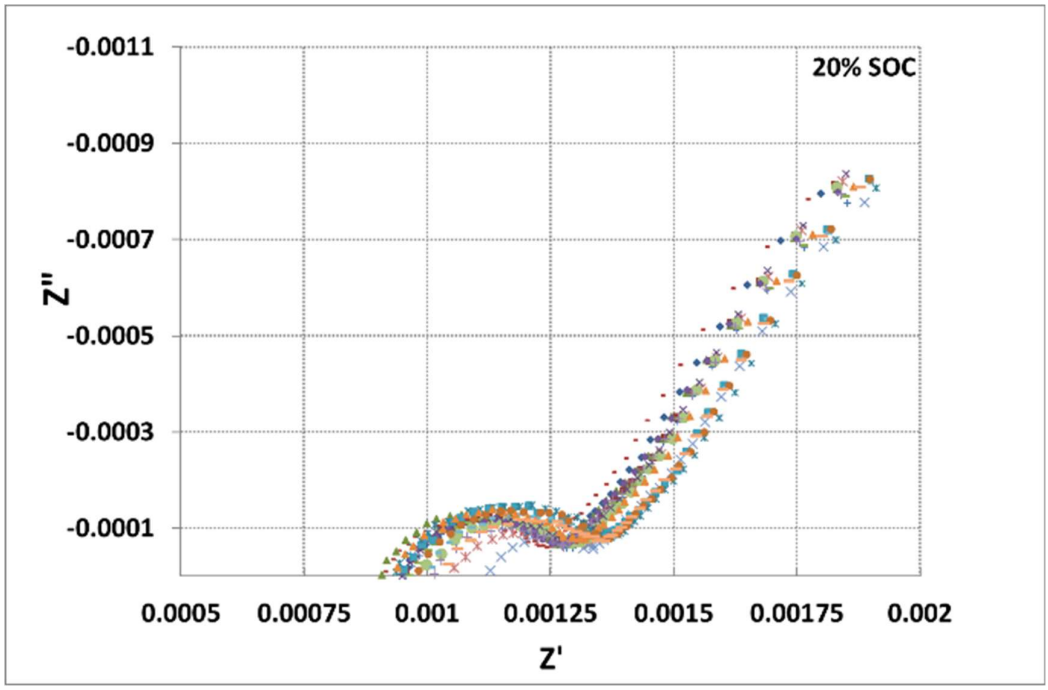

Figure 41: EIS data of all cells pre and post storage for 20% SoC

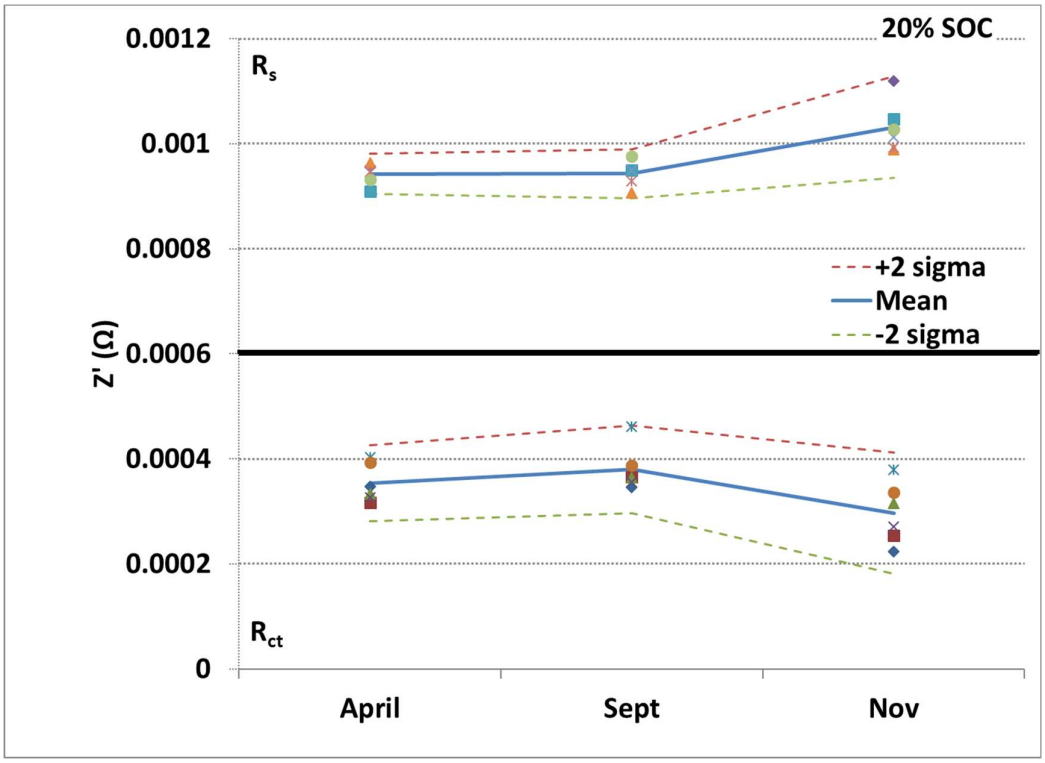

Figure 42: Two sigma analysis of 20% SoC data for R_s and R_{ct} (April – pre storage, Sept/Nov post storage)

Figure 38, Figure 40, and Figure 42 show that the measured series resistances of all three cell groups fell within a two-sigma deviation from the mean. This grouping supports the notion that based on

the three storage conditions there is no discernible difference or impact on the ohmic resistances of the cells. Furthermore, charge transfer resistances similarly fell within a two-sigma deviation from the mean. This provides additional evidence that there is no impact on performance or chemistry of the cell with regards to kinetics when a cell is discharged to 0 V or maintained 0 V for storage when compared to the control cell results.

3.3.3.2 Comparisons of Cell Capacities Pre and Post Storage

During the characterization cycles the capacity for the cells is measured during a 26 A charge (Figure 44) and discharge cycle (Figure 45). Interestingly the capacity of all cells for each storage regime increases after each month of storage. The fact that the control cells exhibit the same behaviour indicates that this phenomenon cannot be solely attributed to any of the three storage regimes. This behaviour is similar to behaviour seen in new LTO cells (total cycle count less than 100) for this manufacturer. It has been seen in their testing that the cell's capacity rises during initial cycles before degrading. This behaviour is seen in the initial cycles of Figure 11, where capacity rises before reducing and shown below Figure 43 from Altairnano's cycle life data for the 13 Ah cell.

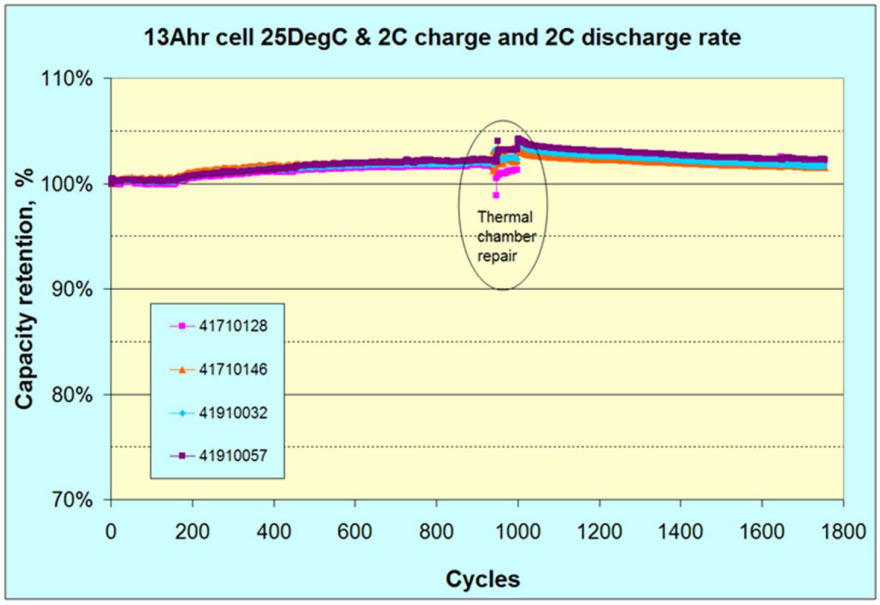

Figure 43: Altairnano 13 Ah cycle life chart showing initial increase in capacity for low count cycles [77]

It is assumed, as the cells in this test have not been cycled extensively, the degradation trend has not begun for these cells. Future work could include extended cycling to ensure the cells long term cycling behaviour mimics that of cells stored per Altairnano's standard operating procedure. The overall capacity difference is less than 2% when compared to the total capacity of the cells.

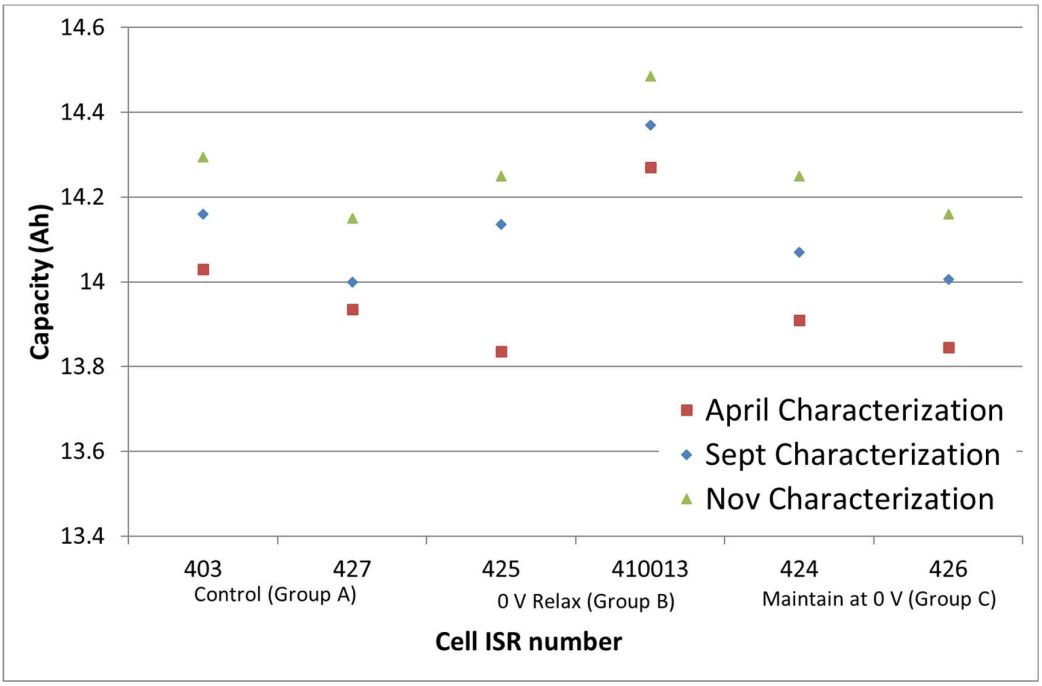

Figure 44: Full cell 26 A charge capacity

For the discharge cycle at 26 A the two cells that did not follow the overall trend of increasing capacity from the April characterization were both control cells, though it should be noted that the overall capacity difference between the various tests is less than 1% of the cell's total capacity.

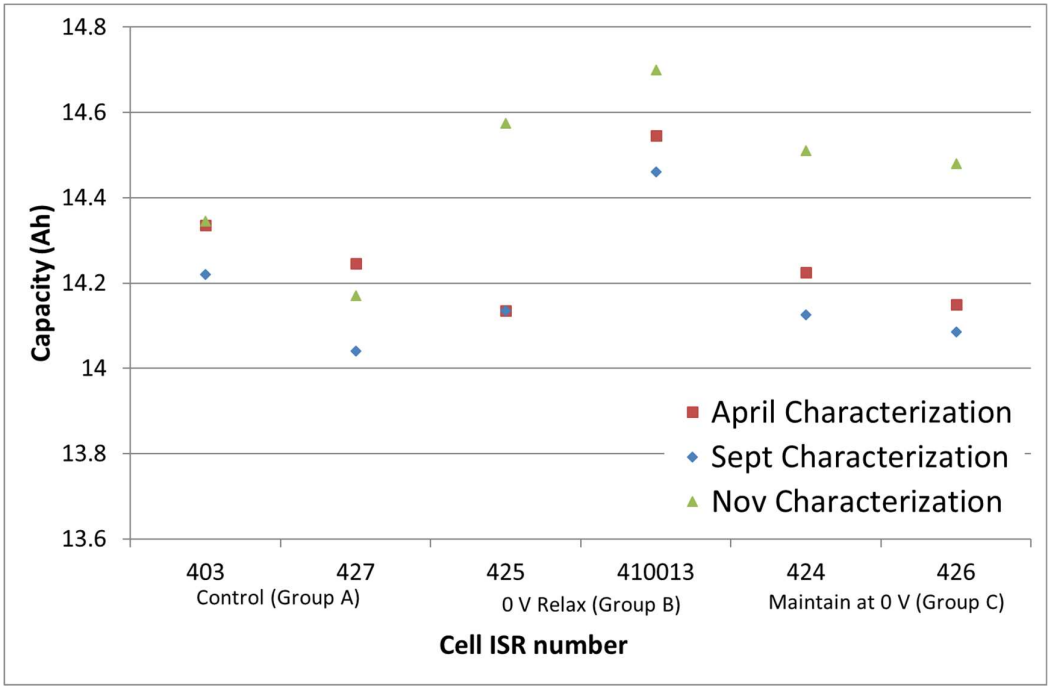

Figure 45: Full cell 26 A discharge capacity

Both the charge capacity and discharge capacity data indicate that the various storage regimes do not cause damage the overall capacity of the cells at a relatively high rate of charge and discharge, in this case a 26 A rate for each cell. Additional storage periods and characterizations would be useful for expanding and identifying any further trends in the data. High precision coulometry, as detailed by Dr Dahn and his team, would be one possible technique for identifying any efficiency impact and the potential effects on longer term cycling. [78]

3.3.3.3 Cycling performance after storage

While 3 A and 5 A cycling is considered a relatively low rate for 13 Ah LTO cells, which are known for their power capabilities and ability to handle high C-rates (up to 20 C or 260 A per manufacturer's specifications), it demonstrates their cycling ability immediately following storage. For each rate, 5 cycles were performed and as seen in Figure 46 below the cycling at both rates (3 A and 5 A) are stable and uniform.

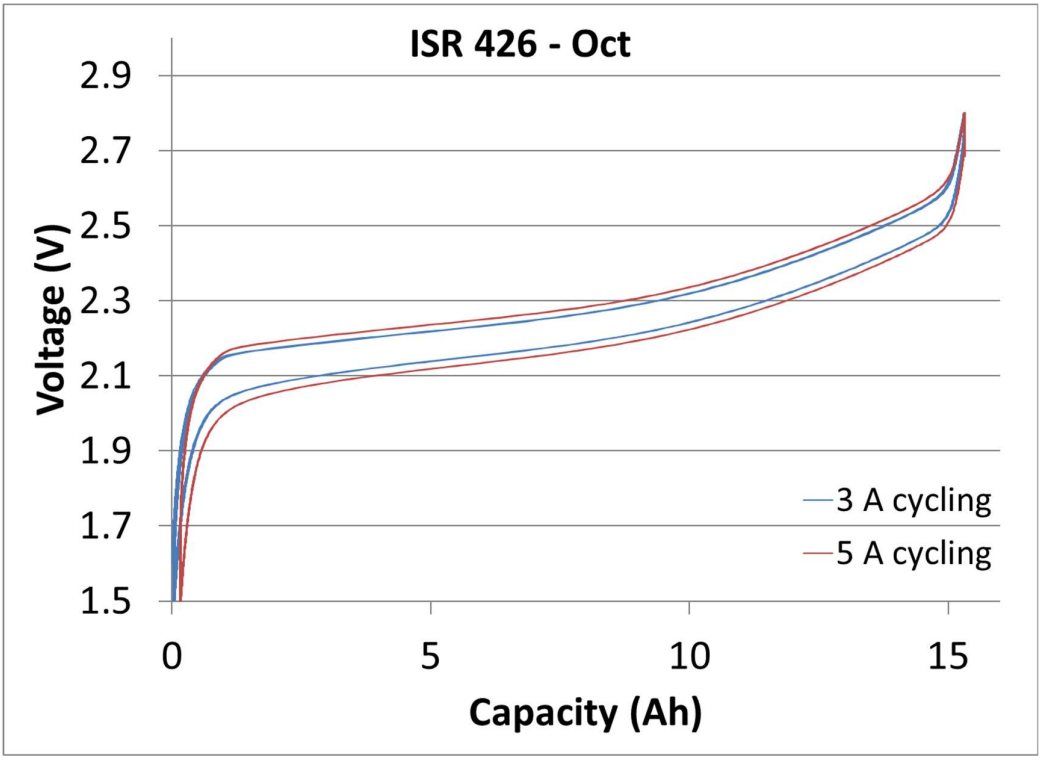

Figure 46: 5 cycles each of 3 A (blue) and 5 A (red) cycling after storage for a cell maintained at 0 V for storage

This data demonstrates the stable cycling ability of the cells immediately after each storage period for each storage regime, which would be important for any system manufacturer who would not want to deal with long or drawn out conditioning cycles to achieve optimal performance of the cells.

Additionally, due to prior experience with the cells' performance following long term storage at 10 °C, it was found that cycling the cells reversed any short-term degradation seen in data caused by the cold storage period. It was found that the performance of the cell returned to levels that matched the performance of the cells prior to storage. It was unknown if this behaviour was exhibited at other storage temperatures, thus while the cells were stored at 25 °C for this testing, the cycling was included to mitigate any potential performance aberrations during the characterization cycle which would impact the results. The cause of the performance degradation following long term cold storage was outside the scope of this research and was not explored. It was considered worthwhile to still include low current cycling after storage, to mitigate any unknown performance degradation despite the cells being stored at higher temperatures.

3.3.4 Three electrode Cell Research

3.3.4.1 Three Electrode Modification

Separate from the six cells discussed above, an additional 13 Ah cell was chosen to be modified into a three-electrode cell. The method for modification of the cell followed the procedure and techniques laid out by Dr Euan McTurk and the University of Oxford team [79].

To modify the cell, it was first discharged to 1.5 V and allowed to rest overnight. Then within an argon glove box a small incision was made in the pouch cell at the midpoint on the small side of the cell adjacent to the negative terminal. This incision would allow for the insertion of a reference electrode.

The reference electrode was created by electro plating lithium on to a copper wire and inserted into the small incision. Once inserted the incision was sealed by epoxy. The epoxy was allowed to set prior to testing. Future work could consider alternate pure metal reference electrodes, such as platinum or lithium, to eliminate possible issues due to the plating technique, but for this research the method presented by Dr McTurk was followed as he was personally assisting with the testing.

While the epoxy was setting the cell voltage was monitored for 24 hours to ensure cell stability. Following the 24 hour rest period the cell was discharged to 0V at 0.4 A, then maintained at a full cell voltage of 0 V while monitoring the full cell's and each electrode's voltage versus the reference which can be seen in Figure 47 and discussed in section 3.3.4.2 Three Electrode Results.

After 24 hours at 0 V, the cell was then charged using constant current constant voltage strategy at 0.4 A to 2.8 V and maintained at 2.8 V for 5 days. This cell voltage float at 2.8 V was not intended to be sustained for 5 days. Following the testing and analysis of the data this extended duration was discovered and was due to an error in programming the cycler. Additional testing time was not available to repeat the test with the intended constant voltage step to a determined current value. Following the charge cycle the cell was discharged in three phases of 0.4 A to 1.0 V, 0.2 A to 0.5 V

and finally 0.1 A to 0 V, where the cell was maintained at 0 V to mimic a storage state. These currents were chosen due to the current limits of the cycler as well as chosen to limit any possible issues from high rate currents. Despite having completed a number of full cell discharges to 0 V for the storage testing, discharging a cell to 0 V was still treated as an unknown and potentially unsafe condition for the testing lab. Additionally, the three different rates were chosen to mimic the step-down manner of a constant voltage discharge, but in a more defined and known square wave step down pattern. Following the three CC steps, the final step was a constant voltage (0 V) step where the cycler was allowed to manage the reduction in current rates.

3.3.4.2 Three Electrode Results

In the first experiment with the three-electrode cell, the cell was discharged from 1.6 V to 0 V at a 0.4 A rate. From the data (Figure 47) we see the LTO anode voltage rising to meet the cathode voltage at approximately 3.6 V as the full cell voltage drops to 0 V. In this case the anode voltage is similar but slightly higher than the voltage that was tested with the half-cell coin cell in previous experiments. In those experiments the LTO anode was tested to 3.5 V. To be noted, the behaviour of the electrodes in this experiment was following the cell resting at an open circuit voltage of 1.5 V for 24 hours, during which each of the electrodes relaxed to a steady state for a full cell voltage of 1.6 V at the time of the discharge to 0 V. As will be seen in the subsequent experiment, the behaviour of each electrode differs when the cell is discharged to 0 V immediately following a complete discharge cycle (i.e. no rest time for voltage relaxation effects to take affect).

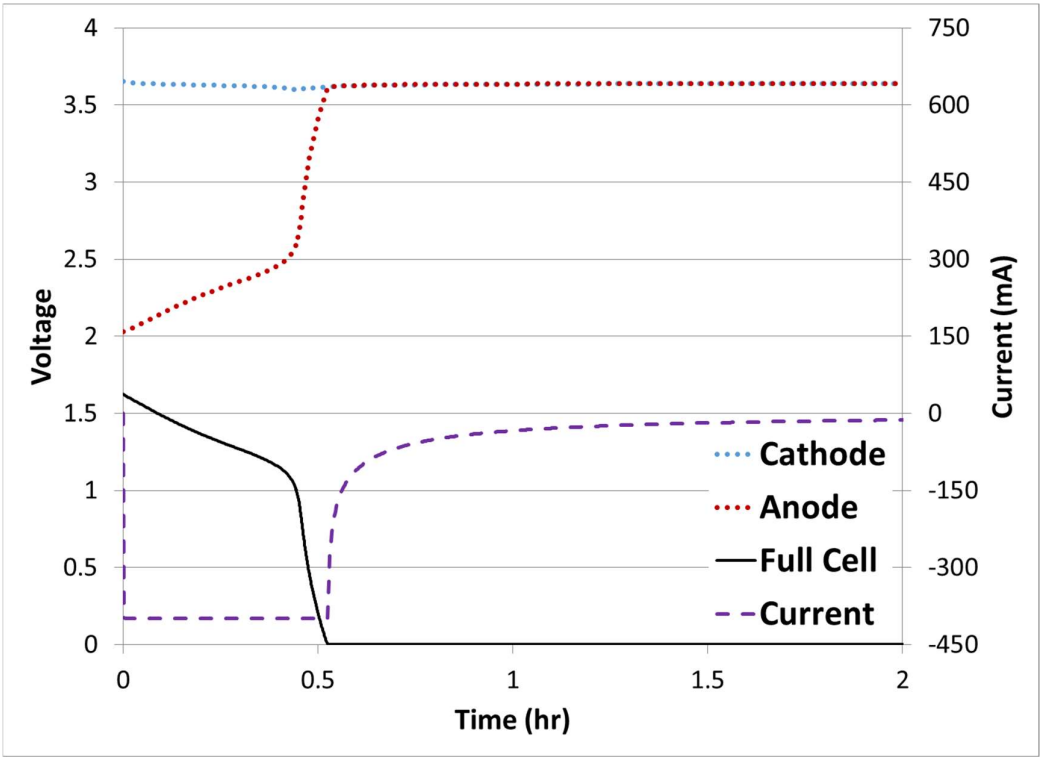

Figure 47: Three electrode voltage diagram of cell being discharged to 0 V, with the 0 V crossing point noted.

In the second experiment, the behaviours of the two electrodes changed significantly. As noted previously, in this experiment the cell was discharged from 2.8 V to 0 V via a single cycle with multiple, sequentially reducing current rates with no rest time to allow for any voltage relaxation effects at open circuit to occur. From the data snapshot shown in , with the chart starting from a cell voltage of 1.6 V to match the previous data set, we see the voltage of the cathode lowering to meet the anode potential. In this situation the full cell 0 V crossover point is at 1.6 V, which is near the 1.5 V plateau LTO is known for [31,67]. There are multiple behaviours seen in this voltage data for each of the electrodes which differed from the previous test. These behaviours would need to be explored in future work.

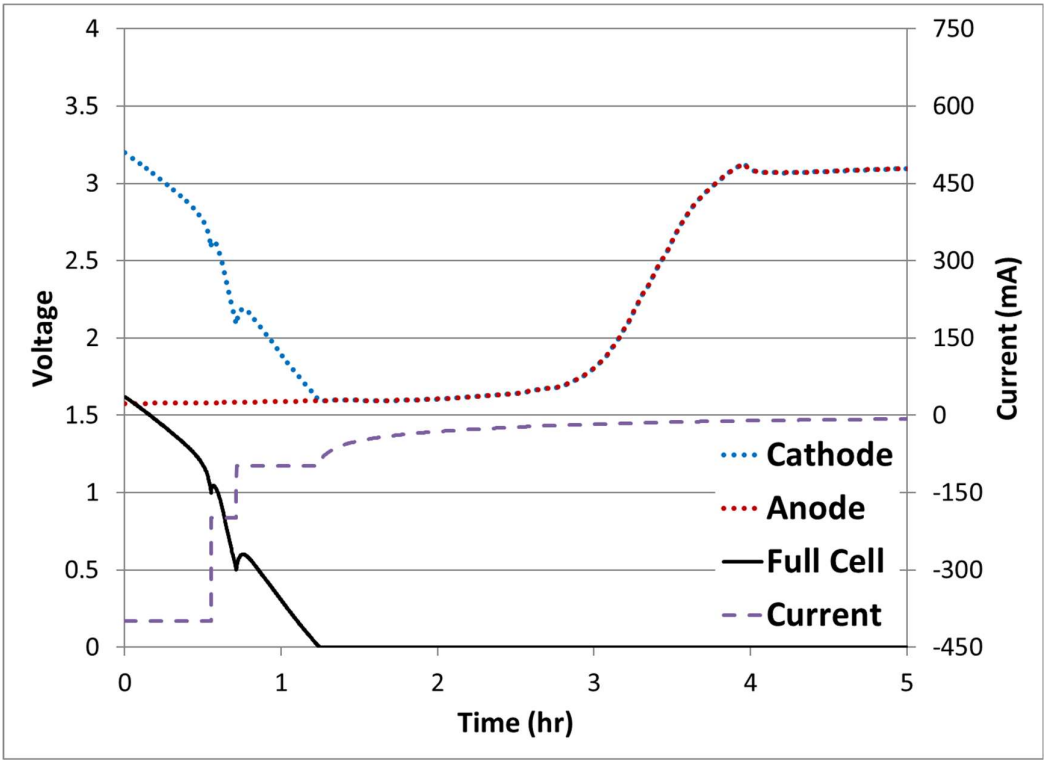

Figure 48: Three electrode voltage diagram of the cell following a full charge discharge cycle, discharging the cell to 0 V in a single cycle with no rest. The 0 V crossing point is noted.

For the first hour, as indicated by the chart, the LTO is slowly lithiating while the cathode is de-lithiating. From then till around 2.5 hours both cells are slowly lithiating before there is a step change in lithiation range. This would indicate that there is unknow reaction happening after the first hour. For both electrodes to be lithiating there must be a source of lithium. Whether this is due to a high concentration of excess lithium in the electrolyte (based on discussions with Altairnano) or there is another source providing lithium such as the inserted reference electrode is currently unknow. The only way for this behaviour to occur is if there is a source providing lithium to both electrodes. In future testing a platinum reference could be used to eliminate the reference electrode as a potential source of the lithium due to the plating providing the excess lithium. Other testing to understand the lithium gradient within each electrode and the electrolyte would be ideal to determine the exact behaviour seen within the data presented.

During the relaxation period both electrode voltages raise to just over 3.0 V, while this does not match the 3.6 V versus lithium seen in the previous testing, 3.0 V is still within normal operating voltages of both electrodes.

As can be seen in Figure 48 above, once the cell reaches 0 V the current trends towards 0 mA, but the current is non-zero for a period of time. This may indicate the presence of side reactions continuing within the cell which have not been explored during this research. Future work would need to identify possible reactions and the appropriate testing protocols to explore those reactions.

3.4 Brief Discussion of Results

Based on preliminary testing of half cells supported by cycling, storage and SEM imaging, it was shown that Altairnano's LTO electrode would remain stable with no identifiable changes when cycled and stored a high potential voltage versus lithium. This voltage condition was chosen to mimic any possible anode potential within a full cell as a demonstration of a worst-case scenario, providing evidence of the behaviour that may exist within a full cell during discharge to and storage at 0 V.

Based on this the half-cell testing, full cell testing including characterization and storage was completed for three cell groups identified previously. The characterisation data from various analysis techniques were used in an effort to identify if the behaviour and health between the three cell groups differed. The hypothesis being that if the behaviour differed between cell groups it would provide evidence that the proposed 0 V storage regime had caused changes within the cell that would need to be explored in a separate project. Otherwise if no significant change could be identified or discerned, this would provide indication and evidence that discharging and/or storing an Altairnano 13 Ah LTO cell at 0 V is a viable and feasible method of storage. Based on the voltage curve, incremental capacity analysis and EIS measurements, there was no discernible or identifiable difference in behaviour. The capacity and performance of the two cell groups which were stored at 0 V and discharged to 0 V then allowed to relax to open circuit voltage, which for any standard

lithium ion battery would be an over-discharged abuse condition, did not differ when compared to the control cell group. This data and subsequent analysis provides support for commercial 13 Ah LTO cells to be stored at a 0 V condition for long periods of time, providing an increase in safety, reduction of risk and reducing potential costs for storage and shipping.

When data from Altairnano was available to review, both published data sheet specifications [68] and internal data (much of which is not published or publicly available), the comparable performance aspects all cells from each three cell groups including measured OCV curves, impedance values at various SoC, EIS measurements and capacity measurements aligned with Altairnano's data. This provided confidence that that the control cell's test data aligned and was comparable to Altairnano's results providing validity to the testing. This validation of the control results in turn supported the validity of the resulting data from the '0 V relax' (group B) cells and the '0 V storage' (group C) cells' tests.

3.5 Innovation and Impact on Industry

It had been identified through a literature review that there was a significant lack of data and information on the zero-voltage operation or storage of large format commercially available cells, especially with regards to lithium titanate cells. While there are multiple studies on the damage caused by over discharging standard lithium ion cells and a few studies which mention replacing the current collector material with alternative material, these studies were mostly for research purposes or small-scale medical devices only, there had been no study on the discharging of a commercial lithium titanate cell to zero volts and the effects of such an operational state.

This gap in research provided a unique opportunity to pursue potentially ground-breaking research with significant potential for impact on industries and companies. The impact includes the lithium ion battery shipping industry which due to the safety inherent in a 0 V cell can reduce costs associated with shipping by reducing the level safety required during transportation. Pending testing by international shipping regulators this research has the possibility to reduce the costs to

the cell, module and system manufacturers who, with a cell that can be safely stored at 0 V, could ship in manners, such as air in high volumes, which would not be available to their competition due to the international regulations regarding standard lithium ion batteries. This ability to ship in easier and cheaper methods creates an opportunity for a point of differentiation for Altairnano, the sponsor company. In discussion with Altairnano's test engineer the volume of cells required for UN 38.3 testing is approximately 30 cells. It could be assumed that a similar volume of cells could be used to demonstrate sufficiently to a certifying body the uniqueness and safety of Altairnano's cells if stored or shipped at 0 V. This could provide sufficient evidence for Altairnano to request and receive exemption from some shipping regulation and restrictions in place for the shipping of standard lithium ion batteries.

Additionally, the increased safety inherent in the cells and modules would be a benefit to manufacturers of high voltage system. By keeping operating voltages during manufacture to levels below hazardous, the required training of personnel and safety restrictions can be reduced.

In addition to the data provided of the behaviour of a cell at 0 V, the testing also provided a number of supplemental datasets invaluable to modelling. Firstly, it provided a better understanding of a complete voltage curve of the cell from 0 V to 2.8 V, which had not previously been explored. Secondly, while not often modelled, storage conditions can have a significant impact on the life of a battery. It is often overlooked but batteries are often in a state of storage, shipping from company to customers the cells are sat in a storage condition for weeks and even months at a time due to shipping by ocean and delays at customs. Beyond that, even once received by a customer the cells will often be put into inventory until they are needed to be put into use, with some customers storing batteries for month or years due to backlog or the timing of their production flow. Even once put into use, batteries can often sit in standby with periods of downtime, such as when used in a grid application where there may be periods of days or weeks where the unit is taken offline for maintenance either on the unit itself or on local connections where due to safety the battery must

be disconnected or turned off. By understanding the behaviour of Altairnano's cell during and after storage periods where the cells can be stored at 0 V, there can be a higher degree in the confidence in the predicted performance of an aging model. Additionally, via the characterization and the very low current testing conducted (0.12 A on a 13 Ah cell), a pseudo open circuit voltage curve was established, providing a high fidelity continuous OCV curve. In addition to providing new knowledge of the chemistry, providing the benefit and stability of a new and novel storage method, unique data sets generated can support the effort for increasing the accuracy in modelling and have been incorporated into the modelling efforts discussed in following sections.

4 Continued Development and Integration of Altairnano's Model

4.1 Altairnano Model Background

Altairnano had previously developed an in-house battery modelling tool, that was used to support engineering design and to provide an insight into the proposed battery system's behaviour to customers. As the tool is proprietary work it will be discussed in an appropriate level of detail to circumnavigate any Intellectual property infringement. Accordingly, this tool has not been previously discussed publicly or presented at conferences, and so this work constitutes the first-time publication regarding Altairnano's modelling tool. Because the tool was designed in-house, it has no formal name and was referred colloquially as a "cycling calculator" or" modelling tool". When utilised in 'calculator' mode, it was formulated as a collection of multiple excel workbooks that constituted portions of a battery model.

The separate pieces included:

- Temperature-dependant impedance versus voltage reference tables
- Two performance modelling workbooks
    - One for initial performance
    - One for aged performance modelling
- A system thermal response model

All documents were pseudo-independent with no direct interaction between workbooks. Any information that was needed from one document had to be manually copied to another document. All documents were implemented into excel which allowed for graphically representing the model's output efficiently.

A visual representation of the workflow is provided below (Figure 49). Greater detail of the various pieces is provided in the following paragraphs.

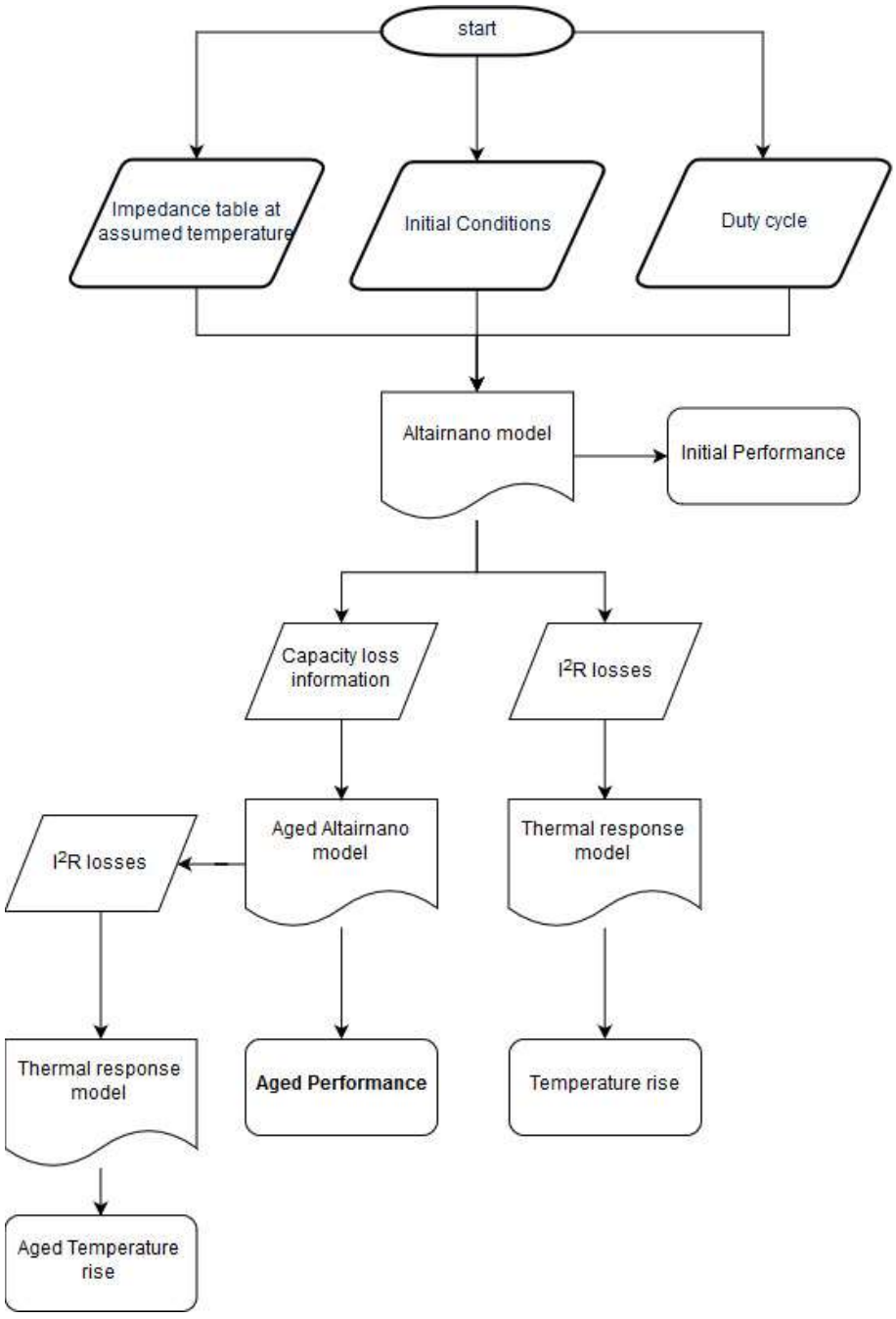

Figure 49: Altairnano performance modelling flow chart

The impedance values were based upon one and ten second pulse testing across a range of temperatures and voltages. This data was processed and compiled into a reference table of one table per temperature step.

The performance model workbooks incorporated the impedance tables to be able to model performance through several calculations, such as voltage under load, capacity changes, resulting states of charge and capacity loss estimations. The inputs for the tool were time series tables of power values and starting conditions - initial state of charge, battery system configuration including series/parallel and cell type, assumed operation temperature. The base workbook accepted only power in terms of megawatts (MW), and due to the design of the original formulae signification modifications were needed to accept any other power ratings (Watt, kilowatt, etc.). Alternatively, two separate performance modelling workbooks were created to accept time series current values for initial and aged performance.

The performance model is considered a zeroth order model [80], which implies that all calculations are based on the direct equation of V=IR. Despite having impedance values for a range of operating temperatures, the model was implemented in such a way that the temperature was assumed to be a single static value. This required inputting a separate impedance reference table into the performance models for each distinct temperature that one wished to model. By assuming a static operational temperature, the model removed the temperature effect on impedance due to internal heating or cooling, which a battery system would experience in actual operation.

Supplemental to the first performance model, which was used to estimate the performance of a battery system in a new state, a second excel file was created that would utilize information from the first file to estimate the performance of a system following a set period of operation and aging. The build of the second model was similar the first model but added an assumption on the loss of capacity due to operation and incorporated an impedance degradation factor due to time aging effects.

To estimate the aged capacity of the system, a capacity loss factor was calculated from the first file into a capacity loss index (CLI) metric. This metric is an output of the initial performance model. The CLI is based on half cycle (i.e. no sign change in direction of power) data and the number of cycles

estimated for the battery at the assumed temperature. The cycles are based on the power or current profile, provided by Altairnano's customer. The CLI was then converted into a CLI/hr metric based on the length of the profile provided by the customer. This metric was subsequently manually copied and inserted into the second performance modelling file, which would combine the metric with the estimated operating life of the system over a specified number of years. This created an estimation of the reduction in capacity the battery cell would experience over the operational period, which could then be used to model the battery performance in the aged state. Additionally, an estimation based on a reference table for the growth of the impedance values was incorporated to reflect assumed ageing impedance for the modelling.

With regards to thermal modelling, a separate tool was developed that could utilize the calculated I^2R loss values from the performance models, new or aged, and based on a selected battery module type to create a thermal performance profile. The limitation to this implementation of the thermal response model was that it had no real-time influence on the temperature-based impedance table used in the performance models. As is widely known, the temperature of cells under load can vary and change dramatically [81], and as such the impedance values based on temperature of the cell are constantly changing. A static temperature assumption in the performance models would not capture these thermal dynamics.

An additional limitation of the original tools was the training necessary to fully utilize and manage the interactions and dependencies between the various models and tools. Even within a technically trained group, the use of the models and tools was limited to specially trained personnel within the engineering department. This created a knowledge silo and created a risk that losing the single trained employee would mean that the company could no longer utilize the tools it had previously developed.

4.2 A Technical Brief of Modelling

Modelling provides a window into the behaviour of a cell or a system of cells. This window can provide a wide range of information, from informing choices on battery materials to making system engineering decisions. This window can also provide a prediction of behaviour in an application to help inform expectations of performance or life. The view provided by modelling is somewhat obscured by a number of factors, such as imperfect information on a system (the cell) and a system which is in a state of constant change with numerous coupled interactions happening internally, as demonstrated in Figure 50. In addition, many of these processes and their interactions are often not fully understood.

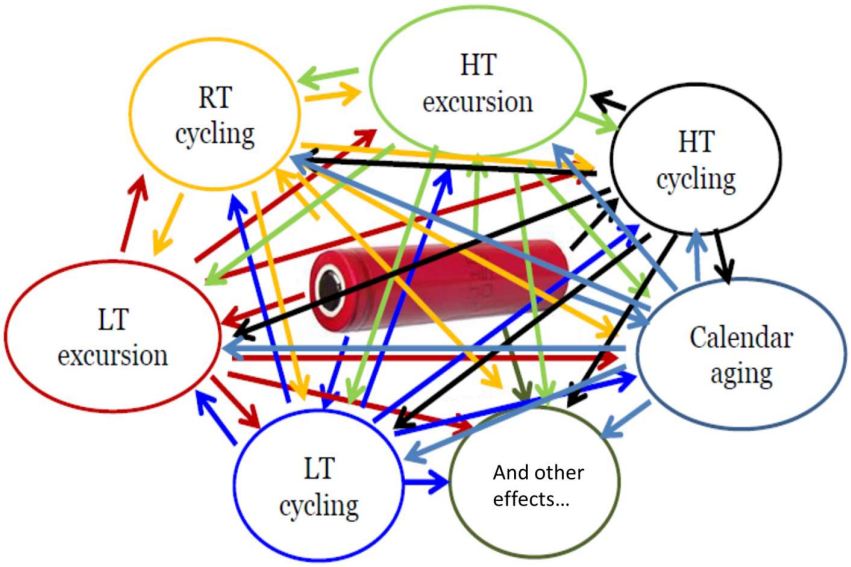

Figure 50: Schematic illustration of interdependent influential mechanisms that can affect aging in cell and create challenges in modelling [50] **(RT – room temperature, LT – low temperature, HT – high temperature)**

These various interdependent interactions complicate the ability to create a simple, computationally lightweight, and accurate model capable of describing the behaviour of a cell or number of cells connected in series or parallel systems under a wide range of conditions. Further complications are added to modelling efforts by trying to predict the future, aged performance of the system in 5 or even 10 years, especially after a cell has been aged in any number of ways and used in numerous different usage profiles.

It is this future prediction of performance and predicted state-of-health (SoH) for the battery, which has value to Altairnano. Altairnano is able to reduce total system costs by correctly configuring and minimizing the number of cells in series and parallel in the initial battery system, while still being able to address the application's future performance needs (usable energy, power) after the system has degraded due to operation and age. Altairnano can achieve this cost reduction by minimizing the initial battery configuration as informed by their performance models, by modelling and estimating both the initial and aged performance of the system. This prevents the need to over specify system attributes, such as excess energy capacity, due to aged performance uncertainty, and to create an end-of-life performance safety margin that is greater than necessary. This better enables Altairnano to create a correctly configured product that minimizes upfront system costs while still meeting the actual performance criteria of the application in future years.

4.3 Model Integration

As noted in the introduction, a goal of the research was the integration of the various tools and models, and increased accessibility of the tool by employees. Additionally, whilst building the new tool and models, an additional goal was to link the various workbooks so that the dynamics of the models would create the appropriate interdependencies such as temperature response and impedance behaviour. This goal was set as an effort to improve the accuracy of the models. Additionally, proper implementation would create the opportunity to change the processes within the organization in novel ways when compared to previous operational processes utilizing the tools and model. One example of a novel process change would be allowing a customer to create system configurations, model performance and present to Altairnano their preferred solution. This would have the effect of reducing the workload upon Altairnano's engineering team which no longer needs to do the initial configuration work and would now be able focus on optimization with the customer, work that has a higher value to Altairnano. Altairnano's purpose and goal was defined by the research as a former employee of Altairnano as well as informal and unstructured discussions with

the researcher's former supervisor who was also acted as the industrial advisor for the sponsoring company. All other discussions with former and current Altairnano employees around the various projects and research were informal in nature.

In an homage to the colloquial use of 'calculator' to describe the excel based implementation of the performance models, combined with the internally used shortening of the company name to Alti, the new modelling tool was designated as AltiCalc. A decision was made by the research to implement the work within a MATLAB environment as it would allow the tool to be compiled into a standalone executable program, able to be installed without MATLAB being present on various computer system. An additional benefit of the MATLAB environment was in direct response to increasing the accessibility of the tools, as by utilizing MATLAB, it would allow for the development of a graphical user interface (GUI). This could then be packaged easily, with the deployment of the tool and provide a richer environment, to deal with the complexities and interdependencies of the various tools. The following Figure 51, Figure 52, and Figure 53 show a progression of the screens that the user will interact with when using the AltiCalc.

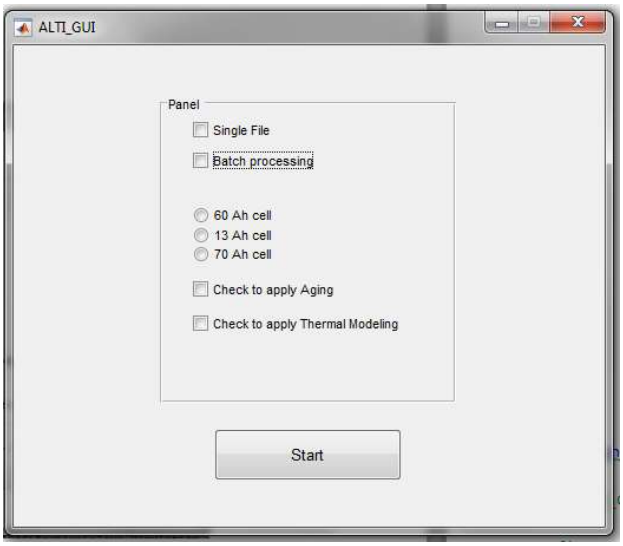

Figure 51: Initial interface shown when the program is first initialized

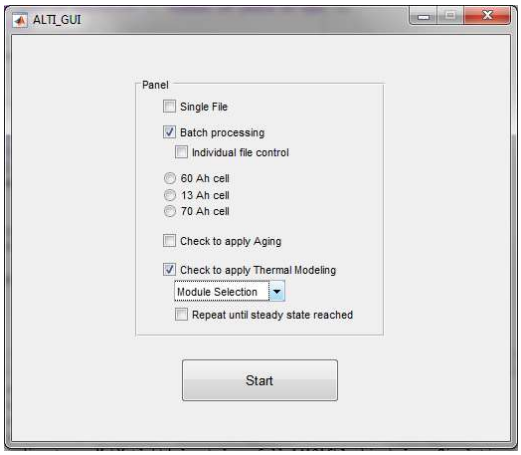

Figure 52: Interface shown with selections that expand to show the various options including batch processing control (single input for all files versus input for each file) and module selection

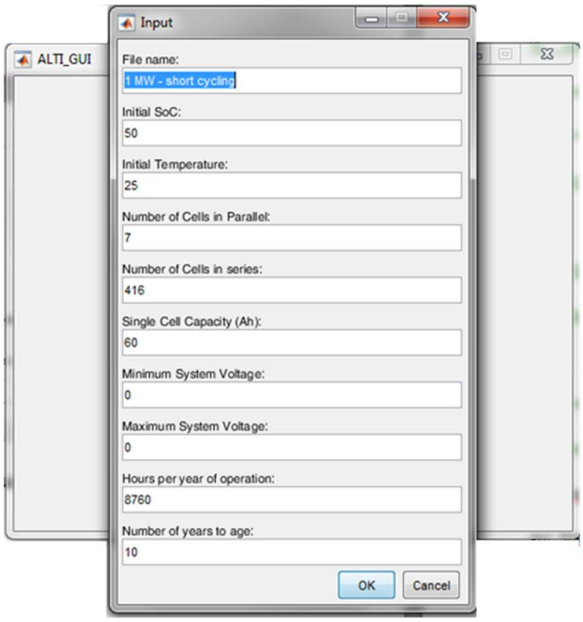

Figure 53: Example of initial input parameters to be entered by the user based on choices selected from the previous screen

The first step required was to reverse engineer the models to understand how the various tools could be interlinked, e.g. changing temperature of the system during cycling should be reflected in the change of impedance for each time-step modelled. Interviews were conducted with employees who had background knowledge of the model, as well as incorporating the researcher's previous experience with the model during prior employment with the company. The information from the employees was limited, but information was scattered throughout various documents located on the

company's servers. Prior to this work, the information had not been collected into a single source. This provided a knowledge base from which to build upon, with the development of a single point of interaction incorporating all the previous tools and models. The development was carried out within the MATLAB script environment which allowed for continuous testing and validation of the code base as it was being developed. The complete MATLAB code can be found in the researcher's third submission titled 'EngD Submission 3: Altairnano Lithium Titanate Modelling including Aging and Thermals Code Base'. Additionally, as seen above, a GUI was integrated into the program to provide ease-of-use functionality.

When compared to the process flowchart (Figure 49) outlining the workflow of the previous implementation of modelling, integration of the various components within the AltiCalc greatly simplifies the process as seen below in Figure 54.

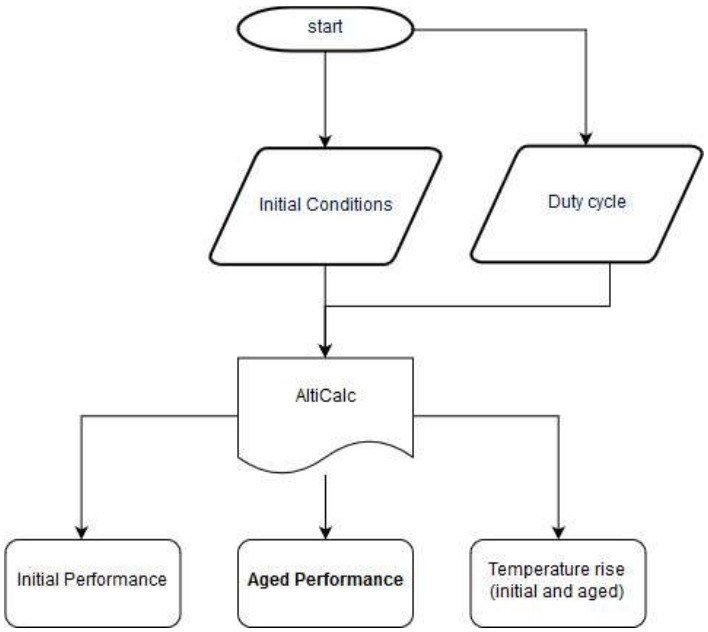

Figure 54: An example of the AltiCalc workflow

Figure 55 shows the internal workflow of the AltiCalc, highlighting the integration and feedback loop from the thermal response of the system. Additionally, the workflow captured within the AltiCalc block no longer requires interaction from the user, as was required for each step previously.

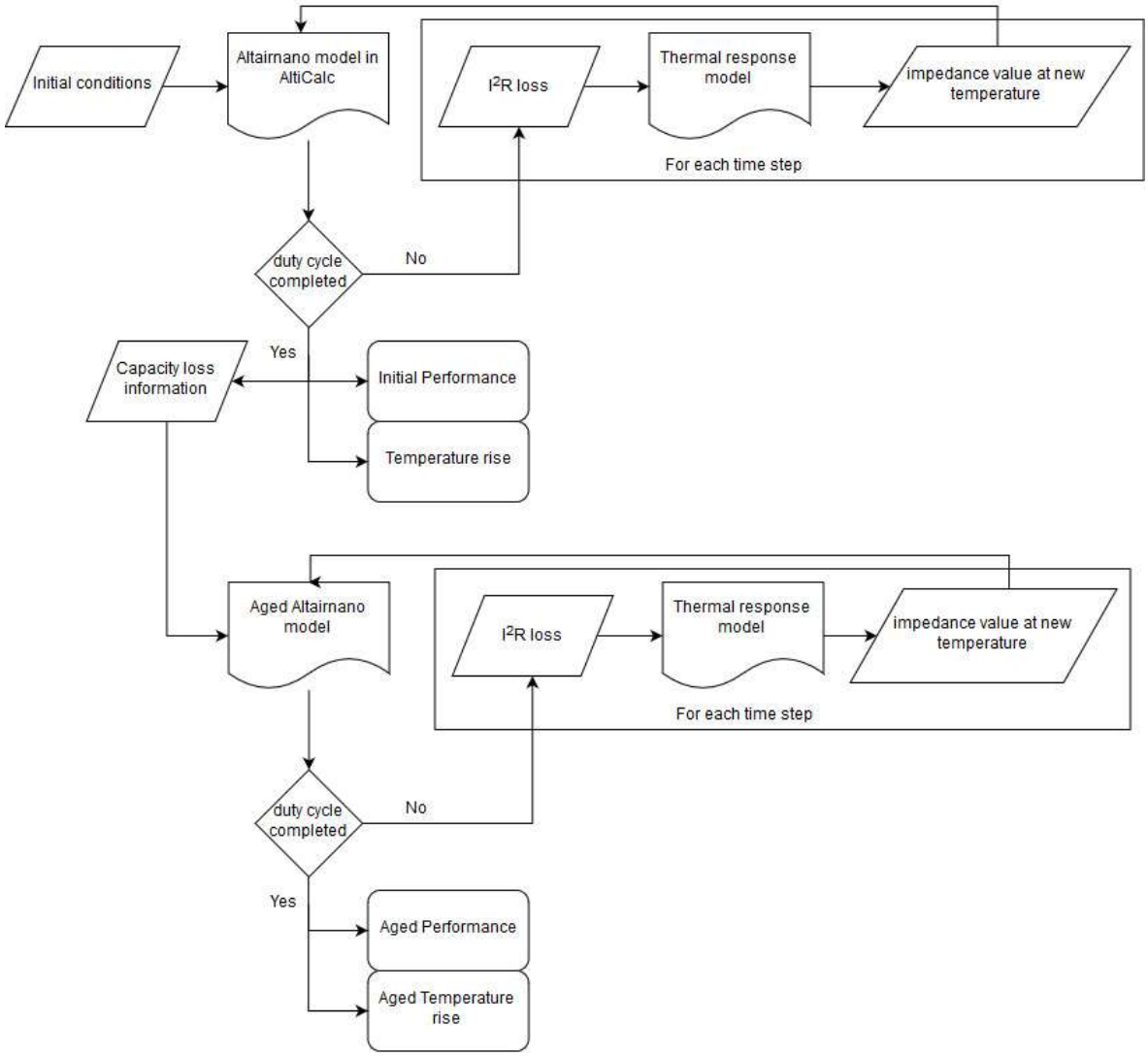

Figure 55: Expanded view of the interactions within the AltiCalc

4.4 Innovation and Impact on Altairnano

The first impact to the company was a change in process of how a customer profile was evaluated. Previously a customer provided a time-based duty cycle profiling with some additional basic information including voltage limitations, temperature and operational life expectancy. This information was provided to the Application Engineer, who then utilized the tools and models to

provide several charts to graphically represent the behaviour of the proposed system. As noted previously, only those directly trained in the engineering team were able to manage the various tools to create the feedback. Following the roll-out of the AltiCalc program, following simple training, others within the engineering team, the members of the sales team and even a customer were able to engage and utilize the tool to provide self-sufficiency. This enabled an understanding with regards to the modelling of the behaviour of a proposed system that was previously unfeasible. This represented a significant departure from previous processes and capability internally within the organization, but also externally.

Such a change in process has the potential effect of improving the process flow by allowing the sales team to engage with a customer and better evaluate their application, creating a higher quality sales funnel prior to engaging with a limited and potentially expensive resource (the engineering team.) The engineering team must still qualify the results if the sales member believes the lead and application may fit well, but this burden is born by the sales team rather than the engineering team. Previously, the engineering team had to engage with every inquiry due to the need for the tool to evaluate possible fits with the company's technology. Higher quality sales funnels reduced unnecessary engagement with unsuccessful inquiries for the engineering team, and increased accessibility to the knowledge contained within the tool provides opportunities to improve the company's process flow. In addition, having the ability to enable a partner and customer to utilize the tool also eliminates possible unproductive engagements, as with the sales team, the customer is now able to self-qualify concepts and systems to efficiently engage with successful designs. Qualitatively, through implementation by the researcher within day to day operations of Altairnano response time to the sales team and customer need on the modelling of a duty profile has reduced from generally few weeks of time to often returned within a few days. This improved response time has allowed the customer and Altairnano's sales team to engage quicker on a number of projects.

Separately, the various models embedded within the tool create innovation for Altairnano as they are now able to dynamically interact and influence the model during each time step. This previously was not possible with the prior arrangement of multiple non-linked tools and excel sheets. This improvement can serve to improve the accuracy and fidelity of the model, improving the ability of the company to research future battery chemistries and provide better feedback to customers. As chemistry development is a continuing process, this tool allows Altairnano to model potential performance gain or losses in field applications. This allows Altairnano to provide valuable feedback to the research and development team on their advancements and changes to the chemistry of the cell.

5 Development of New Parametrization Signal and Implementation into an Equivalent Circuit Model

The final project looked to build upon the previous work while developing new skills and knowledge. First by taking the knowledge gleaned from developing the AltiCalc, it looked to further develop Altairnano's knowledge and capabilities in two ways: First it looked to create a new model for Altairnano. While Altairnano uses equivalent circuit (EC) calculations in its battery management software, and EC are not new to modelling in academia and the wider industry [47], Altairnano does not use ECs anywhere else within the organization including its modelling. To build upon the AltiCalc tool and expand both the software's and Altairnano's capabilities it was decided to develop a model around equivalent circuit calculation which in future iterations could be implemented within the framework of the AltiCalc which had been developed in the previous work.

Second, this project sought to develop new knowledge and skills by developing a novel way to generate parameters for an EC model. ECs were familiar to Altairnano and are standard in industry [47] so the risk of introducing a new model as a basis for the work was minimized. This allowed taking the risk, and focusing the research, on an alternate method for generating the parameters for a 1st order EC model. The novel test signal developed was based upon data directly available from a target application of Altairnano, and many other battery system suppliers, the PJM frequency regulation signal. This data is publicly available in large volumes (2 second data for multiple years) and was used to generate a 24-hour test signal, which was then used to parameterize the EC model. This signal operated the cell dynamically throughout the entire SoC at various power levels. This signal differed from many characterization test profiles which focus the on testing in distinct, discrete SoC steps as well as at a consistent load, such as the hybrid pulse power test (HPPC [82]) profile.

Finally, the resulting equivalent circuit utilized characterization data from the 0 V research for its open circuit voltage curves, as well as utilizing portions of the testing data as inputs against which to validate the model.

The novelty of the work laid in the conception of a testing profile to achieve parameters for a model in a unique way whose source could be traced directly to a real-world application usage profile, while new knowledge and skills were created for Altairnano as an organization building upon work from the previous projects.

5.1 Common Issues with Testing for Parameterization and Model generation

5.1.1 Simulating Actual Conditions in Testing and Models

One of the biggest issues with most models can be the lack of semblance to real life conditions and capability of the model to handle the dynamically various conditions that may be experienced by a cell while in real-world operation. By not testing the performance of a cell in the laboratory to conditions similar to those that would be experienced in an application, and then using that data set to characterize a model, one could develop a model that provides erroneous results. When compared to actual usage the model would generate performance and behaviours that would not be representative of actual performance of a cell in operation. Whilst the goal of laboratory testing is to simplify the complexities of a system to a manageable degree, ignoring and not testing in conditions similar to what is seen in actual operation be can misleading.

5.1.2 Hybrid Pulse Power Characterization (HPPC)

One method often used for parameterizing a cell or system model is hybrid power pulse characterization (HPPC) profile as seen in Figure 56, specified by USABC a US battery consortium. The HPPC profile is designed to test the pulse power capability of a battery system at various states

of charge [35,73,82–88]. From these pulses open circuit behaviour and impedances can be determined, which can then be used to parameterize a battery model.

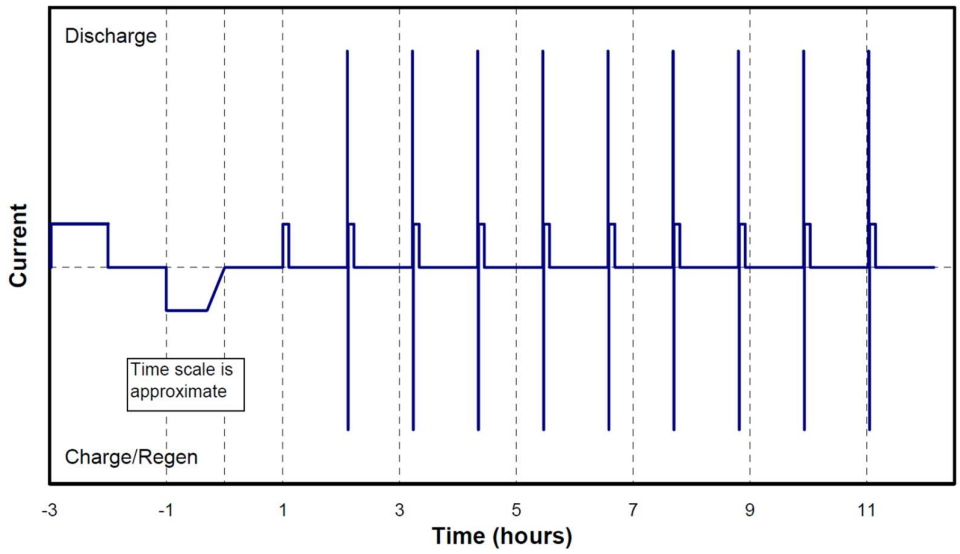

Figure 56: Complete HPPC profile – USABC Battery test manual for plug-in hybrid electric vehicles [82]

The issues with parameterizing a model with HPPC profile include the significant amount of time the characterization takes to complete. HPPC testing is done in non-operational, unrealistic fixed states of charge, usually in 10% intervals with significant rest intervals (1 hours) between each pulse.

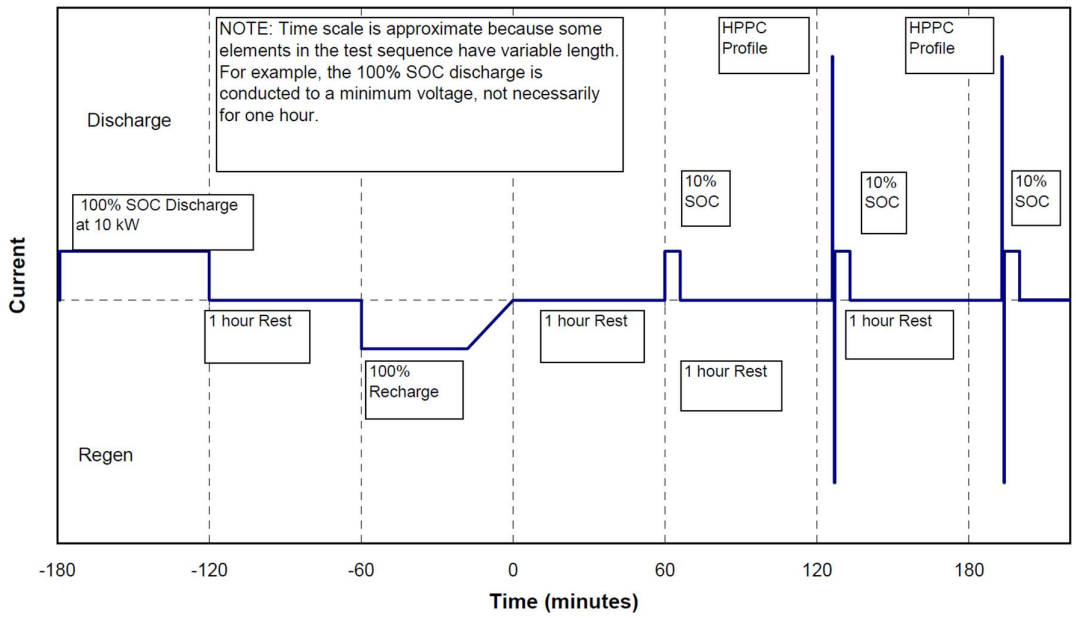

Figure 57: Initial sequence of the HPPC profile [82]

The test is conducted at specific states of charge (SoC), with SoC step as large as 10% between pulse testing. This is a significant change in SoC, over which the behaviour (impedance and slope of voltage change) of the cell can change quite significantly. This is especially true at the higher or lower states of charges, where a small change in capacity can result in large changes in voltage and impedance. Large changes in SoC have the potential to hide or miss significant behaviours in the middle SoCs, where the voltage changes tend to be smaller. The behaviour not captured by the test, when characterizing a model has the potential to influence the predicted modelling results and provide erroneous responses.

Additionally, a HPPC profile is very dissimilar to the actual operation of a hybrid vehicle, which does not experience large rest periods between each current event (such as braking accelerating, etc.) An example comparison of such phenomena can be seen in Figure 58 below.

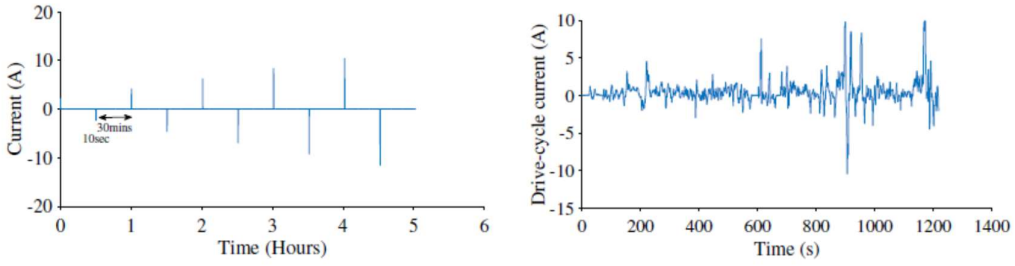

Figure 58: Comparison of a Pulse Power profile versus a drive validation test for an actual vehicle [89]

Because of these issues, the HPPC test is not very representative of the actual performance of a battery, often missing the dynamic behaviour of a cell. A HPPC profile would not be seen in actual operation of a hybrid vehicle. The current or power flow seen during actual operation of a battery system is dynamic, seen in the right-hand image of Figure 58. This variation in amplitude is seen for various reasons:

- In grid frequency regulation applications, the amplitude varies as loads are turned on and off with sources varying their output to match the load changes

- In vehicle the load changes based on the pressure the driver puts on the pedals and the demand of the car, speeding up or slowing down.

This variation in amplitude can have a number of effects on the battery, some of which are discussed in a previous section (2.3 Aging and Degradation), and include current load, changes in the state of charge of the battery, and impact to internal cell temperature. A HPPC test controls and limits the variation on current, SoC and temperature and tests the cell under ideal conditions under limited parameters. For current, each event is a constant current value with a set duration for the pulse. For state of charge, the cell is adjusted to the desired state of charge prior to the test, then for the test itself the current pulse alternate in equal magnitude to minimize the change in SoC. The cell is then adjusted for any additional SoC desired. For temperature, the cells are tested under climate-controlled conditions with parameters set to limit the test if the cell exits a narrow allowable temperature window. Additionally, depending on the specific test, a large rest period after a pulse is part of the test plan. This rest period reduces or eliminates any impact that prior pulses may have had on the current pulse, including any hysteresis effects [90]. The result of this testing produces cell parameterization that assumes linearity, with no path dependence or hysteresis effects [91]. These limitations are not to say that the HPPC testing does not produce valid parameters but to point out possible shortcomings. This work looks to provide a possible alternative parameterization signal which also may be sufficient for modelling while incorporating operational usage into the testing.

In an actual application the controls and limits are set much wider. Current loads are dynamic, constantly varying in amplitude, time and direction (charge, discharge). This behaviour has an impact on the state of charge and temperature of the cell which is not controlled in real-world usage to the level of control seen in laboratory testing. In an actual application state of charge can vary as needed, with operating ranges (e.g. 20-80% SoC, 40-60% SoC) depending on chemistry and goals or needs of the application. While most applications seek to control the temperature of the cells and

their operating environment with climate control, it is not to the degree of control that is exhibited during testing. As an example, from Altairnano's operation of an energy storage system: the climate control was set to provide 25 °C air but the cell temperature varied depending on location within the system. The cells temperatures would range from 30-40 degrees Celsius with the temperature of the cell constantly changing a few degrees within minutes due to the application's varying load demands. The events prior to the current pulse influence the response of the cell to subsequent pulses. Cells in applications do not always operate under ideal conditions but are generally tested under ideal conditions.

5.1.3 Development of a Novel Parameterization Signal and Method

As noted previously, some of the largest issues with the HPPC characterization method are its inability to capture cell dynamics outside of the pulse and unrealistic semblance to how a cell is actually used in an application. The limitations of the method offered an ideal opportunity to research and develop a novel parametrization technique that would ideally capture cell dynamics across the full range of the cell, and which would be based upon realistic cell usage.

Based on this criterion, a suitable source of data for a profile was needed, with sufficient size to be able to capture as many cell excitation behaviours as possible. A suitable data source identified was PJM's fast response frequency regulation signal, referred to as RegD [92–94]. The signal is a normalized signal ranging from +1 to -1, to provide a signal that scales independently of the connected system's size. Energy storage devices which participate in this market receive a new signal once every two seconds, directing a specific response needed by the grid operator. Ideally for this project PJM records, and provides to the public, a historical record of this signal covering multiple years. This provides a source of data that is independent of system size and is an actual usage experienced by battery systems connected to this service. Over the course of a single year, this dataset provides 15,768,000 data points from which to develop a testing profile that can then be used to characterize a signal.

To develop a suitable testing signal that would not take a full year to test, an analysis technique was needed that could reduce the complete dataset down to a representative signal. This would need to capture the behaviour of the signal over the course of a year to one that fit within a shorter timeframe, such as multiple hours of testing.

Parallel work within WMG provided a starting point for the analysis and generation of such a signal. Dr Widanage et. al [89,91,95] had developed a technique to combine sine waves of multiple magnitudes with a known signal such as a pulse power signal. This combination is graphically represented below in Figure 59.

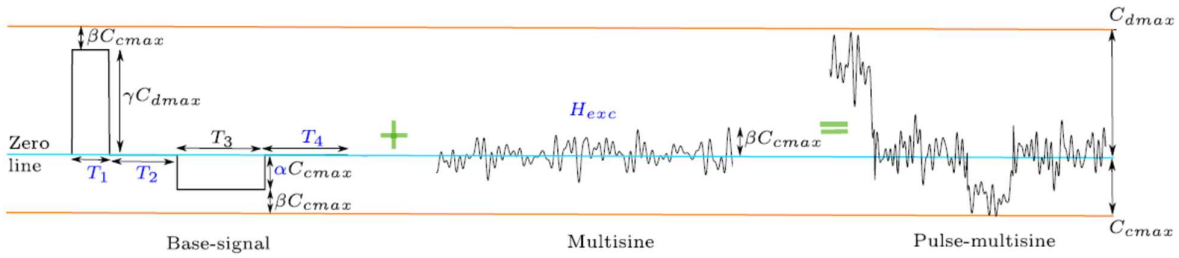

Figure 59: Combination of a known pulse power signal with a multisine generated signal [89]

The idea behind the concept was that by combining the two signals, the pulse-multisine signal generated via frequency analysis would better match for the frequency distribution of an actual drive cycle as seen below in Figure 60 and Figure 61.

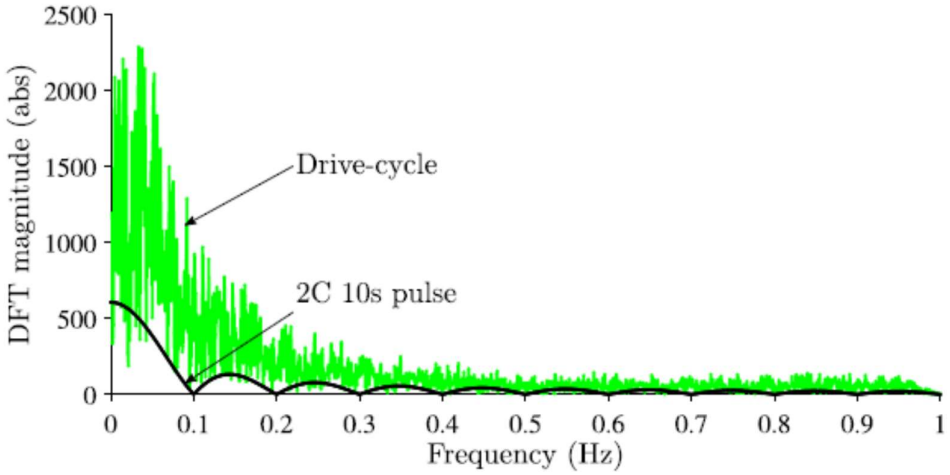

Figure 60: Frequency spectrum analysis of a drive cycle versus a 2C ten second pulse power signal [89]

By combining the two signals Dr Widanage and his team were able to create a shorter profile with a similar frequency distribution and magnitude that matched the drive cycle, an indication that it matched actual usage and would allow the ability to better capture the dynamics of the drive cycle.

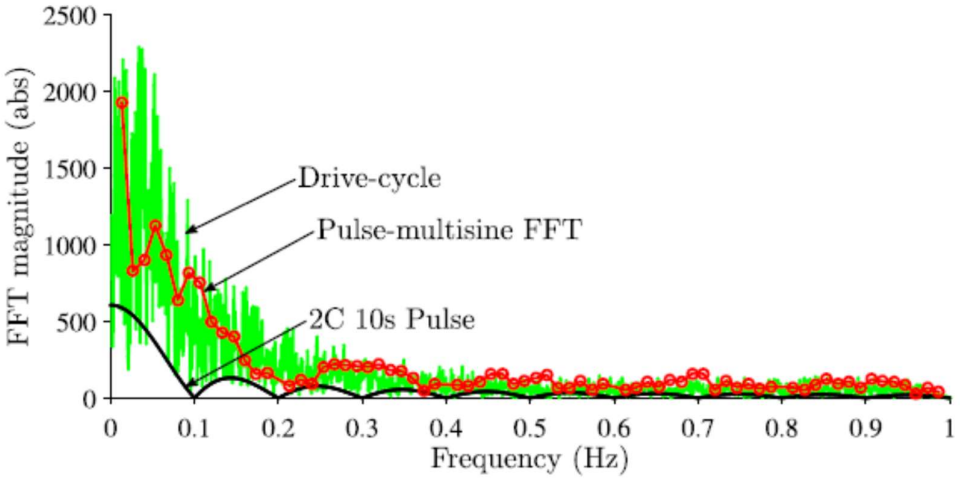

Figure 61: Magnitude and frequency comparison between the drive cycle, the pulse power test and the combined signal [89]

This ability to take a signal and generate a shorter signal would aid in the goal of taking a full year's worth of signal data from PJM's RegD signal and reduce it down to a shorter duration test signal. It was a unique application of Dr Widanage's work and required consultation with him and his team.

One limitation of the technique the researcher identified was that while the generated signal was able to better match the drive cycle signal in terms a distribution, it was limited in that the pulse-multisine signal had to be tested multiple times in approximately 5% State of Charge (SoC) increments. This meant an example testing protocol would charge a cell to 95% SoC, run the cell to the signal, change SoC and repeat down to 5% SoC, similar to the HPPC's 10% increments. For characterization the signal was only valid in 5% increments meaning that at each 5% SoC step there was a valid parameter from data, and in between the parameterization was interpolated. Given that the behaviour of a cell can change significantly within a very small SoC change, this meant that the model may be missing or losing intermediate information for some states of charge, similar to the limitation of the HPPC signal.

The second limitation to the researcher was that by introducing a tuneable multisine signal to a pulse power, the signal was still in effect a random signal not based on an actual usage profile. Thus, there can be arguments that while the signals relatively match as seen in Figure 61, the signal was for all intents and purposes a randomly generated signal.

To solve the second issue first, Dr Widanage's technique was modified so that it would analyse a full year worth of the PJM data, attempting to match the frequency distribution. Both PJM's RegD frequency spectrum (blue circles) for one year's worth of data and a fitting curve for the distribution can be seen in Figure 62 below.

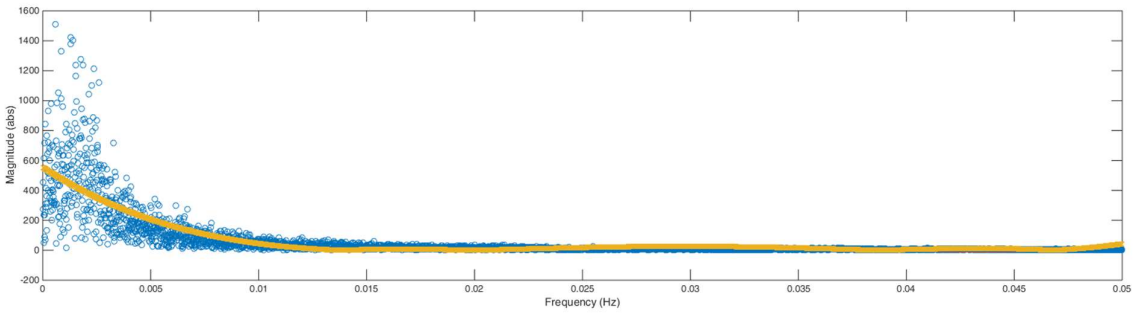

Figure 62: Frequency analysis with magnitude and phase of the PJM signal. A fitted curve (orange) would provide the basis of the multisine generation signal.

Then based on the frequency spectrum analysis shown above, Dr Widanage's multisine technique would generate a signal of a user defined time length that would match the magnitude, frequency and distribution of the provided PJM signal. The MATLAB source code to analyse and generate the signal was provided by Dr Widanage to the research for modification as needed, with guidance and feedback from Dr Widanage.

The resulting outputs from the script are shown below in Figure 63 and Figure 64. Outputs include comparisons of the original and generated normalized power signal, histograms of the two signals, frequency and amplitude curves, as well as root mean square error analysis of the final iteration. Following the analysis of the input data, a generated signal was iteratively processed over multiple fits to provide a best fit signal within an acceptable error threshold seen in Figure 64 (centre top).

The initial iteration's distribution can be seen in Figure 63 and the final iteration in Figure 64. The length (total time) of the resulting signal was tuneable as a user definable input (i.e. 2-hour profile, 24-hour profile).

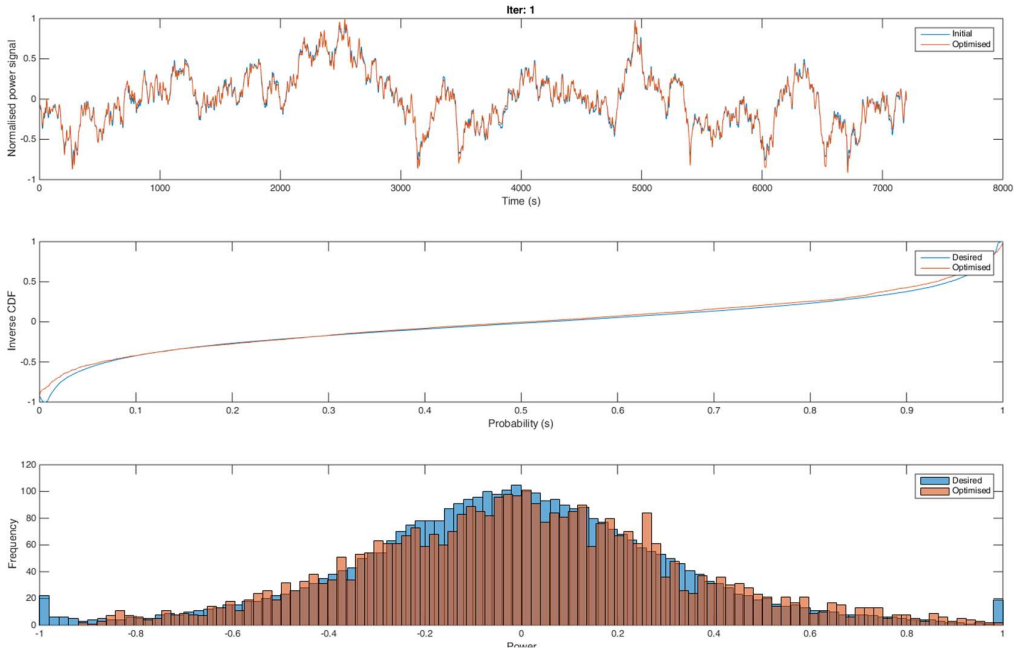

Figure 63: Initial step of the MATLAB tool comparing the original signal (blue) to the initial generated signal (orange). From the top normalized signal (top), inverse cumulative distribution function, and the distribution of both signals.

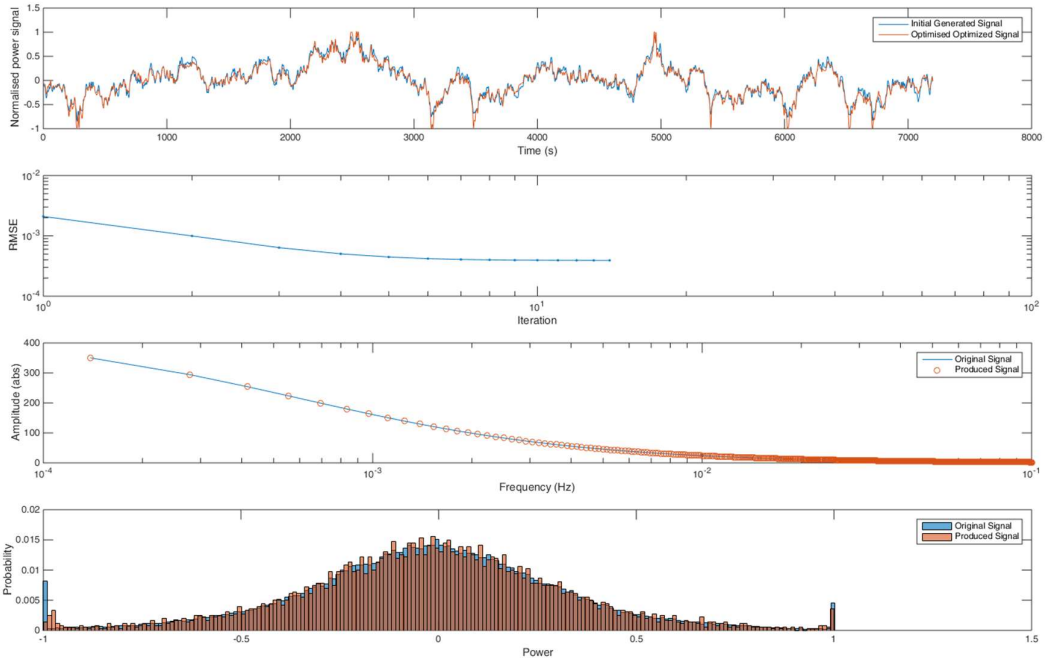

Figure 64: Output from the MATLAB code showing the original signal (blue) compared to the generated signal (orange). From the top normalized signal (top), the root mean square error of the signals (centre top), the amplitude and frequency distribution of the signal (centre bottom), and the distribution of both signals (bottom).

Theoretically, this output would create a signal on the basis of an actual usage profile used in a real-world application. Thus, it could be argued that the generated signal would better reflect the realities and randomness of an actual signal the battery would experience in a real-life application and not a sterilized tightly controlled signal created in a laboratory. This signal would theoretically include the dynamic effects of prior current pulses, prior-step temperature changes, changes in state of charge change , and hysteresis effects.

As seen in Figure 64, there exists a fit between the original signal and the generated signal. To further support the fit between the original and generated signal, each signal was averaged to compare the means between the two. The original signal is non-neutral as it has a slight bias towards -1 due to the RegD signal being designed for energy storage systems. This means that the signal incorporates a bias towards charging (-1) to generate a signal that, after system losses, allows the energy storage device to remain relatively energy neutral over a period of time. The resulting generated signal produced a profile with an identical bias and mean, with a matching frequency distribution, and signal distribution implying that the generated signal was reflected and represented of the original signal. This shows that the generated signal preserves the nuances, such as charging bias and general distribution of power, of the original signal. This would indicate that a system operated to either signal would behave in a similar fashion.

Once there was a satisfactory match between the original and generated signal, the signal was to be used for testing. It was decided to move forward with this signal as it met the goal discussed in section 5.1.1 Simulating Actual Conditions in Testing and Models of creating a testing profile whose source could be traced back to an actual real-world application signal versus an HPPC signal a similar comparison as demonstrated in Figure 58, shown previously.

To minimize the time necessary for testing due to resource constraints, a time a signal length of 24 hours was chosen. A profile of 24 hours would produce a duty cycle of 43,200 steps which varied in signal direction and power, between +1 and -1. This length was chosen for the initial testing as it

was assumed the signal would generate a significantly large enough data set which could be parameterized for the model successfully. Additionally, the time frame was chosen in hopes that the signal would provide enough events over the entire SoC of the cell from 0% to 100%, to capture a full dynamic signal across the entire voltage spectrum with varying power demands. This would solve the first issue identified with Dr Widanage's technique which originally was limited to discrete 5% increments. The generated signal was intended to dynamically test the cell versus across the entire SoC in a single test protocol.

Currently this data has only been collected for 25 °C, additional testing would be needed to expand the data set for the complete temperature range in which the cells would operate under. Future work may look at how to incorporate a dynamically changing temperature regime, but that would require additional resources and time.

5.1.4 Implementation into an Equivalent Circuit Model

5.1.4.1 Equivalent Circuit – Physical model Background

One method often used to model the behaviour and voltage response of a cell is the equivalent circuit model (ECM) [43,96–100]. An equivalent circuit model usually includes a number of resistors and capacitors in series and parallel configurations, as well as other components such as an inductor. These circuit components are used to represent the various parts in a cell such as anode, cathodes, capacitance layers, connectors, other the various resistances and their resulting cell behaviours. These equivalent circuits can be used in a model to determine the response of the voltage under a load.

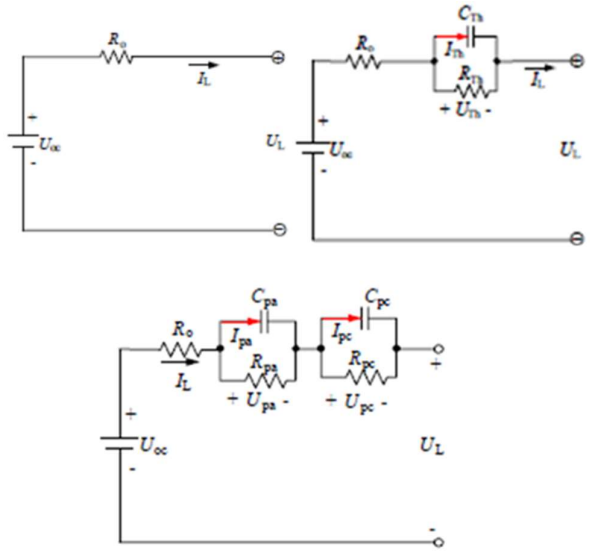

Figure 65: General equivalent circuit models. (Upper left: 0th order - Upper Right: 1st order - Bottom: 2nd order)

Equivalent circuits can be parameterized in two ways: through Electrochemical Impedance Spectroscopy (EIS) discussed or characterization testing [23,101–103] such as HPPC.

5.1.4.2 Implementation into an 1st Order Equivalent Circuit Model

Cell cycling based upon the generated signal was completed in a 25 °C climate-controlled chamber, with data collection every 2 seconds, in time with the application duty cycle. Based on the data collected the parameters Ro, Rp, and Tau for a 1st order equivalent circuit was extracted through the use of a MATLAB script developed by Dr Widanage [91] for EC parameterization. For these equivalent circuit parameters Ro is the ohmic resistance of the cell, Rp is the polarization resistance, and Tau is the time constant for the RC pair. [104]

The generated signal was designed as a ban-limited (a finite number of frequency components) and periodic signal with the maximum frequency set to be less than 0.5Hz (time step of 2 seconds). However in practice, the measurement of current and voltage response can differ from the ideal band-limited periodicity as the measurement equipment is not perfectly ideal due to imperfections which can introduce measurement noise, and the voltage response may not reach a steady state response both of which introduces leakage.

Both these errors are minimized during the parameter estimation stages. The influence of noise is reduced by averaging the measured current and voltage over the applied periods and the leakage error is accounted for when estimating the frequency response function (relating the applied current to the measured voltage). Traditionally, leakage is minimized by multiplying the signals with a window function (for example by a Hanning window [105]). However, for this work a method employed by Dr Widanage that advances on windowing methods is applied [91]. The unknown frequency response and leakage term are approximated over a narrow frequency windows via polynomials and estimated simultaneously, leading to a frequency response estimate with a lower variance (known as the local polynomial method, the details on the frequency window length and estimation method are given in [91,105]). This estimated frequency response is then parameterized via an ECM to obtain the equivalent circuit parameters (as the current is the input and voltage is the output, the frequency response estimate also corresponds to an electrochemical impedance in this occasion). When fitting the ECM, the parameterization scheme utilises the estimated frequency response variance to perform a weighted least squares minimisation via the Levenberg-Marquardt algorithm.

The EC parameterization script was further modified, by the researcher to enable user defined incremental SoC steps used for generating the parameter values within distinct SoC ranges. Due to intent of the generated profile, which was to utilize the full dynamics during operation throughout the complete SoC based on a currents of varying magnitudes and signs, and the method by which the parameterization script generated its parameters, the data was binned based on SoC. The binned SoC values were recorded with the corresponding voltage and current values measured during that SoC step. This resulted in the data was no longer being sorted based on time order but by recorded relative SoC. This reordering of the data allowed the parameterization script to build its parameters based on the user defined SoC increments.

Due to the coarseness, or largeness of the data collection time, step it was necessary to implement the ability to define various SoC steps for parameterization. This was due to the fact that with high enough requested current the change in SoC could be rapid which meant that the response of the battery could be changing significantly if the SoC step was too large. Generally, data is collected at sub-second time step to minimize unmeasured changes in cell responses but due to the length of the profile, and the possible volume of data that could be generated, data was only collected every 2 seconds. This would mean the fidelity of the data would be significantly lower than most testing protocol used to generate model parameters. This would later prove beneficial in establishing that coarse data when properly processed can be used to parameterize accurate models, with benefits in terms of the amount of data that is needed to be collected.

Due to the data collection rate and the resulting availability of the data, the researcher was unsure how to handle the processing that would be required to achieve a useful output. Through research of equivalent circuit models, a paper discussing a layering technique applied by Jackey et. al. [106] was found which was used to minimize parameterization of an ECM into smaller tasks. From that work three SoC incremental ranges were then chosen for the parameterization of this work. The resulting parameters were then combined to provide consistent, continuous parameters across a range of SoCs.

The first SoC step chosen was a 2% incremental step. As an example, the parameters derived for 4% was comprised of all data values greater than 2% and all values to 4%, the next step was comprised of all value greater than 4% to 6% and so on for the entire SoC range. The resulting parameter values can be seen below in Figure 66.

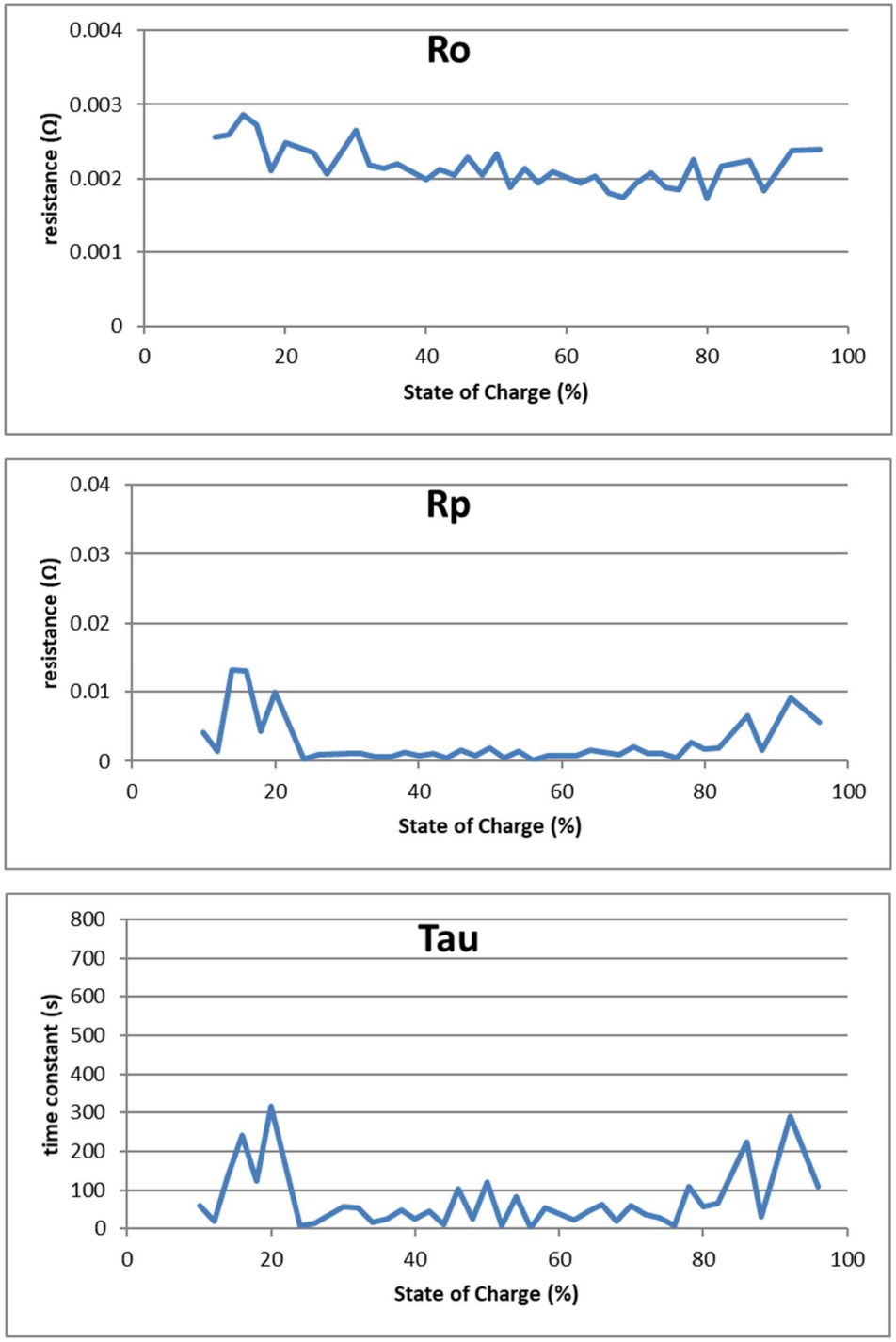

Figure 66: 2% incremental step equivalent circuit parameters. The x-axis in all charts is state of charge. For Ro and Rp the Y-axis is ohms. For Tau the y-axis is the RC time constant of the parallel circuit.

The second SoC increment was a layered technique based upon work by Jackey et al. [106], in this case the layering value was 2%, so all SoC steps were based on values ±2% the actual target SoC. As an example, the parameters for 4% were based on all values from greater than 2% and less than 6%,

the parameters for 6% were based on values greater than 4% and less than 8%, and so on. The reasoning behind the layering effect was that the parameters are continuous functions as such every value should be dependent on the values greater or less than it in a smooth function. Thus, by layering the SoC increments, each SoC step should have a greater continuity with the values nearby. The resulting values can be seen below in Figure 67.

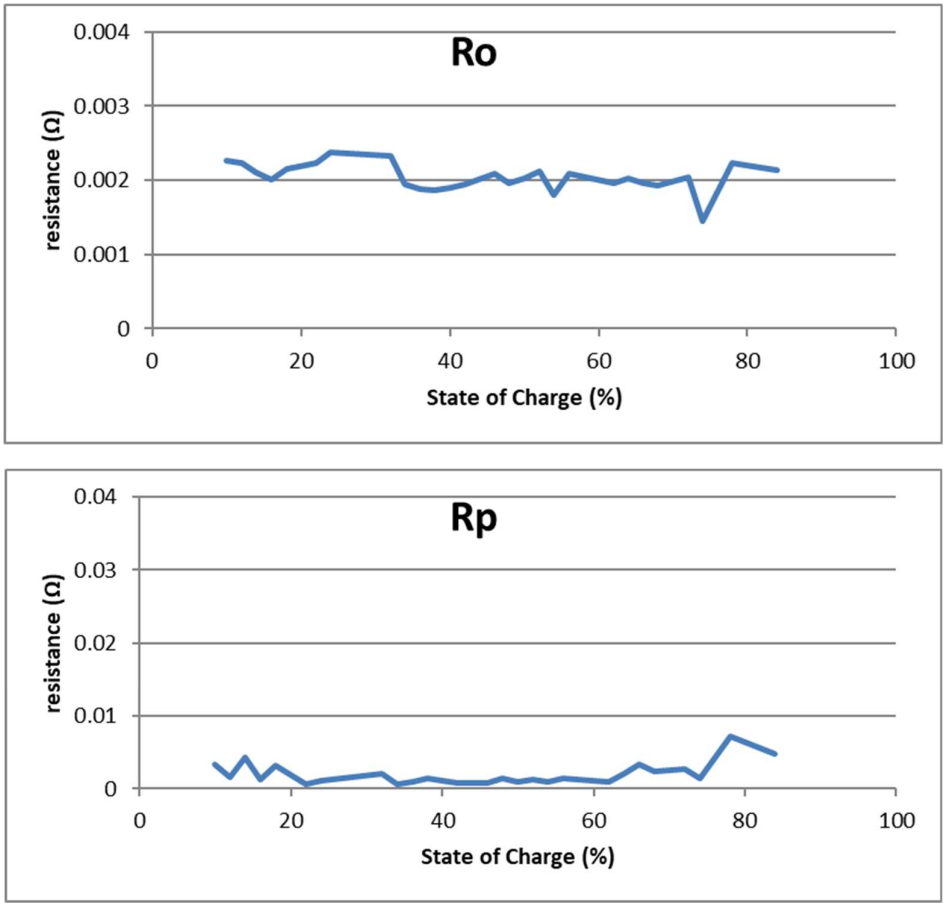

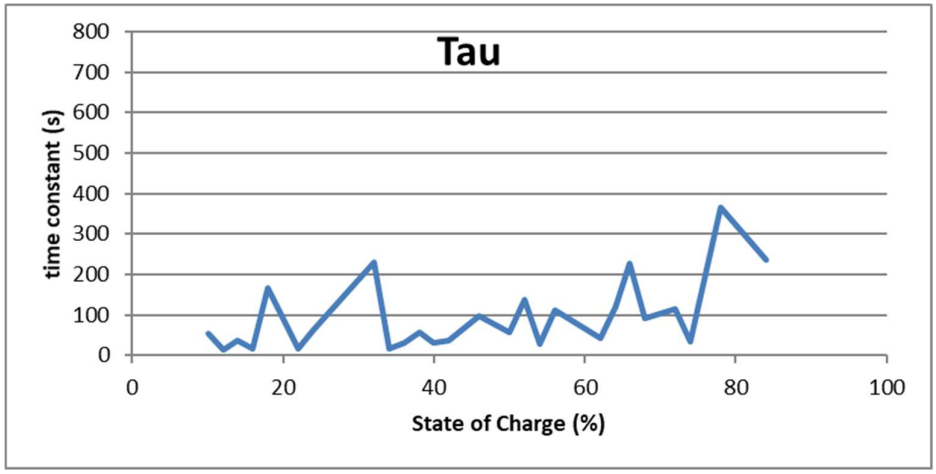

Figure 67: 2% layered incremental step equivalent circuit parameters. The x-axis in all charts is state of charge. For Ro and Rp the Y-axis is ohms. For Tau the y-axis the RC time constant of the parallel circuit.

The final SoC increment chosen was Dr Widanage et al.'s original range of 5%. As with the 2% increment, values for 5% were based on values from greater than 0% until 5%, incremented to 100% SoC. The resulting values can be seen below in Figure 68.

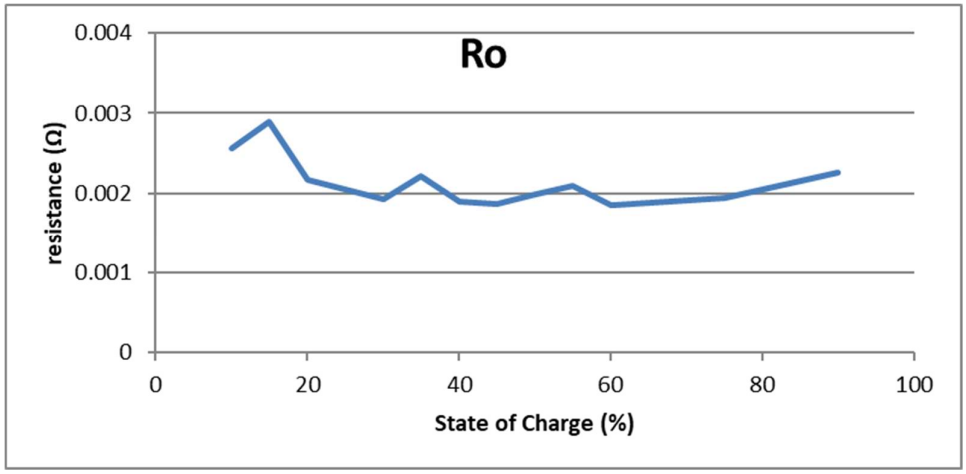

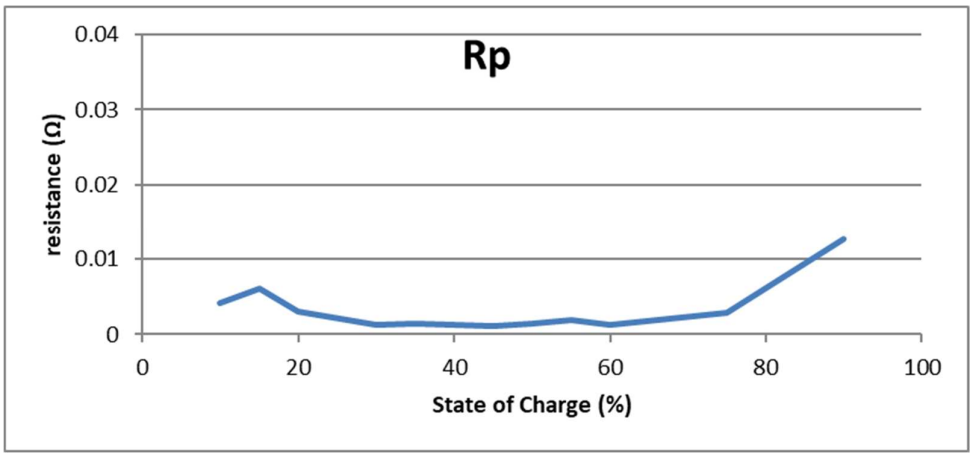

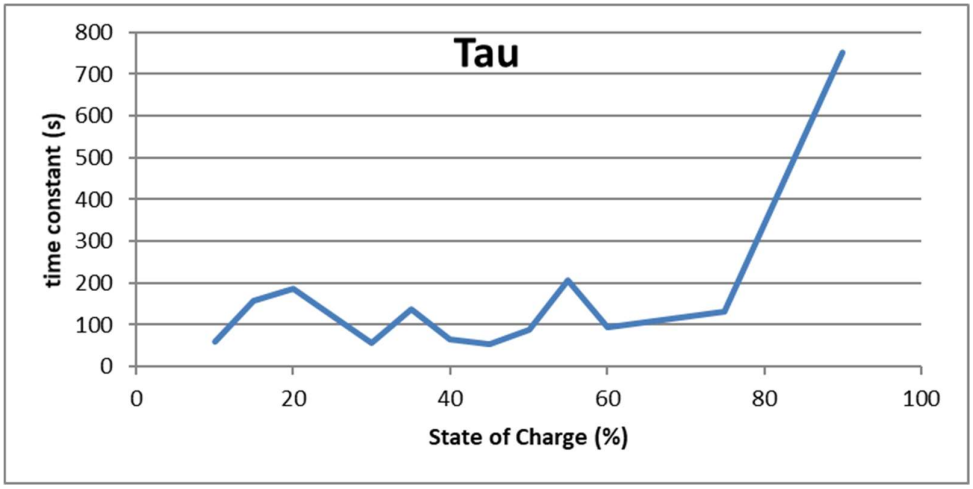

Figure 68: 5% incremental step equivalent circuit parameters. The x-axis in all charts is state of charge. For Ro and Rp the Y-axis is ohms. For Tau the y-axis the RC time constant of the parallel circuit.

The data was processed eliminating significant outliers in the data. Outliers were determined to be any value which had a result which was multiple magnitudes greater then surrounding data. Additionally, as can be noted from the charts, values above and below certain SoC values are not present. This is one limitation to the technique; future projects will be needed to explore how to improve the parameterization at the upper and lower SoCs. It is hypothesized that higher fidelity data may help to improve the results at the extreme SoCs, but this would need to be explored with further work.

Once all three parameterization sets were collected and processed, a final step merged the three data sets into a single continuous data set[106]. First, for each SoC, a table was generated with 1% incremental steps. For each 1% SoC increment Ro, Rp, and Tau were calculated by interpolating between the nearest values in the raw data to generate a single data set for each SoC with specific delineated SoC increments. Each table was bound by the limiting data set's minimum and maximum SoCs (lower limitation of 10% set by all three data set, upper limitation of 83% set by the 2% layered data set). This ensured that there were three data points for each SoC increment for the composite parameter table. Finally, all three tables were averaged into a single table with the same 1% SoC incremental steps. The combined table ranged from 10% to 83%, same as the individual data set

limits. 1% increments were chosen to simplify inclusion into the modelling. The resulting values can be seen in Figure 69 below.

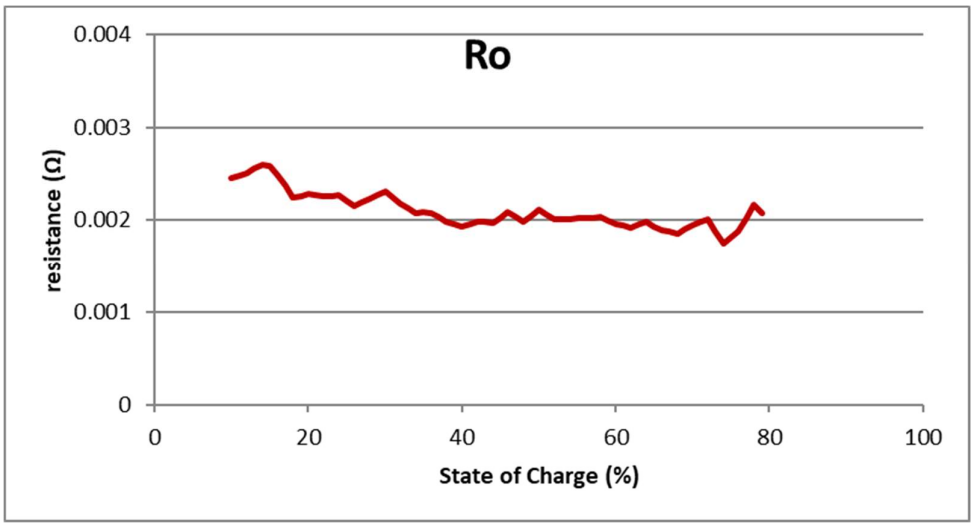

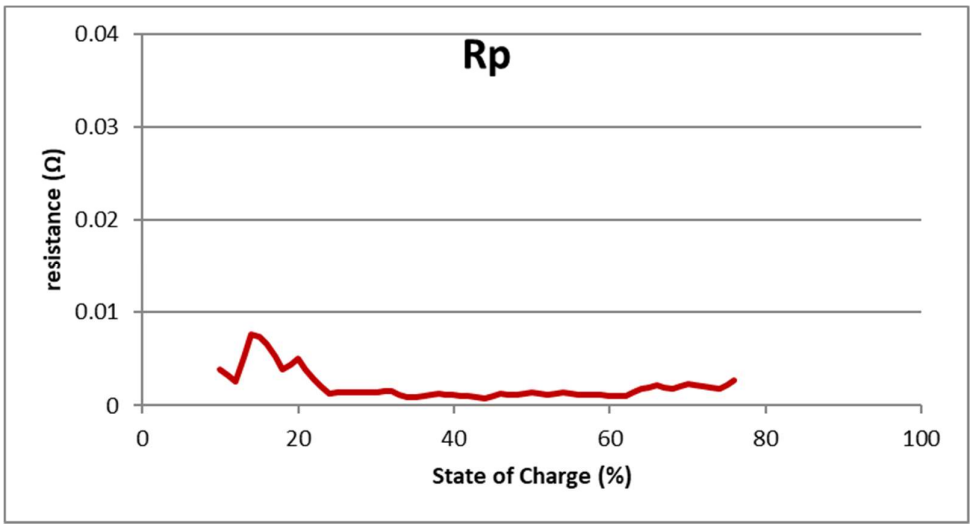

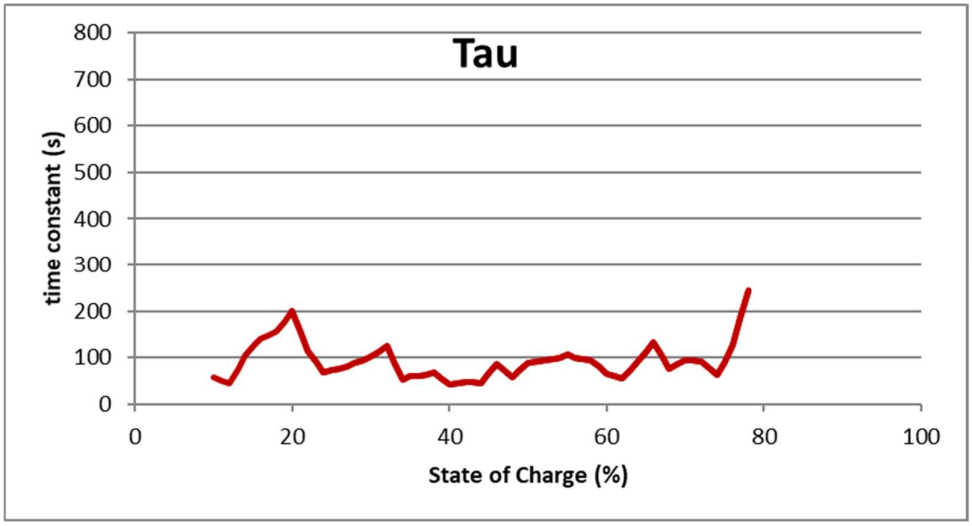

Figure 69: Combined Ro, Rp and Tau parameters plotted 1% incremental steps

The parameters generated were then implemented into a reference table based, equivalent circuit model for Altairnano's lithium titanate cell. The accuracy of the model would be validated against cell data from various testing regimes. Validation of this model would provide support towards validating the technique of utilizing an actual application signal to generate a test profile for model parameterization. Additionally it would also assess the practicality of using data with a coarse fidelity to be utlized in a model and still produce valid and accurate results.

A comparison of the calculated resistance for a 13 Ah cell based on Altairnano's standard 10 second pulse power testing versus the frequency regulation based, multisine signal which was used to parameterize a 1st order equivalent circuit can be seen below in Figure 70. The equivalent circuit resistance is calculated with a 10 second time step input, to approximate the pulse time used in calculating resistance used traditionally by Altairnano. Altairnano's resistance for the 13 Ah cell is calculated based on HPPC testing with a 10 second, 130 A pulse in 25 °C chamber, in 17 increments. Altairnano's increments are approximately as follows, the increments are approximate as the incremental steps for Altairnano vary from test to test and for each of temperatures they tested at:

- One meaurement at 0% SoC
- Three measurements for 0-4% SoC (one 0.5% and two 1.5% increments)

- One measurements between 4%-10% SoC (approximately 5% increment from previous step)
- Eight measurements for 10%-90% SoC in approximately 10% steps
- Three measurements for between 90% and 100% SoC (two 3% increments and one 1.3% increments)
- One measurement at 100% SoC

Because of the relatively flat resistance response in the middle SoC, Altairnano reduces the incremental steps in the middle sections and increases the number of measurements at the extreme upper and lower SoCs in an effort to capture the rapid change in cell resistance which happen in those regimes.

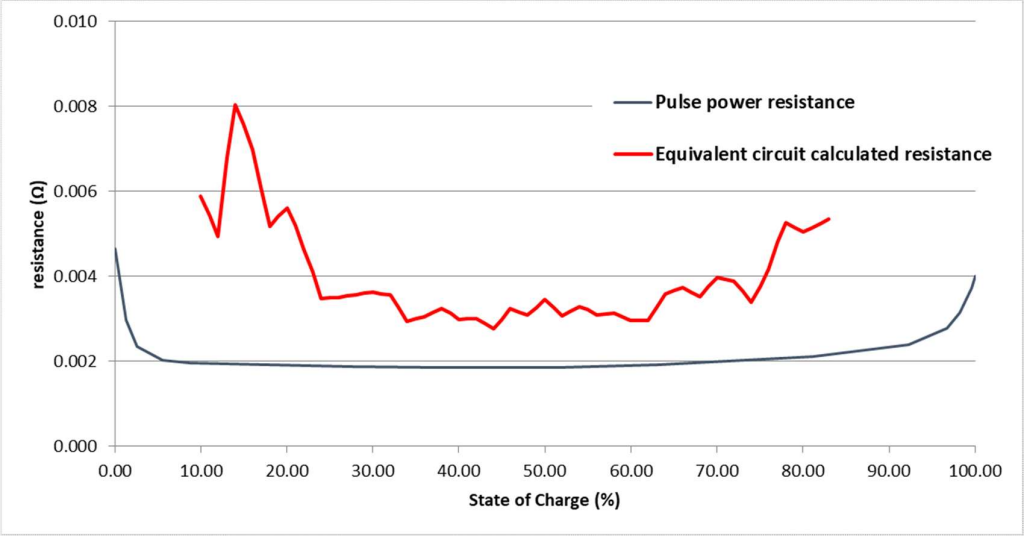

Figure 70: Comparison of Altairnano's pulse power resistance values and equivalent circuit based on parameterization from the frequency regulation based multisine singal testing.

There is difference between the values, with the equivalent circuit resistance being overall higher in addition to apparent noise in the calculated values. This difference could be due to the nature of the HPPC calculation, as dependant on which voltages are used in the calculation, the calculated resistance can vary slightly (for example the difference between initial OCV and ending OCV following the pulse, versus the difference between last measured loaded voltage and the first resting

voltage following the end of the pulse). In discussions with Altairnano, both calculations have been used for various purposes within the organization.

The accuracy of the calculated resistance values when used for modelling is discussed in the following sections with focus on the performance of Altairnano's standard method versus the ECM based model parameterized based upon the generated signal. The following sections will compare the predicted voltage response and SoC performance, based on each method's resistances, utilizing with actual measure cell data over a broad range of operating conditions as the models' inputs.

5.1.4.3 Model Validation

The models were validated to 6 distinct data sets covering various operating states. Due to the limitation of the equivalent circuit model, the data sets were limited to an operating SoC range between 10% and 83%. Three of the data sets were selected from the data collected during the testing of the 13 Ah cell which was used to generate the paramerization values. Validation against this data is useful for checking the performance of each model versus a wide range of dynamically varying current values across a wide range of SoC, to asses accuracy of the model versus the data used to generate it.

The first data set, due to the SoC resitrictions, was selected from time stamps 9,146 seconds to 31,470 seconds, for a data set comprised of 11,163 data points. The second data set, was selected from the same test but at later time stamps of 33,348 seconds to 49,150 seconds, creating a data set comprised of 8,082 data points. The third data set, also from the same test included data from time stamps 50,614 seconds to 59,880 seconds, creating a data set comprised of 4,634 data points. All total the three data sets provides a total of 23,879 points for comparison.

In the following sections Altairnano's HPPC based resistance model is referred to as 'Altair model' while the equivalent circuit model is designated as 'EC model'.

5.1.4.3.1 Charge Depeleting Validation

For the first validation data set, the resulting estimated loaded voltage and state of charge for the EC model is show below in Figure 71. This output of the model shows that the validation data is within the designated SoC limits of 10% to 83% and demonstrates a wide range of voltages under varying current loads. This section of the data shows a charge depleting profile.

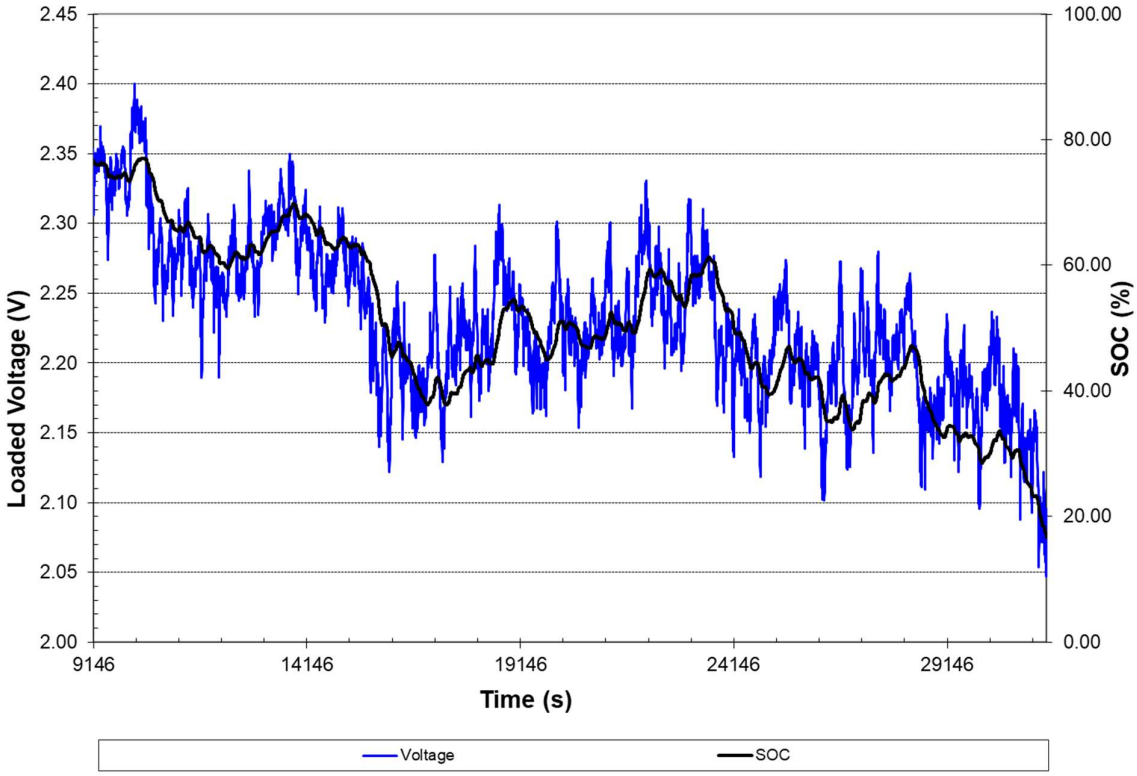

Figure 71: Estimated loaded voltage and SoC based on the equivalent circuit model, parameterized based on the frequency regulation based multisine signal in a charge depleting profile

The absolute error shown in millivolt (mV), the difference between recorded cell data and modelled voltage, for each time step can be seen below Figure 72 for each model. This data set comprised of the highest number of valdiation data points for comparison with 11,163 points from the frequency regulation based, multisine test signal data.

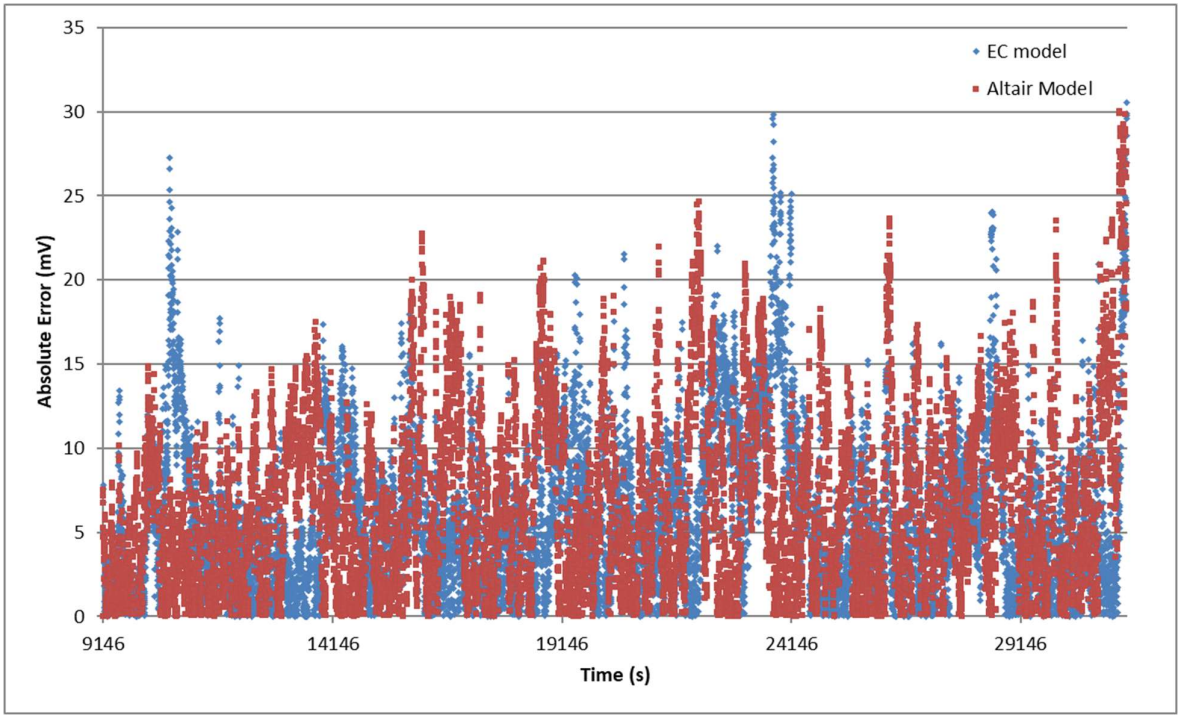

Figure 72: Absolute error between recorded and modelled cell voltages for Equivalent circuit model (blue) and Altair's model (red) for a charge depleting profile

To further clarify each model's performance, the following table summarizes the accuracy of the models against a number of criteria.

Table 2: Charge Depleting Test Profile - Summarization of errors for each model

	# of pts > 10 mV error	# of pts > 20 mV error	# of pts > 25 mV error	max error (mV)	average error (mV)	rms error (mV)
Altair model	2683	176	45	30.0	6.65	8.4
EC model	2021	153	29	30.5	5.99	7.6

From the analysis it can be seen that the EC model has a lower overall error rate than the Altair model. It should be noted that for errors greater than 25 mV, all of the errors for the Altair model are seen at the end of the run where the SoC is nearing 20%. This is in contrast with the EC model which has its large errors distributed throughout the data. This may indicate that there is a greater error in Altair's model at lower SoCs.

As the EC model was parameterized utlizing the vary data to which it was validated against, it can be assumed that some bias exists in the performance of the model. As the EC model was parameterized

based on the data while the Altair model has not. Still despite this possible bias, the results show an improvement, but no analysis has been completed if a bias truly exists only assumed.

5.1.4.3.2 Charge Sustaining Validation

The second validation data included 8,082 data point for comparison. This second validation set, seen in Figure 73, exhibited a differing behaviour over the course of the profile. This profile exhibited a realtively energy neutral profile, as opposed to the energy depleting profile seen in the first validation data set. This gives the models an opportunity to exhibit a different behaviour over the course of the profile.

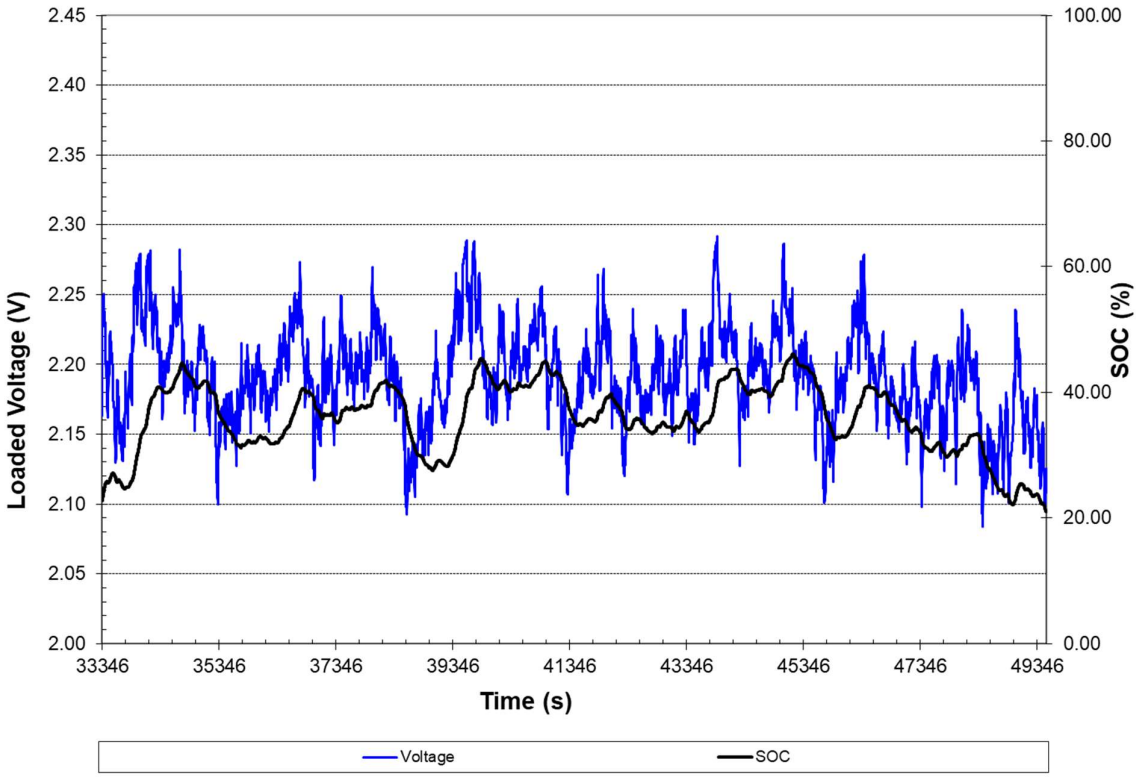

Figure 73: Estimated loaded voltage and SoC based on the equivalent circuit model, parameterized based on the frequency regulation based multisine signal in an charge sustaining profile

Figure 74 shows that the error in the Altair model trends higher over the course of the profile which has an impact on the resulting accuracy summarized below. This could be due to a cumulative error throughout a profile present in Altiair's modelling methodology.

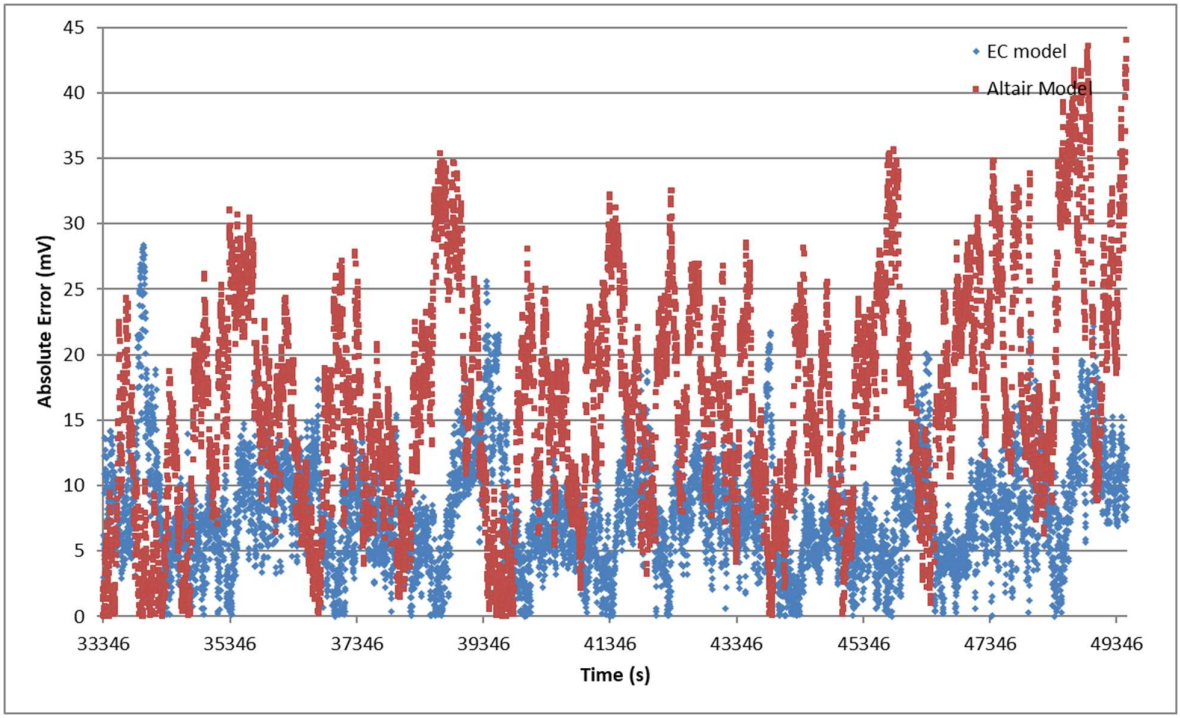

Figure 74: Absolute error between recorded and modelled cell voltages for Equivalent circuit model (blue) and Altair's model (red) for an energy neutral profile

As seen in the following table, the EC model has a greater accuracy over Altair's model with a lower maxiumum error and average error.

Table 3: Charge Sustaining Test Profile - Summarization of errors for each model

	# of pts > 10 mV error	# of pts > 20 mV error	# of pts > 25 mV error	max error (mV)	average error (mV)	rms error (mV)
Altair model	6080	2777	1322	44.0	16.49	18.6
EC model	2183	105	27	28.3	7.85	8.9

5.1.4.3.3 Charge Increasing Validation

The third and final validation data set from the data collected for the equivalent circuit model parameterization, includes 4,634 data points for comparison. As can be seen in Figure 75 this data set exhibits a charge increasing profile trend.

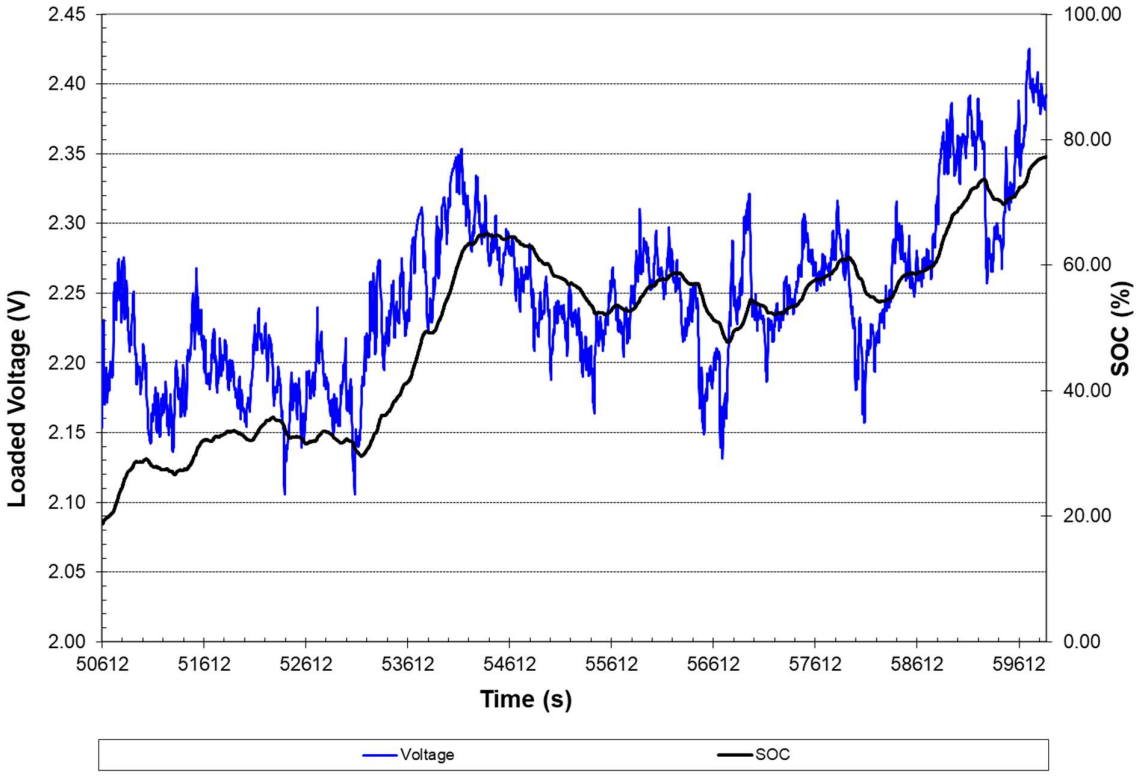

Figure 75: Estimated loaded voltage and SoC based on the equivalent circuit model, parameterized based on the frequency regulation based multisine signal in a charge increasing profile

From this validation set we see that the EC model has a significant number of errors, with its highest error in the low state of charge range at the beginning of the profile, seen in Figure 76. A significant number of these errors are exhibited between approximately 18 and 23% SoC. Refering back to Figure 70, it can be seen that this SoC range is where a sharp increase in the calculated resistance values for 24% SoC or less happens. This may indicate that a higher resolution data set needs to be collected at lower states of charge to properly parameterize the model.

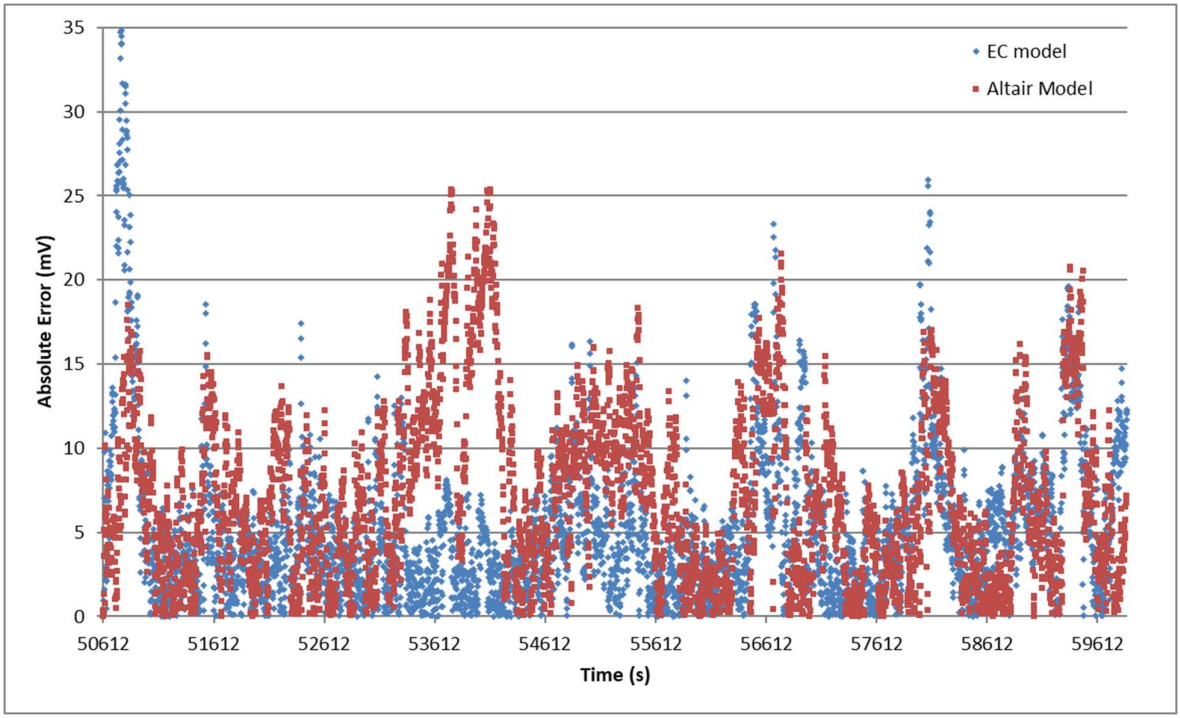

Figure 76: Absolute error between recorded and modelled cell voltages for Equivalent circuit model (blue) and Altair's model (red) for charge increasing profile

As seen in Table 4 below, overall the EC model has a much better accuracy than the Altair model. If the initial portion of the run is excluded the max error for the EC model becomes 25.9 mV, with only two points greater than 25 mV and sixteen points greater than 20 mV. This indicates that better paramaterization of lower SoC is critical for the accuracy of the model across a wide range of operating SoC.

Table 4: Charge Increasing Test Profile - Summarization of errors for each model

	# of pts > 10 mV error	# of pts > 20 mV error	# of pts > 25 mV error	max error (mV)	average error (mV)	rms error (mV)
Altair model	1258	102	7	25.4	7.08	8.8
EC model	583	73	46	35.2	5.07	6.9

5.1.4.3.4 Constant Current Charge and Discharge Validation

The fourth and fifth validation data sets come from the characterization testing of a cell during the previously discussed 0 V project. This data set represents the pseudo-open circuit voltage curve for both charge and discharge cycles at 0.12 A continous, which provides 5,115 and 4,890 data points respectively. As neither model has been trained on or developed from this data it should show the performance of each model versus a continuous charge or discharge cycle at very low current rates.

Figure 77 shows the estimated loaded voltage and SoC for the EC model based on a 0.12 A constant current charge.

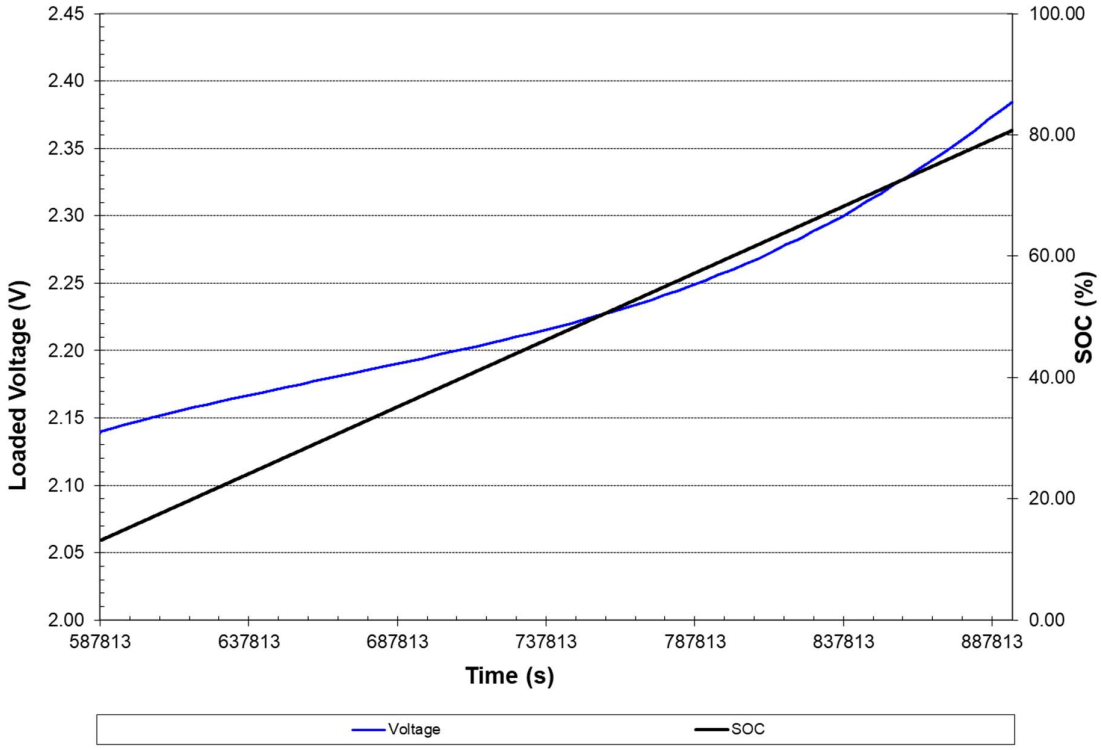

Figure 77: Estimated loaded voltage and SoC based on the equivalent circuit model, parameterized based on the frequency regulation based multisine signal in a 0.12 constant current charge profile

Figure 78 shows the absolute error between measured voltage and modelled voltage for both models. It should be noted that the range of the error values was much smaller over the course of the profile with all errors being less than 3.1 mV, versus the larger error seen in prior validation runs.

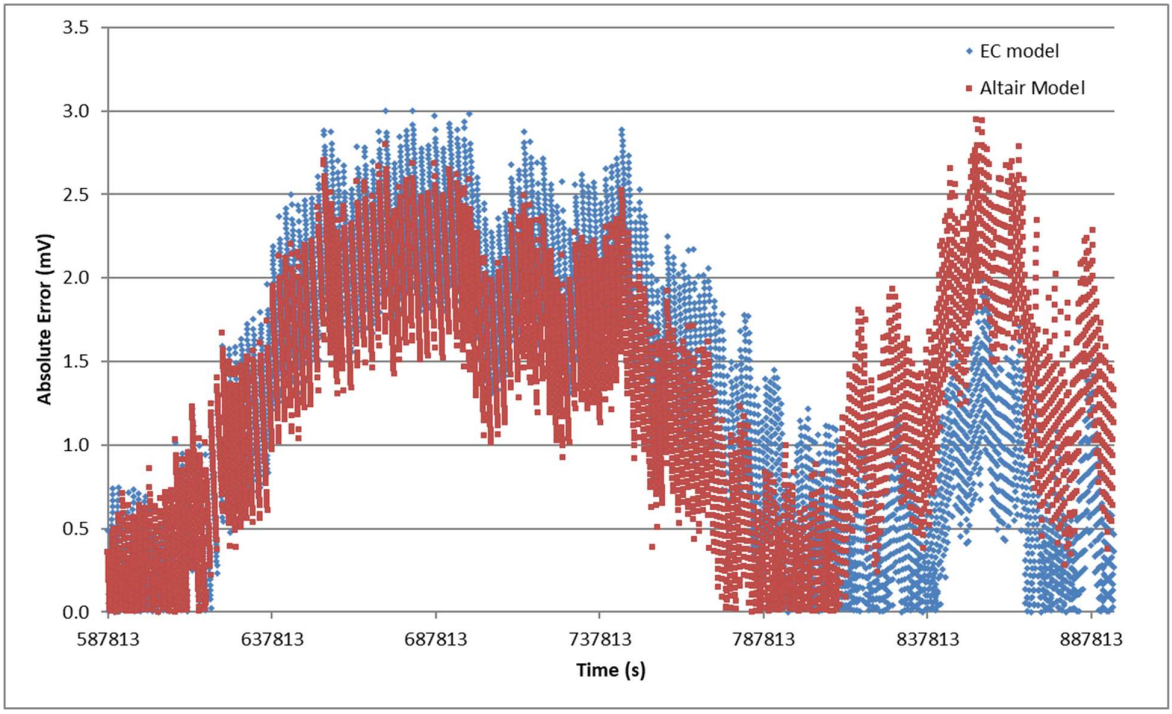

Figure 78: Absolute error between recorded and modelled cell voltages for Equivalent circuit model (blue) and Altair's model (red) a 0.12 constant current charge profile, please note the Absolute error scale change versus prior charts

Both models perform similarly with the Altair model having a small advantage in accuracy for errors greater than 2 mV. To better asses the viablity of both models the EC model would need to be expanded to full paramaterization from 0-100% SoC so that a fullly modeled charge from 1.5 V to 2.9 V could be achieved and compared.

Table 5: Low Constant Current Charge Test Profile - Summarization of errors for each model

	# of pts > 1 mV error	# of pts > 2 mV error	# of pts > 2.5 mV error	max error (mV)	average error (mV)	rms error (mV)
Altair model	3346	905	109	2.9	1.30	1.6
EC model	2916	1249	331	3.0	1.27	1.5

Figure 79 shows the estimated loaded voltage and SoC for the EC model based on a 0.12 A constant current discharge.

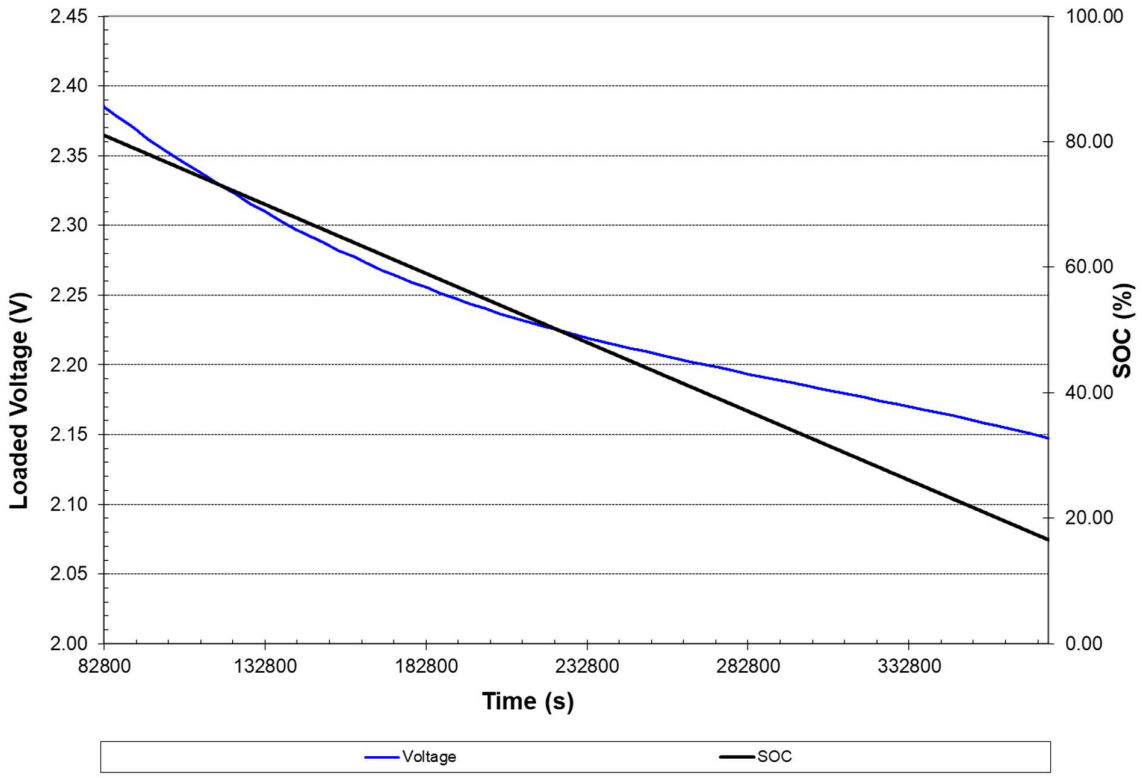

Figure 79: Estimated loaded voltage and SoC based on the equivalent circuit model, parameterized based on the frequency regulation based multisine signal in a 0.12 constant current discharge profile

While the overall error to this validation data is lower than the previous validation runs, there is a noticeable trend exhibited by both models. This trend shows an increasing error while modelling a low constant current discharge behaviour of the cell. It is unknown the cause of this drifting error, and as it was exhibited by Altair's model, it was beyond the scope of this research to identifying the errors in their methodology with regards to their models and these results. As both models were independently developed multiple years apart by differing techinques this error is not believed to be inherent to the model methodologies. As both have the a similar pattern in the error with regards to an independent data set it is is something which should be explored further in future projects and models.

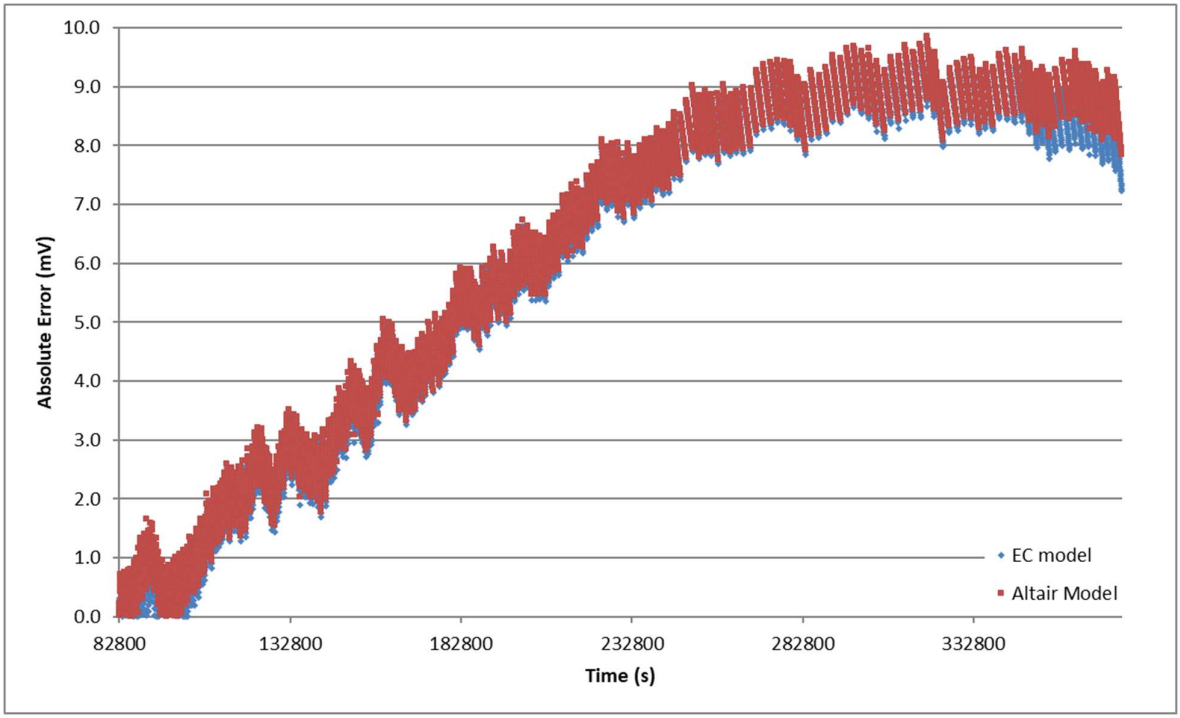

Figure 80: Absolute error between recorded and modelled cell voltages for Equivalent circuit model (blue) and Altair's model (red) a 0.12 constant current discharge profile

Table 6 looks at a summary of the errors with both models performing similarly with no accuracy advantage to either.

Table 6: Low Constant Current Discharge Test Profile - Summarization of errors for each model

	# of pts > 5 mV error	# of pts > 7.5 mV error	# of pts > 9 mV error	max error (mV)	average error (mV)	rms error (mV)
Altair model	3346	2406	738	9.8	6.22	6.9
EC model	3252	2353	460	9.7	6.07	6.7

5.1.4.3.5 Pulse Power Testing with Rest Periods

The sixth and final data set looks at the performance of the models versus pulse power testing at a cell voltage of 2.259 V. This data was collected during the the characterization testing of a cell during the 0 V project. The data set represents an ideal and extreme dynamic response of the cell. It is believed that this data set should provide a good estimation on the performance of the models to handle such a dynamic behaviour as well as large rest periods. The complete data set is comprised of 90,751 data points. The pulse testing was conducted at 20 A, 40 A, and 60 A. The large number of data points contained within the set is due to the data collected during rest periods between each pulse. The data set should provide insight into the behaviour of the models during

OCV events as well as high current pulses, as would be seen during a HPPC or pulse power test.

Figure 81 shows the estimated loaded voltage and SoC for the EC model based on 20 A, 40 A and 60 A pulses with rest periods.

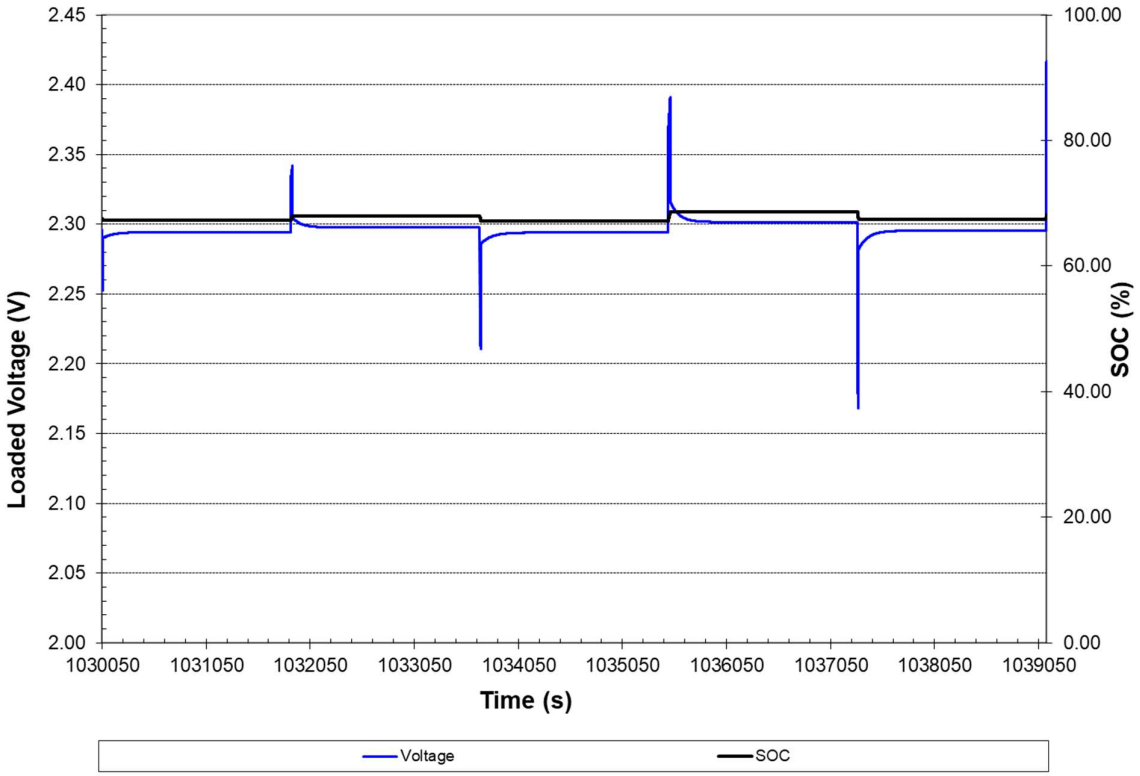

Figure 81: Estimated loaded voltage and SoC based on the equivalent circuit model, parameterized based on the frequency regulation based multisine signal, in a pulse power test with rests

Both models show a significant number of error points as a result of the offset during the rest periods as seen in Figure 82.

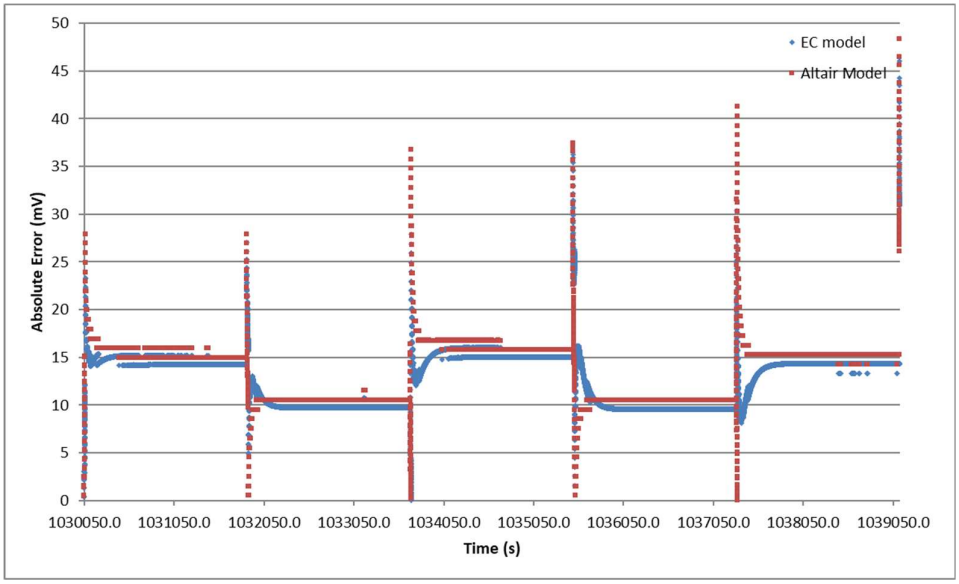

Figure 82: Absolute error between recorded and modelled cell voltages for Equivalent circuit model (blue) and Altair's model (red) for a pulse power profile

Figure 83 shows the actual error for the EC model showing a significant offsett in the negative direction, which corresponds to a discharge offset. This is something that follows on from the previous validation work against the 0.12 A discharge, and as noted previously the cause of this error should be explored in a future project.

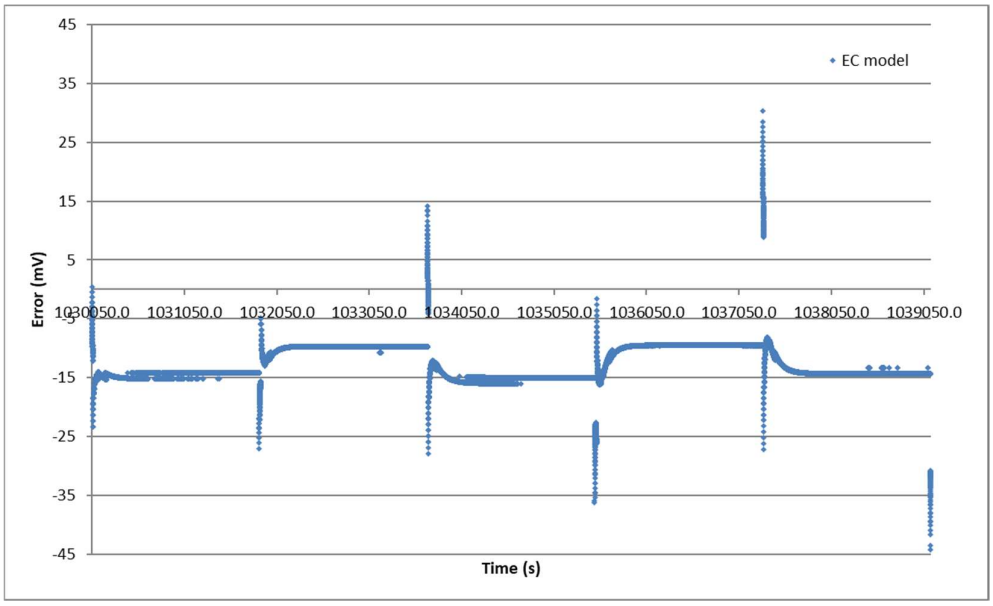

Figure 83: Error for EC model prior to adjustment showing an offset

To allow a better comparison, an offest was determine for both data sets. This value was based on the average error for each profile. This value was then subtracted from the error of the respective

model, in an effort reduce the average offest during rests to 0V. The results of the adjusted error for the EC model is seen below in Figure 84.

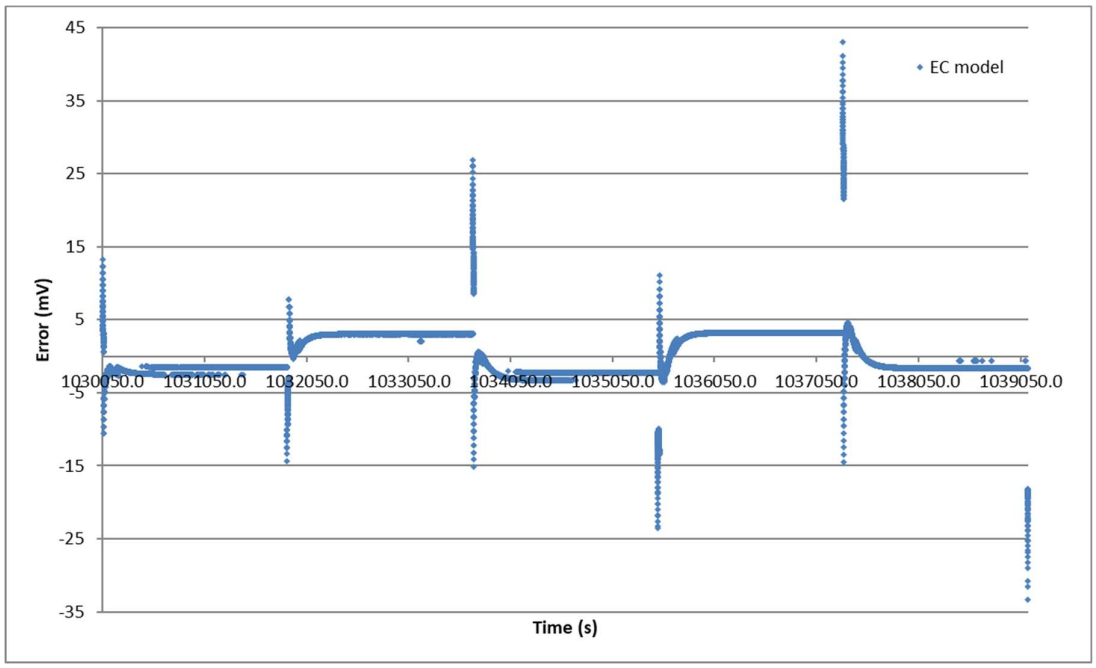

Figure 84: Adjusted error for EC model, charge values are negative and discharge values are positive

This correction allowed for a comparison of the two models, as the errors were focused on the response to the pulse power tests and less on the offset during rest. The adjusted absolute error for both models can be seen in Figure 85.

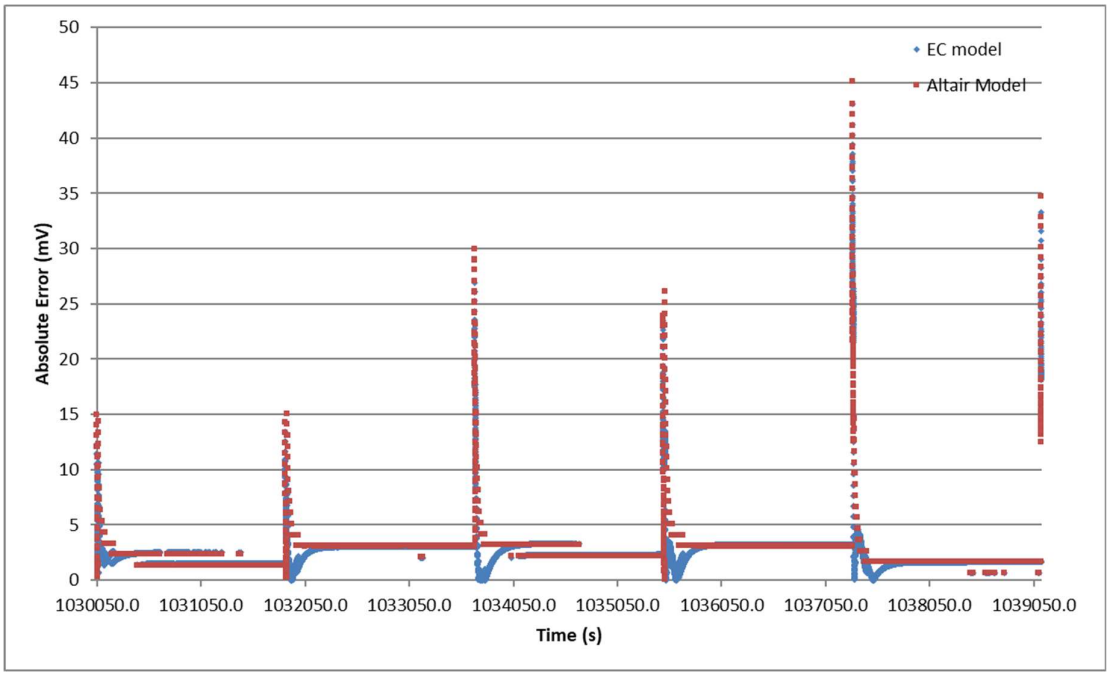

Figure 85: Adjusted absolute error between recorded and modelled cell voltages for Equivalent circuit model (blue) and Altair's model (red) for a pulse power profile

It should be noted, for the adjusted data, that the error is greater for discharge events than for the charge events. This behaviour, combined with the 0.12 A discharge error, would tend to indicate that there is a methodolgy error in the data collection and parameterization for both models with regards to discharge.

Based on the adjusted data, the two models perform similar with minor differences between the two as seen in Table 7.

Table 7: Pulse Power Test Profile - Summarization of errors for each model after adjustment

	# of pts > 5 mV error	max error (mV)	average error (mV)	rms error (mV)
Altair model	3346	45.1	2.6	3.1
EC model	3252	43.1	2.4	2.8

5.1.4.3.6 Discussion of EC model results versus Altairnano's HPPC based model results

Based on the validation work, it was shown that the EC model parameterized from a frequency regulation based multisine signal has an increased accuracy over Altair's current method of modelling based on 10 second pulse power testing. The comparison was done against a number of distinct operating regime in an effort to ascertain if there were deficiencies in either method.

Battery systems are operated in a wide range of conditions and usages, so a model must be able to accurately reflect all of these usages. The EC based model was able to demonstrate increased accuracy over a number of operating scenarios including dynamic charge depleting, charge sustaining, charge increasing, energy neutral signals, and both high and low current rate applications.

Through this validation a limit to the accuracy of the models and source for improvement was identified in both models with regards to a constant current C/100 discharge profile and pulse power testing with rest profiles. Both models showed issues with a drift in the error that increased throughout the data sets for those two tests. This drift is not noticibly present in the same low rate constant current charge profile or the dynamic charge- depleting/sustatin/increasing profiles. The source of this drifting and increasing error needs to be identified and addressed in future work. But as this error was present in both models it implies that it is not a result of the researchers work shown here, but is a systemic issue that needs to be addressed with both models. Future work on identifying if this issue exists with other models would be of interest.

5.2 Innovation and Impact on Altairnano

As previously discussed, many testing and parameterization methods do not accurately represent the applications that the battery cells under test are intended for. In addition, these non-representative methods are used to parametrize models which are then used to predict the performance of the cells in various situation and conditions. The development and validation of a new and novel techniques which builds upon prior work within WMG has been demonstrated as a suitable method for generating data for model parameterization. This technique utilized a reduced data set generation with 2 second data sample rate. Though it is believed that higher fidelity data would serve to enhance and improve the parameterization and the model's accuracy.

As noted by Barai et al. [107] the work by Widanage et al. [89,91] is relatively new and the implementation of this method for characterisation is still under development. The work in generating a signal for parameterization presented here is a step in that direction.

It should be noted that the testing profile generated for the parameterization was based on historical data from PJM fast response frequency regulation signal, and as such provides a realistic basis for the cycle. This contrasts with the HPPC test, which has unrealistic rest periods between each pulse, and the pulse-multisine technique developed by WMG which utilizes synthetic sine waves as part of the signal. While the pulse-multisine may better represent a duty cycle, still has its basis in random generation of sine waves overlaid upon a HPPC signal.

Additionally, while the basis of the model, a 1st order equivalent circuit is not new in modelling, it is a new modelling method for Altairnano. This has the benefit of providing alternative methods for expanding their testing and modelling capabilities. This validation work also served to provide additional 3rd party validation of the capabilities of their present model, which was a project goal. It is intended that this work will continue with Altairnano to apply this technique to their newest generation chemistry.

6 Conclusions

Whilst the scope of this innovation report targeted different directions of research, all three projects described contributed to or built upon each other. In addition, each of the projects contributed towards fulfilling parts of the three main goals set by Altairnano with respect to the introduction of data generation, development of the MATLAB tool and IP. The goals were as follows:

- Data generation
    - Validation of Altairnano's model
    - Additional cycle life data
- MATLAB tool for aging models
    - Initial code to be based on current model
    - MATLAB tool with friendly user interface
    - Code to be improved based upon research and data
- Journal publications and IP generation
    - Undefined but it had been anticipated by both Altairnano and WMG that there would IP and paper generation

The 0 V project provided new and novel data that has been captured in the development of a journal paper. Unfortunately, this paper was never completed and published due to the lack of support from the organization in finalizing and submitting for publication. Additionally, this work is scheduled to be carried out on Altairnano's newest generation chemistry as testing resources are made available. This work will seek to confirm that the new chemistry behaviour is similar to that of the second generation, upon which this work was originally carried out on, as well as strengthening pieces of the research that required additional data to confirm conclusions. Additionally, characterization techniques used within the research provided updated and improved open circuit values, which were then incorporated into the MATLAB modelling tool developed and used in the

equivalent circuit model. This data helped to update and improved the accuracy of the models. The data generated during characterization of the cells was also used for validation of both models.

The integration of Altairnano's performance, aging and thermal models into a single MATLAB program called AltiCalc met the second goal of the company, while contributing data towards the first goal. Once complied, the AltiCalc was used in validating Altairnano's model against multiple operating profiles in conjunction with the work of validating the new parameterization technique. This work also created a framework for which future models, such as the equivalent circuit model used in the parameterization research, to be incorporated into the AltiCalc. This allows for a single point of interface for Altairnano's capability and modelling needs, while providing for the flexibility in updating or incorporating other models for use in the future.

The development of the novel parameterization technique and incorporation into a standard equivalent circuit model met the needs of the 2nd goal. It achieved this by improving upon the previous model, by increasing the modelling accuracy, and providing an alternate model for Altairnano's modelling needs. This work also supported the 1st goal by generating new data and creating new techniques for generating useful data. Additionally, there is scope for further collaboration work regarding the modification and implementation of the technique for parameterizing models based on actual application usage data. It is possible that this future work may allow for the capture of a wider range of dynamics of a system in a single test. With additional work to be carried out at Altairnano with their current generation chemistry it is anticipated that conference presentations will be created. This work is limited and has not been completed due to limitations in the testing resources of Altairnano which have been focused on basic characterization of Altairnano's newest generation chemistry and have not been expanded to include additional testing outside of the standard operating procedures. It is concluded that the research conducted has created new knowledge and innovation with value added to Altairnano based on the research completed and its ability to be applied to future work as resources become available.

Supplemental to the main goals, the development of the AltiCalc provided the experience of coding within the MATLAB environment which was later necessary for data processing of the 0 V study and the parameterization work.

Additionally, the AltiCalc is in constant use within Altairnano. It is utilized by multiple users and has been deployed to a customer for use. A 0 V study is currently being applied to their current generation in an effort to solve a manual manufacturing safety concern with a newly developed pack until an automated manufacturing line is created.

6.1 Limitations

It is acknowledged that there are limitations to the research, but these limitations can and should be view as opportunities for future work. Limitations of the work to be considered:

- 0 V storage study
    - While three voltage states for storage were studied (a standard storage voltage, an open circuit naturally relaxed voltage after discharging to 0 V, and 0 V) there was limited work on studying the long-term behaviour of the open circuit cell. This storage method may be an alternative to 0 V storage as it would not require a method to keep the cell at 0 V via a wired connection
    - Consideration on a method of maintaining the cell at 0 V while within a manufacturing environment. The study created a connection between the cell's terminals by clamping the leads a resistor to each current collector tab, which many not be feasible in a manufacturing environment. Second, in a manufacturing environment the method for connecting the two terminals may also impede connections to bus bars during module construction.
    - This work was completed with Altairnano's second-generation chemistry which is no longer being manufactured. Altairnano is now manufacturing their fourth-generation chemistry which has a number of chemistry changes which may impact

the cell's ability to achieve 0 V storage without degradation or performance changes. As such to apply this work would require repeating the work with the new chemistry.

    - A longer-term study over the course of one year would be beneficial in support of the conclusions drawn within this work.

- Continued Development and Integration of Altairnano's Model
    - Better modularity of the code - As the code currently exists a large amount of work is required to implement new models into the framework.
    - Additional model integration – the current version of AltiCalc currently uses Altairnano's original model but significant code changes are required to implement the ECM model developed here. This work was not completed prior to completion of the research and is still in development currently.
    - Greater error correction – while there are controls built into limit errors from inputs, there still exists opportunity for a greater control to prevent additional situations and inputs which create errors during runtime.
    - The output of the model is exported to Excel, which has limitations on the number of rows of data that can be written. Very large modelling data sets, while rare, may run into this limitation. An example would be a one-year profile with 2 second time step, such as the PJM signal used for creating the multisine signal, would have greater than 15 million data points exceeding the limit of Excel.
- Development of New Parametrization Signal and Implementation into an Equivalent Circuit Model
    - The data collected only allowed for parameterization for state of charge range from 10% to 83%. Altairnano often uses the full range of states of charge in its application so any modelling method would need to encompass the complete state of charge range from 0% to 100%.

- There was obvious noise in the final impedance and time constant results used for parameterization. This required the combination of three separate state of charge filters in an effort to minimize the noise. Additional data collection on multiple cells as well as higher fidelity data collection may help to minimize this issue.
- The data collected was for a single operating temperature, 25 °C. While Altairnano's battery systems are designed with climate control, their cell's actual operating temperatures range across their full stated operating temperature range of negative 55 °C to 65 °C depending on the application.
- The time frame for completing the test and parameterization can be long. A 24-hour testing profile was used to collect an assumed sufficient data set, but future work could look at the feasibility of shorter profiles (4, 6, 8 hours etc.).
- The current data set used to create the signal was based upon the PJM frequency regulation data with 2 second time step. A data set which has shorter time steps (higher resolution) may need to be evaluated for impact on the parameterization values. Such a data set could be collected from other sources such as electric vehicle operational data, other utility grid signals, or applications.

6.2 Future Work and Opportunities

Already Altairnano has taken steps to implement and utilize various pieces of the work presented here, but as the limitations indicate, there still remains much work to be done. One of the largest pieces of future work to be completed is repeating the testing upon their newest generation chemistry to start developing the knowledge and tools for use in commercial applications.

- 0 V storage study needs to be duplicated and expanded with Altairnano's most recent generation chemistry.
    - This includes extending the total storage time to one year

    - Increasing the sample of cells used for testing to better improve the validity of the data
    - Utilizing additional analysis techniques such as in situ imaging of the cell at 0 V or during discharging to 0 V
    - Additional analysis and understanding of the open circuit voltage behaviour after discharging a cell to 0 V
- Continued Development and Integration of Altairnano's Model
    - Implement the equivalent circuit model into the AltiCalc in conjunction of extending the parameterization data to include the full range of operating states of charge and temperatures
    - Implement the ability to accept wider range of customer profile input options including various units of power currently not accepted (watt, kilowatt, megawatt) or current values
    - Incorporate data for the newest generation of chemistry to be able to model its expected performance in applications
- Development of New Parametrization Techniques and Implementation into an Equivalent Circuit Model
    - Expand the parameterization to the full operating state of charge - 0% to 100%
    - Include additional operational temperature ranges – negative 55 degrees Celsius to 65 degrees Celsius
    - Evaluated alternative input data sets to generate the parameterization signal such as automotive, industrial or other grid applications
    - Develop a testing regime that includes temperature changes over the course of the parameterization signal testing to reduce the need to repeat the parameterization signal testing for multiple temperature regimes

7 Conference Presentations

The 0 V work was presented at PRiME 2016 held by ECS in Honolulu, Hawaii under the title “Effect of Zero Volt Storage on Commercial LTO Cells”.

8 References

[1] D. Ahn, X. Xiao, Extended lithium titanate cycling potential window with near zero capacity loss, Electrochem. Commun. 13 (2011) 796–799. doi:10.1016/j.elecom.2011.05.005.

[2] M. Moorthi, Lithium Titanate Based Batteries for High Rate and High Cycle Life Applications, (2010) 1–8. http://neicorporation.com/white-papers/NEI_White_Paper_LTO.pdf.

[3] H. Maleki, J.N. Howard, Effects of overdischarge on performance and thermal stability of a Li-ion cell, J. Power Sources. 160 (2006) 1395–1402. doi:10.1016/j.jpowsour.2006.03.043.

[4] R. Guo, L. Lu, M. Ouyang, X. Feng, Mechanism of the entire overdischarge process and overdischarge-induced internal short circuit in lithium-ion batteries., Sci. Rep. 6 (2016) 30248. doi:10.1038/srep30248.

[5] H.-F. Li, J.-K. Gao, S.-L. Zhang, Effect of Overdischarge on Swelling and Recharge Performance of Lithium Ion Cells, Chinese J. Chem. 26 (2008) 1585–1588. doi:10.1002/cjoc.200890286.

[6] ALTAIR NANOTECHNOLOGIES INC - FORM 10-K - May 18, 2017, (n.d.). http://getfilings.com/sec-filings/170518/ALTAIR-NANOTECHNOLOGIES-INC_10-K/ (accessed May 30, 2017).

[7] N. Tran, M. Holzapfel, J. Dollinger, A. Pollner, M. Eisgruber, G. Nuspl, S.C. Ag, New Lithium Titanate as Anode Material for Lithium Ion Batteries, (2008). http://www.phostechlithium.com/documents/ECS_214th_Meeting_Honolulu_2008.pdf.

[8] T.-F. Yi, Y. Xie, Y.-R. Zhu, R.-S. Zhu, H. Shen, Structural and thermodynamic stability of Li4Ti5O12 anode material for lithium-ion battery, J. Power Sources. 222 (2013) 448–454. doi:10.1016/j.jpowsour.2012.09.020.

[9] T.-F. Yi, Z.-K. Fang, L. Deng, L. Wang, Y. Xie, Y.-R. Zhu, J.-H. Yao, C. Dai, Enhanced electrochemical performance of a novel Li4Ti5O12 composite as anode material for lithium-ion battery in a broad voltage window, Ceram. Int. 41 (2015) 2336–2341. doi:10.1016/j.ceramint.2014.10.041.

[10] P. Svens, R. Eriksson, J. Hansson, M. Behm, T. Gustafsson, G. Lindbergh, Analysis of aging of commercial composite metal oxide – Li4Ti5O12 battery cells, J. Power Sources. 270 (2014) 131–141. doi:10.1016/j.jpowsour.2014.07.050.

[11] K. Nakahara, R. Nakajima, T. Matsushima, H. Majima, Preparation of particulate Li4Ti5O12 having excellent characteristics as an electrode active material for power storage cells, J. Power Sources. 117 (2003) 131–136. doi:10.1016/S0378-7753(03)00169-1.

[12] M.R. Harrison, P.P. Edwards, J.B. Goodenough, The superconductor-semiconductor transition in the Li 1+x Ti 2-x O 4 spinel system, Philos. Mag. Part B. 52 (1985) 679–699. doi:10.1080/13642818508240629.

[13] H. Ge, N. Li, D. Li, C. Dai, D. Wang, Study on the Theoretical Capacity of Spinel Lithium Titanate Induced by Low-Potential Intercalation, J. Phys. Chem. C. 113 (2009) 6324–6326. doi:10.1021/jp9017184.

[14] T. Spitler, J. Prochazka, Process for Making Lithium Titanate - United States Patent US006890510B2, 2005. https://drive.google.com/viewerng/viewer?url=patentimages.storage.googleapis.com/pdfs/US6890510.pdf (accessed November 13, 2014).

[15] C.P. Sandhya, B. John, C. Gouri, Lithium titanate as anode material for lithium-ion cells: a review, Ionics (Kiel). 20 (2014) 601–620. doi:10.1007/s11581-014-1113-4.

[16] X.L. Yao, S. Xie, C.H. Chen, Q.S. Wang, J.H. Sun, Y.L. Li, S.X. Lu, Comparisons of graphite and spinel Li1.33Ti1.67O4 as anode materials for rechargeable lithium-ion batteries, Electrochim. Acta. 50 (2005) 4076–4081. doi:10.1016/j.electacta.2005.01.034.

[17] K. Zaghib, M. Simoneau, M. Armand, M. Gauthier, Electrochemical study of Li4Ti5O12 as negative electrode for Li-ion polymer rechargeable batteries, J. Power Sources. 81–82 (1999) 300–305. doi:10.1016/S0378-7753(99)00209-8.

[18] Y.-B. He, M. Liu, Z.-D. Huang, B. Zhang, Y. Yu, B. Li, F. Kang, J.-K. Kim, Effect of solid electrolyte interface (SEI) film on cyclic performance of Li4Ti5O12 anodes for Li ion batteries, J. Power Sources. 239 (2013) 269–276. doi:10.1016/j.jpowsour.2013.03.141.

[19] W.-S. Cho, J.-H. Song, M.-S. Park, J.-H. Kim, J.-S. Kim, Y.-J. Kim, Reaction Behavior of Li 4+x Ti 5 O 12 Anode Material as Depth of Discharge, J. Electrochem. Sci. Technol. 1 (2010) 85–91. doi:10.5229/JECST.2010.1.2.085.

[20] T.-F. Yi, L.-J. Jiang, J. Shu, C.-B. Yue, R.-S. Zhu, H.-B. Qiao, Recent development and application of Li4Ti5O12 as anode material of lithium ion battery, J. Phys. Chem. Solids. 71 (2010) 1236–1242. doi:10.1016/j.jpcs.2010.05.001.

[21] K.M. Colbow, J.R. Dahn, R.R. Haering, Structure and electrochemistry of the spinel oxides LiTi2O4 and Li43Ti53O4, J. Power Sources. 26 (1989) 397–402. doi:10.1016/0378-7753(89)80152-1.

[22] N. Takami, H. Inagaki, Y. Tatebayashi, H. Saruwatari, K. Honda, S. Egusa, High-power and long-life lithium-ion batteries using lithium titanium oxide anode for automotive and stationary power applications, J. Power Sources. 244 (2013) 469–475. doi:10.1016/j.jpowsour.2012.11.055.

[23] X. Han, M. Ouyang, L. Lu, J. Li, Cycle Life of Commercial Lithium-Ion Batteries with Lithium Titanium Oxide Anodes in Electric Vehicles, Energies. 7 (2014) 4895–4909. doi:10.3390/en7084895.

[24] S. Scharner, Evidence of Two-Phase Formation upon Lithium Insertion into the Li1. 33Ti1. 67 O 4 Spinel, J. …. 146 (1999) 857–861. http://jes.ecsdl.org/content/146/3/857.short (accessed August 27, 2014).

[25] A.. Jansen, A.. Kahaian, K.. Kepler, P.. Nelson, K. Amine, D.. Dees, D.. Vissers, M.. Thackeray, Development of a high-power lithium-ion battery - LTO, J. Power Sources. 81–82 (1999) 902–905. doi:10.1016/S0378-7753(99)00268-2.

[26] C.-C. Yang, H.-J. Hwu, S.J. Lin, W.-C. Chien, J.-Y. Shih, Preparation of High-rate Performance Li4Ti5O12/C Anode Material in Li4Ti5O12/LiFe0.5Mn0.5PO4 Batteries, Electrochim. Acta. 125 (2014) 637–645. doi:10.1016/j.electacta.2014.01.156.

[27] W. Liu, Y. Wang, X. Jia, B. Xia, The Characterization of Lithium Titanate Microspheres Synthesized by a Hydrothermal Method, J. Chem. 2013 (2013) 1–9. doi:10.1155/2013/497654.

[28] Y. Qin, Z. Chen, I. Belharouak, K.A. Pi, Mechanism of LTO Gassing and potential solutions, (2011). http://www1.eere.energy.gov/vehiclesandfuels/pdfs/merit_review_2011/electrochemical_storage/es112_amine_2011_p.pdf.

[29] T.T. Ohzuku, A. Ueda, N. Yamamoto, N. Yamamota, Zero-Strain Insertion Material of Li[Li1/3Ti5/3]O4 for Rechargeable Lithium Cells, J. Electrochem. …. 142 (1995) 4–8. doi:10.1149/1.2048592.

[30] K. Zaghib, A. Mauger, H. Groult, J. Goodenough, C. Julien, Advanced Electrodes for High Power Li-ion Batteries, Materials (Basel). 6 (2013) 1028–1049. doi:10.3390/ma6031028.

[31] L. V. Nowack, O. Waser, O. Yarema, V. Wood, Rapid, microwave-assisted synthesis of battery-grade lithium titanate (LTO), RSC Adv. 3 (2013) 15618. doi:10.1039/c3ra43237h.

[32] Y. Shi, L. Wen, F. Li, H.-M. Cheng, Nanosized Li4Ti5O12/graphene hybrid materials with low polarization for high rate lithium ion batteries, J. Power Sources. 196 (2011) 8610–8617. doi:10.1016/j.jpowsour.2011.06.002.

[33] J. Mcdowall, UNDERSTANDING LITHIUM-ION TECHNOLOGY, 2008. http://www.battcon.com/papersfinal2008/mcdowallpaper2008proof_9.pdf.

[34] M. Dubarry, B.Y. Liaw, M.-S. Chen, S.-S. Chyan, K.-C. Han, W.-T. Sie, S.-H. Wu, Identifying battery aging mechanisms in large format Li ion cells, J. Power Sources. 196 (2011) 3420–3425. doi:10.1016/j.jpowsour.2010.07.029.

[35] J. Vetter, P. Novák, M.R. Wagner, C. Veit, K.-C. Möller, J.O. Besenhard, M. Winter, M. Wohlfahrt-Mehrens, C. Vogler, A. Hammouche, Ageing mechanisms in lithium-ion batteries, J. Power Sources. 147 (2005) 269–281. http://www.sciencedirect.com/science/article/pii/S0378775305000832 (accessed October 31, 2013).

[36] B. Markovsky, A. Rodkin, Y.. Cohen, O. Palchik, E. Levi, D. Aurbach, H.-J. Kim, M. Schmidt, The study of capacity fading processes of Li-ion batteries: major factors that play a role, J. Power Sources. 119 (2003) 504–510. http://www.sciencedirect.com/science/article/pii/S037877530300274X (accessed October 31, 2013).

[37] N. Williard, M. Osterman, M. Pecht, Remaining useful performance analysis of batteries, 2011 IEEE Conf. Progn. Heal. Manag. (2011) 1–6. doi:10.1109/ICPHM.2011.6024341.

[38] V. Ramadesigan, P.W.C. Northrop, S. De, S. Santhanagopalan, R.D. Braatz, V.R. Subramanian, Modeling and Simulation of Lithium-Ion Batteries from a Systems Engineering Perspective, J. Electrochem. Soc. 159 (2012) R31–R45. doi:10.1149/2.018203jes.

[39] C. Masquelier, M. Morcrette, J.-M. Tarascon, C. Delmas, S.-W. Eom, M.-K. Kim, I.-J. Kim, S.-I. Moon, Y.-K. Sun, H.-S. Kim, Life prediction and reliability assessment of lithium secondary batteries, 2007. http://www.sciencedirect.com/science/article/pii/S0378775307013389 (accessed October 31, 2013).

[40] M. Ecker, J.B. Gerschler, J. Vogel, S. Käbitz, F. Hust, P. Dechent, D.U. Sauer, Development of a lifetime prediction model for lithium-ion batteries based on extended accelerated aging test data, J. Power Sources. 215 (2012) 248–257. http://www.sciencedirect.com/science/article/pii/S0378775312008671 (accessed October 31, 2013).

[41] Y. Takeda, J. Yamaki, Z. Ogumi, M. Broussely, P. Biensan, F. Bonhomme, P. Blanchard, S. Herreyre, K. Nechev, R.J. Staniewicz, Main aging mechanisms in Li ion batteries, J. Power Sources. 146 (2005) 90–96. http://www.sciencedirect.com/science/article/pii/S0378775305005082 (accessed October 31, 2013).

[42] X. Han, M. Ouyang, L. Lu, J. Li, Y. Zheng, Z. Li, A comparative study of commercial lithium

ion battery cycle life in electrical vehicle: Aging mechanism identification, J. Power Sources. 251 (2014) 38–54. doi:http://dx.doi.org/10.1016/j.jpowsour.2013.11.029.

[43] B.Y. Liaw, R.G. Jungst, G. Nagasubramanian, H.L. Case, D.H. Doughty, Modeling capacity fade in lithium-ion cells, 2005. http://www.sciencedirect.com/science/article/pii/S0378775304008808 (accessed October 31, 2013).

[44] L. Kang, X. Zhao, J. Ma, A new neural network model for the state-of-charge estimation in the battery degradation process, Appl. Energy. 121 (2014) 20–27. doi:10.1016/j.apenergy.2014.01.066.

[45] E.V. Thomas, I. Bloom, J.P. Christophersen, V.S. Battaglia, Statistical methodology for predicting the life of lithium-ion cells via accelerated degradation testing, J. Power Sources. 184 (2008) 312–317. http://www.sciencedirect.com/science/article/pii/S0378775308012032 (accessed January 8, 2014).

[46] E.V. Thomas, I. Bloom, J.P. Christophersen, V.S. Battaglia, Rate-based degradation modeling of lithium-ion cells, 2012. http://www.sciencedirect.com/science/article/pii/S0378775312002078 (accessed January 8, 2014).

[47] A. Millner, Modeling lithium ion battery degradation in electric vehicles, Innov. Technol. an Effic. …. (2010) 349–356. doi:10.1109/CITRES.2010.5619782.

[48] S. Sankarasubramanian, B. Krishnamurthy, A capacity fade model for lithium-ion batteries including diffusion and kinetics, Electrochim. Acta. 70 (2012) 248–254. http://www.sciencedirect.com/science/article/pii/S0013468612004021 (accessed July 22, 2014).

[49] J. Yan, G. Lidén, D. Chiaramonti, W. Waag, S. Käbitz, D.U. Sauer, Experimental investigation of the lithium-ion battery impedance characteristic at various conditions and aging states and its influence on the application, Appl. Energy. 102 (2013) 885–897. http://www.sciencedirect.com/science/article/pii/S030626191200671X (accessed October 31, 2013).

[50] M. Dubarry, C. Truchot, A. Devie, B.Y. Liaw, Battery Modeling - Bridging academic & industrial understandings, in: 2014.

[51] M. Dubarry, A. Devie, K. Stein, M. Tun, M. Matsuura, R. Rocheleau, Battery Energy Storage System battery durability and reliability under electric utility grid operations: Analysis of 3 years of real usage, J. Power Sources. 338 (2017) 65–73. doi:10.1016/J.JPOWSOUR.2016.11.034.

[52] Siemens, How can power plant operators be ready for today's challenges , and tomorrow's?, 2011. http://www.siemens.co.uk/pool/about_us/businesses/energy/energy-service/documents/siemens-essf-brochure.pdf.

[53] D. Nichols, M. Brunell, ALTI-ESS an Advanced Technology Power Plant for Grid Stabilization Applications, (2011) 1–6. http://scholar.google.com/scholar?hl=en&btnG=Search&q=intitle:ALTI-ESS+an+Advanced+Technology+Power+Plant+for+Grid+Stabilization+Applications#0 (accessed July 22, 2014).

[54] G. Crabtree, J. Misewich, Integrating renewable electricity on the grid, … ENERGY II USING …. (2011). http://scitation.aip.org/content/aip/proceeding/aipcp/10.1063/1.3653865 (accessed July 22, 2014).

[55] H.F.F. Xiang, X. Zhang, Q.Y.Y. Jin, C.P.P. Zhang, C.H.H. Chen, X.W.W. Ge, Effect of capacity matchup in the LiNi0.5Mn1.5O4/Li4Ti5O12 cells, J. Power Sources. 183 (2008) 355–360. doi:10.1016/j.jpowsour.2008.04.091.

[56] V. Manev, M. Coleman, B. Hanauer, Altairnano Large Format Batteries for Stationary Power and Automotive Application, in: 30th Int. Batter. Semin., Fort Lauderdale, 2013.

[57] K. Zaghib, M. Dontigny, a. Guerfi, P. Charest, I. Rodrigues, a. Mauger, C.M. Julien, Safe and fast-charging Li-ion battery with long shelf life for power applications, J. Power Sources. 196 (2011) 3949–3954. doi:10.1016/j.jpowsour.2010.11.093.

[58] P. Huang, Q. Wang, K. Li, P. Ping, J. Sun, The combustion behavior of large scale lithium titanate battery., Sci. Rep. 5 (2015) 7788. doi:10.1038/srep07788.

[59] A.W. Golubkov, S. Scheikl, R. Planteu, G. Voitic, H. Wiltsche, C. Stangl, G. Fauler, A. Thaler, V. Hacker, Thermal runaway of commercial 18650 Li-ion batteries with LFP and NCA cathodes – impact of state of charge and overcharge, RSC Adv. 5 (2015) 57171–57186. doi:10.1039/C5RA05897J.

[60] G.A. Kerchner, Shipping Lithium ion Cells , Implications on State of Charge, 2014.

[61] H. Zheng, Q. Sun, G. Liu, X. Song, V.S. Battaglia, Correlation between dissolution behavior and electrochemical cycling performance for LiNi1/3Co1/3Mn1/3O2-based cells, J. Power Sources. 207 (2012) 134–140. doi:10.1016/j.jpowsour.2012.01.122.

[62] S.-T. Myung, Y. Hitoshi, Y.-K. Sun, Electrochemical behavior and passivation of current collectors in lithium-ion batteries, J. Mater. Chem. 21 (2011) 9891. doi:10.1039/c0jm04353b.

[63] H. Tsukamoto, C. Kishiyama, M. Nagata, H. Nakahara, T. Piao, Quallion US8637184B2 - zero volt technology.pdf, 2014.

[64] J. Shu, M. Shui, D. Xu, D. Wang, Y. Ren, S. Gao, A comparative study of overdischarge behaviors of cathode materials for lithium-ion batteries, J. Solid State Electrochem. 16 (2012) 819–824. doi:10.1007/s10008-011-1484-7.

[65] A. Fay, M. Nagata, Zero-Volt and Long Life Chemistry Enhancements to Rechargeable Batteries for Medical Devices, Meet. Abstr. MA2014-01 (2014) 102. http://ma.ecsdl.org/content/MA2014-01/1/102.abstract (accessed September 23, 2015).

[66] S.-T. Myung, H. Yashiro, Electrochemical stability of aluminum current collector in alkyl carbonate electrolytes containing lithium bis(pentafluoroethylsulfonyl)imide for lithium-ion batteries, J. Power Sources. 271 (2014) 167–173. doi:10.1016/j.jpowsour.2014.07.097.

[67] B. Zhao, R. Ran, M. Liu, Z. Shao, A comprehensive review of Li4Ti5O12-based electrodes for lithium-ion batteries: The latest advancements and future perspectives, Mater. Sci. Eng. R Reports. 98 (2015) 1–71. doi:10.1016/j.mser.2015.10.001.

[68] Altairnano, Altairnano 13 Amp Hour Cell, (2011). www.altairnano.com.

[69] M. Dubarry, A. Devie, B.Y. Liaw, The Value of Battery Diagnostics and Prognostics, J. Energy Power Sources. 1 (2014) 242–249.

[70] Gamry, EIS Measurement of a Very Low Impedance Lithium Ion Battery, 2014. http://www.gamry.com/assets/Application-Notes/EIS-on-Very-Low-Z-Battery.pdf.

[71] M.E. Orazem, U. Tröltzsch, O. Kanoun, H.-R. Tränkler, Characterizing aging effects of lithium ion batteries by impedance spectroscopy, Electrochim. Acta. 51 (2006) 1664–1672. http://www.sciencedirect.com/science/article/pii/S0013468605007899 (accessed October 31, 2013).

[72] T. Hang, D. Mukoyama, H. Nara, N. Takami, T. Momma, T. Osaka, Electrochemical impedance spectroscopy analysis for lithium-ion battery using Li4Ti5O12 anode, J. Power Sources. 222 (2013) 442–447. doi:10.1016/j.jpowsour.2012.09.010.

[73] M. Dubarry, V. Svoboda, R. Hwu, B. Yann Liaw, Incremental Capacity Analysis and Close-to-Equilibrium OCV Measurements to Quantify Capacity Fade in Commercial Rechargeable Lithium Batteries, Electrochem. Solid-State Lett. 9 (2006) A454. doi:10.1149/1.2221767.

[74] M. Dubarry, C. Truchot, B.Y. Liaw, Synthesize battery degradation modes via a diagnostic

and prognostic model, J. Power Sources. 219 (2012) 204–216. doi:10.1016/j.jpowsour.2012.07.016.

[75] D. Andre, M. Meiler, K. Steiner, C. Wimmer, T. Soczka-Guth, D.U. Sauer, H. Walz, Characterization of high-power lithium-ion batteries by electrochemical impedance spectroscopy. I. Experimental investigation, J. Power Sources. 196 (2011) 5334–5341. doi:10.1016/j.jpowsour.2010.12.102.

[76] S. Yoon, I. Hwang, C.W. Lee, H.S. Ko, K.H. Han, Power capability analysis in lithium ion batteries using electrochemical impedance spectroscopy, J. Electroanal. Chem. 655 (2011) 32–38. doi:10.1016/j.jelechem.2011.02.013.

[77] V. Manev, D. Ph, J. Shelburne, B. Hanauer, M. Coleman, E. Way, R. Nv, Large Format Li4Ti5O12 Lithium-Ion Batteries and Battery Systems, in: 29th Int. Batter. Semin. Exhib., Fort Lauderdale, 2012.

[78] A.J. Smith, J.C. Burns, D. Xiong, J.R. Dahn, Interpreting High Precision Coulometry Results on Li-ion Cells, J. Electrochem. Soc. 158 (2011) A1136. doi:10.1149/1.3625232.

[79] E. McTurk, C.R. Birkl, M. Roberts, P.G. Bruce, D.A. Howey, Three-Electrode Cells for Open Circuit Voltage Modelling of Commercial Lithium-Ion Batteries, Meet. Abstr. MA2015-03 (2015) 574. http://ma.ecsdl.org/content/MA2015-03/2/574.abstract (accessed November 17, 2016).

[80] A.K. Suttman, Lithium Ion Battery Aging Experiments and Algorithm Development for Life Estimation, Ohio State University, 2011. https://etd.ohiolink.edu/ap:0:0:APPLICATION_PROCESS=DOWNLOAD_ETD_SUB_DOC_ACCNUM:::F1501_ID:osu1306937891,inline (accessed December 19, 2013).

[81] I. Bloom, S.A. Jones, E.G. Polzin, V.S. Battaglia, G.L. Henriksen, C.G. Motloch, R.B. Wright, R.G. Jungst, H.L. Case, D.H. Doughty, Mechanisms of impedance rise in high-power, lithium-ion cells, J. Power Sources. 111 (2002) 152–159. http://www.sciencedirect.com/science/article/pii/S0378775302003026 (accessed October 31, 2013).

[82] J.R. Belt, U . S . Department of Energy Vehicle Technologies Program Battery Test Manual For Plug-In Hybrid Electric Vehicles, 2008.

[83] J. Belt, V. Utgikar, I. Bloom, Calendar and PHEV cycle life aging of high-energy, lithium-ion cells containing blended spinel and layered-oxide cathodes, J. Power Sources. 196 (2011) 10213–10221. http://www.sciencedirect.com/science/article/pii/S0378775311016107 (accessed January 8, 2014).

[84] D.W. Dees, V.S. Battaglia, A. Bélanger, Electrochemical modeling of lithium polymer batteries, J. Power Sources. 110 (2002) 310–320. doi:10.1016/S0378-7753(02)00193-3.

[85] C. Truchot, M. Dubarry, B.Y. Liaw, State-of-charge estimation and uncertainty for lithium-ion battery strings, Appl. Energy. 119 (2014) 218–227. http://www.sciencedirect.com/science/article/pii/S0306261913010556 (accessed January 28, 2014).

[86] J. Cosgrove, J. Gonger, Testing Low-Energy, High-Power Energy Storage Alternatives in a Full-Hybrid Vehicle (Presentation), (2014). http://www.osti.gov/scitech/biblio/1118088 (accessed July 22, 2014).

[87] L. Sánchez, I. Couso, M. González, A design methodology for semi-physical fuzzy models applied to the dynamic characterization of LiFePO4 batteries, Appl. Soft Comput. 14 (2014) 269–288. doi:10.1016/j.asoc.2013.03.020.

[88] Y. Xing, W. He, M. Pecht, K.L. Tsui, State of charge estimation of lithium-ion batteries using the open-circuit voltage at various ambient temperatures, Appl. Energy. 113 (2014) 106–115. doi:10.1016/j.apenergy.2013.07.008.

[89] W.D. Widanage, A. Barai, G.H. Chouchelamane, K. Uddin, A. McGordon, J. Marco, P. Jennings, Design and use of multisine signals for Li-ion battery equivalent circuit modelling. Part 1: Signal design, J. Power Sources. 324 (2016) 70–78. doi:10.1016/j.jpowsour.2016.05.015.

[90] M.A. Roscher, D.U. Sauer, Dynamic electric behavior and open-circuit-voltage modeling of LiFePO4-based lithium ion secondary batteries, J. Power Sources. 196 (2011) 331–336. doi:10.1016/j.jpowsour.2010.06.098.

[91] W.D. Widanage, A. Barai, G.H. Chouchelamane, K. Uddin, A. McGordon, J. Marco, P. Jennings, Design and use of multisine signals for Li-ion battery equivalent circuit modelling. Part 2: Model estimation, J. Power Sources. 324 (2016) 61–69. doi:10.1016/j.jpowsour.2016.05.014.

[92] Case Study: PJM Frequency Regulation, (2015) 2. http://www.res-americas.com/media/2301749/final_frequency-regulation-flyer_v5-26-15.pdf.

[93] K. Tweed, Faster Frequency Regulation Triples in PJM, Greentech Media. (2013). https://www.greentechmedia.com/articles/read/faster-frequency-regulation-triples-in-pjm.

[94] S.N. Labs, Altairnano-PJM Li-ion Battery Ancillary Services Demo, (2013) 0–1. www.energystorageexchange.org/projects/205.

[95] W.D. Widanage, N. Omar, J. Schoukens, J. Van Mierlo, Estimating the frequency response of a system in the presence of an integrator, Control Eng. Pract. 35 (2015) 1–11. doi:10.1016/j.conengprac.2014.10.007.

[96] H. He, X. Zhang, R. Xiong, Y. Xu, H. Guo, Online model-based estimation of state-of-charge and open-circuit voltage of lithium-ion batteries in electric vehicles, Energy. 39 (2012) 310–318. doi:10.1016/j.energy.2012.01.009.

[97] M. Dubarry, N. Vuillaume, B. Yann Liaw, Origins and accommodation of cell variations in Li-ion battery pack modeling, (2010) 216–231. doi:10.1002/er.

[98] M. Dubarry, N. Vuillaume, B.Y. Liaw, From single cell model to battery pack simulation for Li-ion batteries, J. Power Sources. 186 (2009) 500–507. doi:10.1016/j.jpowsour.2008.10.051.

[99] B. YANN LIAW, Modeling of lithium ion cells—A simple equivalent-circuit model approach, Solid State Ionics. 175 (2004) 835–839. doi:10.1016/j.ssi.2004.09.049.

[100] A. Rahmoun, H. Biechl, Modelling of Li-ion batteries using equivalent circuit diagrams, Prz. ELEKTROTECHNICZNY. 2 (2012) 152–156. http://red.pe.org.pl/articles/2012/7b/40.pdf (accessed October 31, 2013).

[101] H. He, R. Xiong, J. Fan, Evaluation of Lithium-Ion Battery Equivalent Circuit Models for State of Charge Estimation by an Experimental Approach, Energies. 4 (2011) 582–598. doi:10.3390/en4040582.

[102] N. Omar, M. Daowd, O. Hegazy, G. Mulder, J.-M. Timmermans, T. Coosemans, P. Van den Bossche, J. Van Mierlo, Standardization Work for BEV and HEV Applications: Critical Appraisal of Recent Traction Battery Documents, Energies. 5 (2012) 138–156. doi:10.3390/en5010138.

[103] S. Thanagasundram, R. Arunachala, K. Makinejad, T. Teutsch, A. Jossen, A Cell Level Model for Battery Simulation, EEVC Eur. …. (2012) 1–13. http://www.researchgate.net/publication/235602059_A_Cell_Level_Model_for_Battery_Simulation/file/d912f511db0c693ca1.pdf (accessed July 22, 2014).

[104] L. Zhang, Z. Mu, Z. Ning, C. Sun, H. Peng, Comparative Research on RC Equivalent Circuit Models for Lithium-Ion Batteries of Electric Vehicles, Appl. Sci. 7 (2017) 1002. doi:10.3390/app7101002.

[105] R. Pintelon, J. Schoukens, G. Vandersteen, K. Barbé, Estimation of nonparametric noise and FRF models for multivariable systems-Part I: Theory, Mech. Syst. Signal Process. 24 (2010) 573–595. doi:10.1016/j.ymssp.2009.08.009.

[106] R. Jackey, M. Saginaw, P. Sanghvi, J. Gazzarri, T. Huria, M. Ceraolo, Battery Model Parameter Estimation Using a Layered Technique: An Example Using a Lithium Iron Phosphate Cell, (2013). doi:10.4271/2013-01-1547.

[107] A. Barai, K. Uddin, M. Dubarry, L. Somerville, A. McGordon, P. Jennings, I. Bloom, A comparison of methodologies for the non-invasive characterisation of commercial Li-ion cells, Prog. Energy Combust. Sci. 72 (2019) 1–31. doi:10.1016/J.PECS.2019.01.001.